SUPERSONIC FLUTTER OF SANDWICH PANELS: EFFECTS OF FACE SHEET BENDING STIFFNESS, ROTARY INERTIA, AND ORTHOTROPIC CORE SHEAR STIFFNESSES

by

Larry L. Erickson

Thesis submitted to the Graduate Faculty of the
Virginia Polytechnic Institute and State University
in partial fulfillment of the requirements for the degree of

DOCTOR OF PHILOSOPHY

in

Engineering Mechanics

APPROVED:

Prof. Daniel Frederick

Prof. G. A. Gray

Prof. C. W. Smith

Prof. R. P. McNitt

Prof. Warren Smith

March 1971

Blacksburg, Virginia

Attention Patron:

Page ii omitted from numbering

ACKNOWLEDGMENTS

The author would like to express his thanks to the National Aeronautics and Space Administration for allowing him to carry out this research as a part of his work assignment at the Ames Research Center. Appreciation is also expressed to Mr. Ralph E. Sutton for coding the computer programs used to obtain numerical results. Special thanks are extended to Professor Daniel Frederick, Head, Department of Engineering Mechanics, Virginia Polytechnic Institute and State University, for his interest and encouragement during the course of this investigation.

TABLE OF CONTENTS

LIST OF FIGURES AND TABLES

SYMBOLS

A_j, B_j, C_j	coefficients appearing in equations (5)
$\overline{A}_j, \tilde{A}_j$	coefficients appearing in equations (94) and (99), respectively
a	length of panel
a_j, a'_j	expressions defined by equations (44a)
a_{11}, a'_{11}	expressions defined by equations (8) and (10), respectively
B	set of bending modes and frequencies
b	width of panel
b_j, b'_j	defined by equations (44b)
c	thickness of a sandwich core
c_j	coefficients appearing in characteristic equations
$c_{ij}, \overline{c}_{ij}, \tilde{c}_{ij}, \hat{c}_{ij}$	elements of frequency determinants given by equations (46), (50), (55), and (56), respectively
D	frequency determinant defined by equation (105)
D_f	face sheet bending stiffness (see appendix A)
D_{q_x}, D_{q_y}	transverse shear stiffnesses of panel in x- and y-directions, respectively (see appendix A)
D_s	panel bending stiffness due to the extensional stiffness of the faces (see appendix A)
$D_8 = D_2 D_6$	differential operators given by equations (84) and (85)
d_1, d_2	distance to elastic axis of panel cross section, measured from middle of faces 1 and 2, respectively (see fig. 2 and appendix A)
d_{ij}	elements of beam frequency determinant obtained by approach of reference 7 (see eq. (102))
E_f	Young's modulus of faces
E_j, F_j	analytic functions of z_j

$\bar{e}$ distance to elastic axis of panel cross section measured from middle surface of core (see fig. 2 and appendix A)

f thickness of face sheets

G_{c_x}, G_{c_y} shear moduli of core in x- and y-directions, respectively

g, g', h, h' defined by equations (22c)

$I( )$ imaginary part of ( )

I_o mass density moment of inertia of face sheets, per unit width, about elastic axis of panel cross section (see appendix A)

$i = \sqrt{-1}$

i, j integers when used as subscripts

K_{ij} partitioned matrices in equations (70)

k_x, k_x' in-plane stress parameters, $\frac{N_x b^2}{\pi^2 D_s}$, $\frac{N_x a^2}{\pi^2 D_s}$

k_y, k_y' in-plane stress parameters, $\frac{N_y b^2}{\pi^2 D_s}$, $\frac{N_y a^2}{\pi^2 D_s}$

L_{ij} differential operators defined by equations (83)

M Mach number

m, n integers designating number of sinusoidal half-waves in x- and y-directions, respectively

$\bar{m}_j = \pi z_j$

N_x, N_y intensity of in-plane force resultants (per unit width) parallel to x- and y-axes, respectively (positive in compression)

$P(z_j) = 0$ characteristic equation

p lateral loading on panel

Q_x, Q_y intensity of internal shears (per unit width) acting in z-direction in cross sections originally parallel to yz- and xz-planes, respectively

q dynamic pressure of airflow

$R( )$ real part of ( )

r, r' — shear flexibility parameters, $\frac{\pi^2 D_s}{b^2 D_Q}$, $\frac{\pi^2 D_s}{a^2 D_Q}$

s, s' — defined by equations (22c)

TS — set of thickness-shear modes and frequencies

TT — set of thickness-twist modes and frequencies

t — time

w — transverse deflection of panel, measured in z-direction

x, y, z — orthogonal coordinates (see fig. 1)

x_j, x_j', y_j, y_j' — defined by equations (12)

z_j — roots of characteristic equations

$\alpha_j = R(\overline{m}_j)$

α_x — rotational contribution to panel slope in xz-plane (see appendixes A and B

$\beta = \sqrt{M^2 - 1}$

$\overline{\beta} = \left(\frac{m}{\eta}\right)^2 + n^2$

$\delta_j = I(\overline{m}_j)$

γ_x, γ_y — shear angles in xz- and yz-planes, respectively (see appendix A) $\frac{Q_x}{D_{Q_x}}$, $\frac{Q_y}{D_{Q_y}}$

ζ — quantity defined by equation (18b)

η — panel length-width ratio, $\frac{a}{b}$

λ, λ' — dynamic pressure parameters, $\frac{2qb^3}{\beta D_s}$, $\frac{2qa^3}{\beta D_s}$

μ — Poisson's ratio of face sheets

$\overline{\rho} = \left(\frac{m}{\eta}\right)^2 k_x + n^2 k_y$

ρ_c mass density of core

ρ_f mass density of face sheets

ρ_m mass per unit area of sandwich panel (see appendix A)

$\tau = \frac{D_{f_1}+D_{f_2}}{D_s}$ (see appendix A)

$$\Phi = \left(w_{,x} - \frac{Q_x}{D_Q}\right)_{,x} + \left(w_{,y} - \frac{Q_y}{D_Q}\right)_{,y}$$

ϕ,ϕ' defined by equations (22c)

χ,χ' rotary inertia parameters, $\frac{\pi^2}{b^2}\frac{I_o}{\rho_m}$, $\frac{\pi^2}{a^2}\frac{I_o}{\rho_m}$

$\overline{\chi}$ function related to w by equation (91)

$$\psi_j = \frac{1}{\frac{1 - r\chi\overline{\omega}^2}{1 - (z_j/n\eta)^2} + n^2 r}$$

ω panel circular frequency

ω_o,ω_o' fundamental frequency of simply supported panel, rigid in shear, with an infinite length or width, respectively, $\frac{\pi^2}{b^2}\sqrt{\frac{D_s}{\rho_m}}$, $\frac{\pi^2}{a^2}\sqrt{\frac{D_s}{\rho_m}}$

$\overline{\omega},\overline{\omega}'$ frequency parameters, $\frac{\omega}{\omega_o}$, $\frac{\omega}{\omega_o'}$

Subscripts

cr critical (minimum) flutter value

1,2 faces 1 and 2, respectively, when used with f

x,y properties in x- and y-directions, respectively

Superscript

* complex conjugate

Notation

$$\nabla^2 = \frac{\partial^2}{\partial x^2} + \frac{\partial^2}{\partial y^2}$$

$$\nabla^4 = \frac{\partial^4}{\partial x^4} + 2\,\frac{\partial^4}{\partial x^2\,\partial y^2} + \frac{\partial^4}{\partial y^4}$$

A comma preceding a subscript denotes differentiation with respect to the subscript.

I. INTRODUCTION

One of the basic structural elements used for exterior skin surfaces of flight vehicles is the flat rectangular panel. The flutter, or dynamic instability, of such panels when exposed to a supersonic flow has received considerable attention since the appearance of the pioneering works of Hedgepeth (ref. 1) and Movchan (ref. 2).

A. Elastic and Inertia Considerations

Most papers in the literature have dealt with homogeneous isotropic and orthotropic panels. However, high-efficiency structural configurations for supersonic vehicles may incorporate sandwich type panels having lightweight orthotropic cores such as honeycomb. Such panels often exhibit properties which are not accounted for by classical plate theory. The primary difference between a homogeneous and a sandwich type panel is that the sandwich panel may experience significant transverse shear deformations due to the lightweight (low stiffness) cores that are often used. In homogeneous panels, this shearing deformation is usually negligible.

The first analytic work dealing with the flutter of sandwich panels appeared in 1964 in a report by McElman (ref. 3). This analysis dealt with simply supported flat and cylindrically curved sandwich panels for which a two-term (mode) Galerkin solution was obtained. In the case of homogeneous panels, this type of solution was known to give qualitatively correct trends, but was not adequate (using only two modes) to predict reliable quantitative results (ref. 1). One of the qualitative results of reference 3 was that the transverse shear

flexibility of an isotropic core could significantly reduce the dynamic pressure required for flutter.

In 1965 an exact closed form solution was published by Anderson (ref. 4) for the flutter of a flat rectangular, isotropic sandwich panel having simply supported or clamped leading and trailing edges and simply supported side edges. This investigation confirmed the significance of the isotropic core shear flexibility and showed that the two-mode Galerkin solution of reference 3 became progressively less accurate as the core shear flexibility increased. The theory developed in reference 4 was employed in reference 5 where numerical results for a wide range of panel parameters were presented for the simply supported edge condition.

The numerical results obtained in references 4 and 5 indicated that the panel theory upon which they were based might be inadequate for certain ranges of parameters. These results showed that under certain conditions involving finite core shear stiffness, an increase in shear stiffness or boundary restraint would cause the dynamic pressure required for flutter to be reduced rather than increased. Because of these unexpected results, it was suggested that a more refined theory describing the panel motion might be necessary. For instance, one of the assumptions of the panel theory used in reference 4 is that the faces behave as membranes (i.e., the face sheet bending stiffness is neglected). Consequently, the governing differential equations turn out to be sixth rather than eighth order, with a resulting loss of one boundary condition per panel edge. An additional refinement in the theory, suggested in reference 5, would be to account for the rotary

inertia. The inclusion of *either* the transverse shear flexibility *or* the rotary inertia in the analysis will lower the in-vacuo panel bending frequencies. The simultaneous inclusion of both the shear flexibility and the rotary inertia, while still affecting the bending motion, will also admit two additional motions. These motions, which were described in reference 6 for a homogeneous isotropic plate, are termed the thickness-shear and thickness-twist modes. In general, both of these motions produce transverse deflections (perpendicular to the panel surface) and influence the aerodynamic loading. The question is whether these additional motions can significantly alter the flutter solution.

The first consideration of the effects of the face sheet bending stiffness was presented by Smirnov in references 7 and 8 for a sandwich beam and panel, respectively. Unfortunately, the flutter analysis of the panel was based on an incomplete differential equation and the solutions presented are correct only for special cases.

Flutter boundaries for sandwich panels having orthotropic shear and bending stiffnesses have been presented by Weidman (ref. 9) for a simply supported panel. As in reference 3, this analysis is based on a two-mode Galerkin solution and gives only qualitative trends.

B. Aerodynamic and Damping Considerations

As in references 1, 3, 4, and 5, the flutter analysis presented herein neglects all damping forces and is based on a simple two-dimensional *static*, inviscid approximation for the aerodynamic forces. In this approximation the aerodynamic loading is proportional to the instantaneous slope of the panel taken in the direction of the airflow. The analyses of references 2, 7, and 8 are based on a two-dimensional

quasi-steady aerodynamic approximation. This has the same mathematical form as the static approximation except for an additional term which is proportional to the panel's transverse velocity and represents an aerodynamic damping force. Flutter boundaries based on these static and quasi-steady aerodynamic theories have recently been compared with results obtained from linearized three-dimensional, unsteady, inviscid (exact) aerodynamic theory (refs. 10 and 11).

For unstressed homogeneous panels, all three theories predict nearly the same flutter dynamic pressure for Mach numbers greater than about 1.6 and for length-width ratios from 0 to at least 6. For Mach numbers less than 1.6 and for length-width ratios less than about 2, the "exact" theory predicts significantly lower flutter dynamic pressures than the other two theories. These lower values are due to a so-called single-degree-of-freedom instability and are very sensitive to structural damping. (The other two theories do not predict this type of instability.) For these low Mach numbers all three theories tend to predict flutter boundaries that disagree with experimental results. This disagreement is apparently due, in part, to the stabilizing effect of the turbulent boundary-layer that occurs in this range of Mach numbers and length-width ratios (refs. 12 and 13). For the higher Mach number range (greater than 1.6) where the theoretical results agree, there is also fairly good agreement with experimental results (obtained at Mach numbers from 2 to 5 and length-width ratios from 0 to 10, ref. 10). For panels that are unstressed or are in tension, the results presented in references 10 and 11 also indicate that, for the higher

Mach number range, the flutter boundaries are insensitive to either structural or aerodynamic damping.

For compressively stressed, unbuckled panels, the results of references 10 and 11 indicate that for Mach numbers greater than about 1.6, the quasi-steady and exact theories predict flutter dynamic pressures that compare very satisfactorily. The static aerodynamics also gives essentially the same results except when compressive stresses cause the in-vacuo values of two bending frequencies to become equal. When this occurs, a zero-dynamic-pressure flutter point is predicted by the static aerodynamics. If the stress levels producing these equal frequencies are less than the buckling stress, then the quasi-steady and exact theories predict small but nonzero flutter values of dynamic pressure. (The zero points predicted by the static theory are prevented by the aerodynamic damping.) However, even these nonzero flutter dynamic pressures significantly underestimate experimental results (ref. 11). In fact, when an equal-frequency stress level coincides with the transition-point value of stress (buckling point of the flutter boundary) even the quasi-steady theory predicts zero-dynamic-pressure flutter (ref. 10, figs. 4 and 5).

In reference 10 it is shown that reasonable quantitative agreement between theory and experiment can apparently be obtained near equal-frequency stress-level conditions, by the use of quasi-steady aerodynamics, if a structural damping term (g_B) associated with the panel bending stress is included in the analysis. In this approach the zero-dynamic-pressure values for transition-point flutter do not occur. The reason for this behavior is not completely clear though since the

further addition of a structural damping term (g_M) associated with stresses produced by in-plane loads gives, for $g_B = g_M$, flutter boundaries which again have zero-dynamic-pressure values for transition point flutter.

To recapitulate, except for cases where compressive stresses cause two in-vacuo bending frequencies to have nearly the same value, the simple static aerodynamic approximation gives nearly the same results as the quasi-steady and "exact" aerodynamic theories for Mach numbers greater than about 1.6. It seems likely then that the results presented herein would not be significantly altered, in most cases, by the use of the more refined aerodynamics. For those cases of nearly equal in-vacuo bending frequencies, however, it would be appropriate to supplement the present analysis with a consideration of damping forces.

C. Scope and Purpose of Investigation

In this investigation an analysis is presented for the supersonic flutter behavior of flat rectangular, biaxially stressed sandwich panels. The mathematical model of the panel accounts for the bending stiffnesses of dissimilar face sheets, rotary inertia, and the orthotropic transverse shear stiffnesses (moduli) of cores such as honeycomb. In the absence of damping forces, for simply supported edges parallel to the airflow, and for the static aerodynamic loading approximation, an exact closed form solution to the problem is obtained for panels with either simply supported or clamped leading and trailing edges. The purpose of the investigation is to determine the effects and importance of the face bending stiffness, rotary inertia, and core shear stiffness orthotropy on the panel's flutter behavior.

II. ANALYSIS

In this chapter the problem is defined and solved. The solution is found to take on different forms according to whether the panel has an orthotropic or isotropic core, or whether the length-width ratio is zero (beam behavior).

A. Panel Configuration and Differential Equations

The panel configuration and coordinate system are shown in figure 1. The panel is flat and is of length a and width b. The panel is subjected to uniform, constant magnitude in-plane force resultants N_x and N_y (positive in compression). The in-plane shear force resultant, N_{xy}, is assumed to be zero. At Mach number M, the flow is over one surface of the panel, is parallel to the x-axis, and is supersonic. Simply supported edges are assumed at $y = 0$ and $y = b$.

The core is of uniform thickness and may possess orthotropic, transverse shear stiffnesses (D_{Q_x}, D_{Q_y}). Its planes of orthotropic symmetry are parallel to the coordinate planes. The face sheets are isotropic but need not be identical (modulus, density, and thickness may differ but Poisson's ratio is assumed to be the same for both faces). The geometry of the core and face sheets is illustrated in figure 2. The quantities d_1, d_2, or $\bar{e}$ locate the elastic axis. Stiffness and inertia properties are given in table I of appendix A.

The extensional stiffness of the core is assumed to be much less than that of the face sheets (i.e., the core contribution to the overall panel bending stiffness is neglected). Also, transverse shear strains in the faces and all normal strains in the z-direction are neglected.

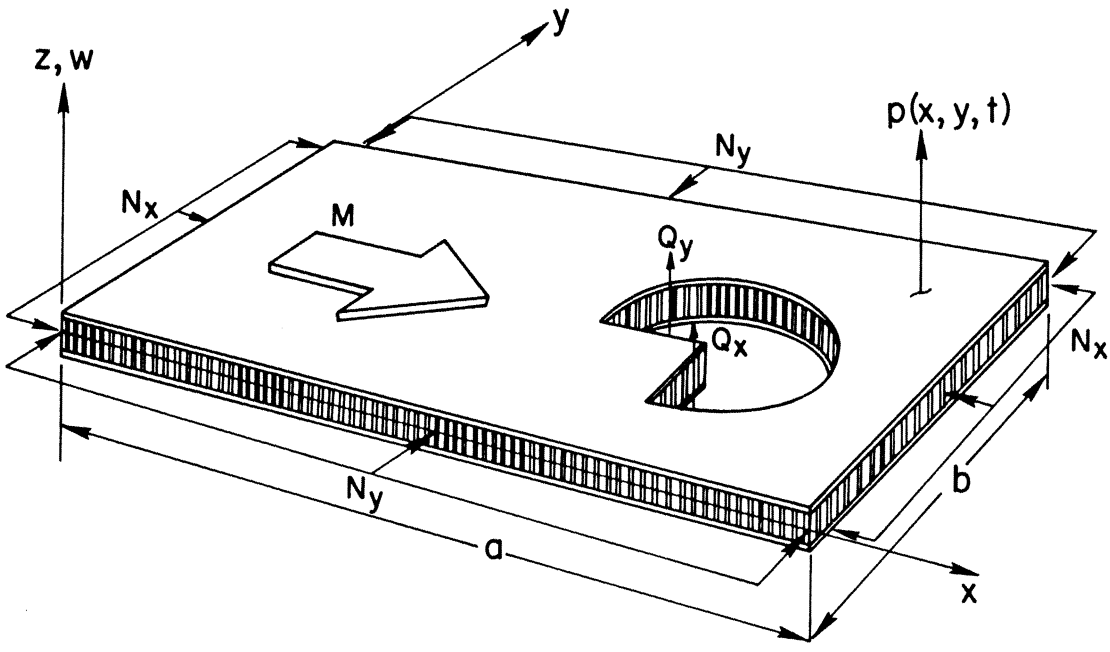

Figure 1.- Panel configuration and coordinate system.

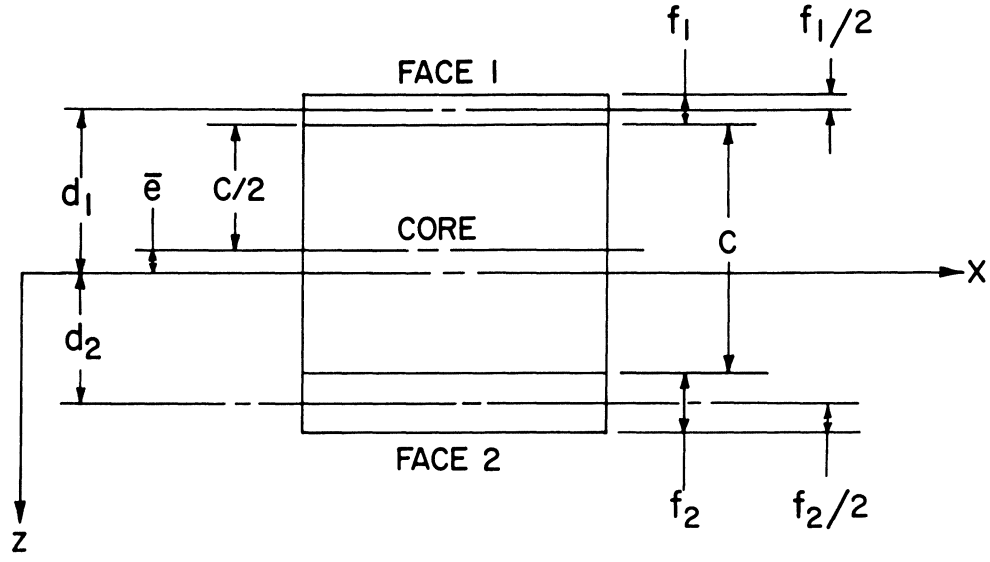

Figure 2.- Geometry of panel faces and core.

The panel face sheets are considered to be thin plates rather than membranes; thus, their bending stiffness contributes to the equilibrium of forces in the z-direction ($\nabla^4 w$ term in eq. (1a)).

For the configuration described, an appropriate set of differential equations of motion can be obtained from either of the sandwich panel theories presented in references 14 and 15. This is done by incorporating the effect of face sheet bending deformations in the sandwich panel theory of reference 14, or by incorporating the effect of orthotropic core shear moduli in the theory of reference 15. With these modifications, and with the addition of rotary inertia terms (see appendix A), both theories yield the following equations of motion.

For equilibrium of forces in z-direction:

$$-(D_{f_1} + D_{f_2})\nabla^4 w - N_x w_{,xx} - N_y w_{,yy} + 2N_{xy} w_{,xy} + Q_{x,x} + Q_{y,y} + p = 0 \tag{1a}$$

For equilibrium of moments about y- and x-axes, respectively:

$$-w_{,xyy} - w_{,xxx} - \frac{Q_x}{D_s} + \frac{1}{D_{Q_x}}\left[Q_{x,xx} + \frac{1-\mu}{2} Q_{x,yy}\right] + \frac{1+\mu}{2}\frac{Q_{y,xy}}{D_{Q_y}} + \frac{I_o}{D_s}\left(w_{,x} - \frac{Q_x}{D_{Q_x}}\right)_{,tt} = 0 \tag{1b}$$

$$-w_{,yxx} - w_{,yyy} - \frac{Q_y}{D_s} + \frac{1}{D_{Q_y}}\left[Q_{y,yy} + \frac{1-\mu}{2} Q_{y,xx}\right] + \frac{1+\mu}{2}\frac{Q_{x,xy}}{D_{Q_x}} + \frac{I_o}{D_s}\left(w_{,y} - \frac{Q_y}{D_{Q_y}}\right)_{,tt} = 0 \tag{1c}$$

For equilibrium of forces in x- and y-directions, respectively:

$$-N_{x,x} + N_{xy,y} = 0 \tag{1d}$$

$$-N_{y,y} + N_{xy,x} = 0 \tag{1e}$$

where

D_{f_1}, D_{f_2} bending stiffnesses of face sheets 1 and 2, respectively

Q_x, Q_y transverse shear forces, per unit width

w transverse deflection

p transverse pressure loading

D_s panel bending stiffness due to the extensional stiffnesses of the face sheets

μ Poisson's ratio of the faces (assumed equal for both faces)

t time

I_o mass density moment of inertia, per unit width, of the face sheets about the elastic axis

In equations (1d) and (1e) the in-plane inertia has been neglected. The last term in each of equations (1b) and (1c) represents the rotary inertia moment about the elastic axis.[1] It is assumed that the z-coordinates of the elastic axes and the centers of mass coincide. This condition is satisfied if the face sheets are of identical material, or if they have equal ratios of Young's modulus to density, E_f/ρ_f. (If this condition is not satisfied, equations (1b) and (1c) couple dynamically with equations (1d) and (1e), respectively (see appendix A).)

[1]A recent flutter paper, in which the rotary inertia moments are incorrectly expressed, is discussed in appendix D.

The assumptions $N_{xy} = 0$, N_x = constant, and N_y = constant satisfy the in-plane equilibrium equations, (1d) and (1e), and eliminate the term $2N_{xy}w_{,xy}$ from the lateral equilibrium equation (1a). The unknowns, to be determined from equations (1a, b, c), are the lateral deflection $w(x, y, t)$ and the two shear angles $Q_x(x,y,t)/D_{Q_x}$, $Q_y(x,y,t)/D_{Q_y}$ (see eq. (A1)). The internal transverse shear force resultants Q_x and Q_y are depicted on the imagined panel cutout of figure 1.

The transverse loading $p(x, y, t)$ is comprised of the inertia force and the pressure due to supersonic flow. The aerodynamic loading is assumed to be given by two-dimensional static aerodynamics so that (ref. 1)

$$p = -\rho_m w_{,tt} - \frac{2q}{\beta} w_{,x} \tag{2}$$

where q is the dynamic pressure, $\beta = \sqrt{M^2 - 1}$, and ρ_m is the panel's mass per unit surface area.

B. Boundary Conditions

Equations (1a, b, and c) constitute a system of eighth order partial differential equations in the spatial coordinates x and y. Corresponding to these equations are four boundary conditions which must be specified at each edge of the panel. Sets of boundary conditions consistent with the assumptions upon which equations (1) are based can be obtained from references 14 and 15. The boundary conditions used herein, in terms of the unknowns w, Q_x/D_{Q_x}, and Q_y/D_{Q_y}, are given below.

Simply Supported Edges at $x = 0$ and a	Clamped Edges at $x = 0$ and a	
$w = 0$	$w = 0$	(3a)
$w_{,xx} - \frac{Q_{x,x}}{D_{Q_x}} + \mu\left(w_{,yy} - \frac{Q_{y,y}}{D_{Q_y}}\right) = 0$	$w_{,x} - \frac{Q_x}{D_{Q_x}} = 0$	(3b)
$w_{,xx} + \mu w_{,yy} = 0$	$w_{,x} = 0$	(3c)
$w_{,y} - \frac{Q_y}{D_{Q_y}} = 0$	$w_{,y} - \frac{Q_y}{D_{Q_y}} = 0$	(3d)

For the simply supported case, equation (3b) specifies that no moment couple is produced by the face sheet axial loads (whose resultant is N_x). Equations (3c) specify that no net moment is acting on the individual face sheets. For the clamped condition, equations (3c) specify a zero edge slope; hence, equations (3b) correspond to a zero shear angle in the x-direction. (Equations (3c) arise because the face sheets are treated as thin plates rather than membranes as was done in refs. 3, 4, 5, and 9.)

Since equations (3a) are true at all points of the boundaries parallel to the y-axis, $w_{,y}$ and $w_{,yy}$ are also zero at $x = 0$ and a. This, together with equations (3c), allows the boundary conditions to be written as follows.

Simply Supported Edges at $x = 0$ and a	Clamped Edges at $x = 0$ and a	
$w = 0$	$w = 0$	(4a)
$\gamma_{x,x} = \left(\frac{Q_x}{D_{Q_x}}\right)_{,x}$	$\gamma_x = \frac{Q_x}{D_{Q_x}} = 0$	(4b)
$w_{,xx} = 0$	$w_{,x} = 0$	(4c)
$\gamma_y = \frac{Q_y}{D_{Q_y}}$	$\gamma_y = \frac{Q_y}{D_{Q_y}} = 0$	(4d)

Note that equations (4d) specify a zero shear angle in the y-direction. (See appendix A for the interpretation of the shear angles.) The boundary conditions at $y = 0$ and b are obtained from equations (4) by interchanging x and y.

Along the edges $x = 0$ and a, the boundary conditions corresponding to equations (1d) and (1e) require that (ref. 15): (1) either N_x is a prescribed value or the translational displacement in the x-direction is zero; (2) either N_{xy} is a prescribed value or the translational displacement in the y-direction is zero. (The boundary conditions at $y = 0$ and b are obtained by interchanging x and y.) As noted earlier, the loads N_x and N_y are assumed to be prescribed and the load N_{xy} is assumed to be zero. If N_x and N_y are prescribed then the in-plane displacements will, in general, be nonzero. Uniform values of N_x and N_y could also be developed by uniform heating of the panel, in which case the in-place displacements could be zero.

C. Solution of Differential Equations for Simply Supported Streamwise Edges

As in references 4 and 5 the solutions to equations (1), which satisfy simple support boundary conditions at $y = 0$ and $y = b$, are sought in the form

$$\left.\begin{aligned} w(x,y,t) &= \sum_j A_j e^{\overline{m}_j(x/a)} \sin\frac{n\pi y}{b} e^{i\omega t} \\ Q_x(x,y,t) &= \sum_j B_j e^{\overline{m}_j(x/a)} \sin\frac{n\pi y}{b} e^{i\omega t} \\ Q_y(x,y,t) &= \sum_j C_j e^{\overline{m}_j(x/a)} \cos\frac{n\pi y}{b} e^{i\omega t} \end{aligned}\right\} \tag{5}$$

The circular frequency is denoted by ω, and n is an integer designating the number of half-sine waves that can form in the y-direction.

The $\overline{m}_j$ are nonrepeated roots of the characteristic equation and are to be determined. As will be seen, the characteristic equation has eight roots, thus giving 24 values for the coefficients A_j, B_j, and C_j ($j = 1$ to 8). However, the coefficients A_j, B_j, and C_j are not all independent quantities since they are related by the three differential equations in w, Q_x, and Q_y. Hence, one coefficient, say B_j, can be expressed in terms of the other two (A_j and C_j) for each value of j. These eight coefficients (B_1 to B_8) are then determined, within an arbitrary constant, by the eight boundary conditions (four at $x = 0$ and four at $x = a$).

Substituting the above expressions for w, Q_x and Q_y into equations (1), and letting

$$z_j = \frac{\overline{m}_j}{\pi} \tag{6}$$

results in the following set of three algebraic equations.

$$\begin{bmatrix} a_{11} & z_j & -n \\ -z_j[\eta^2(n^2-\chi\overline{\omega}^2)-z_j^2] & \eta^2-r_x\left[z_j^2-\left(\frac{1-\mu}{2}\right)n^2\eta^2+\eta^2\chi\overline{\omega}^2\right] & z_j\left(\frac{1+\mu}{2}\right)nr_y \\ -n[\eta^2(n^2-\chi\overline{\omega}^2)-z_j^2] & -z_j\left(\frac{1+\mu}{2}\right)nr_x & 1-r_y\left[\left(\frac{1-\mu}{2}\right)\left(\frac{z_j}{\eta}\right)^2-n^2+\chi\overline{\omega}^2\right] \end{bmatrix} \begin{Bmatrix} A_j \\ \frac{ab^2}{\pi^3 D_s}B_j \\ \frac{a^2b}{\pi^3 D_s}C_j \end{Bmatrix} = \begin{Bmatrix} 0 \\ 0 \\ 0 \end{Bmatrix} \tag{7}$$

where

$$a_{11} = \frac{-\tau}{\eta^2}(n^2\eta^2 - z_j^2)^2 + n^2\eta^2 k_y - k_x z_j^2 + \eta^2\overline{\omega}^2 - \frac{\lambda\eta}{\pi^3} z_j \tag{8}$$

Thus, those values of z_j which satisfy the determinant of the 3 by 3 matrix will determine the nontrivial solutions to the differential equations.

The dimensionless parameters appearing in equations (7) and (8) are defined as

$$\left.\begin{aligned} \eta &= \frac{a}{b} & \tau &= \frac{D_{f_1} + D_{f_2}}{D_s} \\ k_x &= \frac{N_x b^2}{\pi^2 D_s} & k_y &= \frac{N_y b^2}{\pi^2 D_s} \\ r_x &= \frac{\pi^2 D_s}{b^2 D Q_x} & r_y &= \frac{\pi^2 D_s}{b^2 D Q_y} \\ \lambda &= \frac{2qb^3}{\beta D_s} & \omega_o &= \frac{\pi^2}{b^2}\sqrt{\frac{D_s}{\rho_m}} \\ \chi &= \frac{\pi^2}{b^2}\frac{I_o}{\rho_m} & \overline{\omega} &= \frac{\omega}{\omega_o} \end{aligned}\right\} \tag{9}$$

The quantity η is the panel's length-to-width ratio, k_x and k_y are measures of the in-plane loads, r_x and r_y reflect the core shear flexibilities, λ characterizes the dynamic pressure, and χ characterizes the rotary inertia. The ratio designated by τ is a measure of the face sheet contribution to the transverse restoring forces and $\bar{\omega}$ characterizes the panel frequency.

The parameters appearing in equations (9) are all defined in terms of the panel width, b. For length-width ratios $\eta \geq 1$ this is a convenient form, but for $\eta < 1$ it is more convenient to define all parameters in terms of the panel length a. So, for $\eta < 1$ the following primed parameters will be used.

$$
\left.
\begin{aligned}
k_x' &= \frac{N_x a^2}{\pi^2 D_s} = \eta^2 k_x \\
k_y' &= \frac{N_y a^2}{\pi^2 D_s} = \eta^2 k_y \\
r_x' &= \frac{\pi^2 D_s}{a^2 D_{Q_x}} = \frac{r_x}{\eta^2} \\
r_y' &= \frac{\pi^2 D_s}{a^2 D_{Q_y}} = \frac{r_y}{\eta^2} \\
\lambda' &= \frac{2qa^3}{\beta D_s} = \lambda\eta^3 \\
\omega_o' &= \frac{\pi^2}{a^2}\sqrt{\frac{D_s}{\rho_m}} = \frac{\omega_o}{\eta^2} \\
\bar{\omega}' &= \frac{\omega}{\omega_o'} = \eta^2\bar{\omega} \\
\chi' &= \frac{\pi^2}{a^2}\frac{I_o}{\rho_m} = \frac{\chi}{\eta^2} \\
a_{11}' &= -\tau\left[(n\eta)^2 - z_j^2\right]^2 + (n\eta)^2 k_y' - k_x' z_j^2 + \bar{\omega}'^2 - \frac{\lambda'}{\pi^3} z_j = \eta^2 a_{11}
\end{aligned}
\right\} \qquad (10)
$$

It is noted that $\eta^2(n^2 - \chi\bar{\omega}^2) - z_j^2$ appears as a common factor in the coefficients of A_j for both the second and third rows of

equation (7). Also, n appears as a common factor in the coefficients of C_j for both the first and second rows of equation (7). This enables equation (7) to be written as

$$\begin{bmatrix} a'_{11} & z_j & -n\eta \\ -z_j\left(z_j^2-n^2\eta^2+\chi'\bar{\omega}'^2+\frac{1+\mu}{2}r'_y a'_{11}\right) & -x'_j+z_j^2\left(\frac{1+\mu}{2}\right)(r'_x-r'_y) & 0 \\ 0 & -n\eta x'_j & z_j y'_j \end{bmatrix} \begin{Bmatrix} A_j \\ \frac{a^3 B_j}{\pi^3 D_s} \\ \frac{a^3 C_j}{\pi^3 D_s} \end{Bmatrix} = \begin{Bmatrix} 0 \\ 0 \\ 0 \end{Bmatrix} \tag{11}$$

where

$$\left.\begin{aligned} x'_j &= 1+r'_x\left[(n^2\eta^2-z_j^2)\ \frac{1-\mu}{2}-\chi'\bar{\omega}'^2\right] = 1+r_x\left[\left(n^2-\frac{z_j^2}{\eta^2}\right)\frac{1-\mu}{2}-\chi\bar{\omega}^2\right] = x_j \\ y'_j &= 1+r'_y\left[(n^2\eta^2-z_j^2)\ \frac{1-\mu}{2}-\chi'\bar{\omega}'^2\right] = 1+r_y\left[\left(n^2-\frac{z_j^2}{\eta^2}\right)\frac{1-\mu}{2}-\chi\bar{\omega}^2\right] = y_j \end{aligned}\right\} \tag{12}$$

The characteristic equation defining the quantities $\bar{m}_j = \pi z_j$ is obtained by equating the determinant of the square matrix in equation (11) to zero. The form of the characteristic equation varies according to whether the core is orthotropic, isotropic, or whether the length-width ratio is zero.

1. Orthotropic Core ($r_x \neq r_y$) with $\eta > 0$. In this case the characteristic equation is

$$a'_{11}\left[x'_j - z_j^2\left(\frac{1+\mu}{2}\right)(r'_x - r'_y)\right] y'_j - \left[z_j^2-(n\eta)^2+\chi'\bar{\omega}'^2+\left(\frac{1+\mu}{2}\right)r'_y a'_{11}\right]\left[z_j^2 y'_j-(n\eta)^2 x'_j\right] = 0 \tag{13}$$

Since a'_{11} contains z_j^4, and x'_j and y'_j each contain z_j^2, equation (13) is an eighth-order polynomial in z_j. Thus, eight values of $\bar{m}_j$ will appear in equations (5).

2. Isotropic Core ($r_x = r_y$) with $\eta > 0$. For $r'_x = r'_y = r'$, the expressions x'_j and y'_j are equal and equation (13) factors into

$$[a'_{11} - (z_j^2 - n^2\eta^2 + \chi\bar{\omega}'^2)(r'a'_{11} + z_j^2 - n^2\eta^2)]y'_j = 0 \qquad (14a)$$

The six roots of z_j given by the bracketed term depend on λ' (dynamic pressure). However, the two roots (to be designated z_7 and z_8) given by

$$y'_j = 1 - r'\left[(z_j^2 - n^2\eta^2)\left(\frac{1-\mu}{2}\right) + \chi'\bar{\omega}'^2\right] = 0\,, \quad j = 7,\ 8 \qquad (14b)$$

are independent of λ'.

3. Beam Behavior ($\eta = 0$). Equation (13) also factors when $\eta = 0$ (infinitely wide panel of length a). However, it is more instructive to return to equation (11) and set η equal to zero there, giving

$$\left[\begin{array}{c|c|c} a'_{11} & z_j & 0 \\ -z_j(z_j^2+\chi'\bar{\omega}'^2+\frac{1+\mu}{2}r'_y a'_{11}) & -x'_j+z_j^2\frac{1+\mu}{2}(r'_x-r'_y) & 0 \\ \hline 0 & 0 & z_j y'_j \end{array}\right]\left\{\begin{array}{c} A_j \\ \frac{a^3 B_j}{\pi^3 D_s} \\ \frac{a^3 C_j}{\pi^3 D_s} \end{array}\right\} = \left\{\begin{array}{c} 0 \\ 0 \\ 0 \end{array}\right\} \qquad (15)$$

so that

$$\left[1-r'_y\left(z_j^2\,\frac{1-\mu}{2} + \chi'\bar{\omega}'^2\right)\right]\begin{vmatrix} -\tau z_j^4 - k'_x z_j^2 + \bar{\omega}'^2 - \frac{\lambda'}{\pi^3} z_j & z_j \\ -z_j(z_j^2+\chi'\bar{\omega}'^2) & -[1-r'_x(z_j^2+\chi'\bar{\omega}'^2] \end{vmatrix} = 0 \qquad (16)$$

The determinant gives a sixth-order polynomial in z_j from which six roots (j = 1 to 6) can be determined. The bracketed term then gives z_j for j = 7 and 8. From equation (15) it is seen that A_j and B_j

are related but are independent of C_j. The 2 × 2 determinant corresponds to a "beam" solution since the same determinant is obtained by substituting the expressions

$$w(x,t) = \sum_{j=1}^{6} A_j e^{\overline{m}_j (x/a)} e^{i\omega t}$$

$$Q_x(x,t) = \sum_{j=1}^{6} B_j e^{\overline{m}_j (x/a)} e^{i\omega t}$$

into the differential equations for the cylindrical bending of a beam (eqs. (1a) and (1b) with all terms involving derivatives with respect to y set equal to zero).

D. In-vacuo Frequency Equations for All Edges Simply Supported

For no airflow ($\lambda' = 0$) the differential equations and simple support boundary conditions are satisfied by

$$\left.\begin{aligned} w(x,y,t) &= A_{mn} \sin \frac{m\pi x}{a} \sin \frac{n\pi y}{b} e^{i\omega t} \\ Q_x(x,y,t) &= B_{mn} \cos \frac{m\pi x}{a} \sin \frac{n\pi y}{b} e^{i\omega t} \\ Q_y(x,y,t) &= C_{mn} \sin \frac{m\pi x}{a} \cos \frac{n\pi y}{b} e^{i\omega t} \end{aligned}\right\} \qquad (17)$$

where m and n are integers designating the number of half-sine waves that can form in the x- and y-directions, respectively. When equations (17) are substituted into equations (1), with $q = 0$, the characteristic equations (13), (14), and (16) are again obtained except that $\lambda' = 0$ and $z_j^2 = -m^2$. Thus, the characteristic equations become "frequency equations" from which $\overline{\omega}^2$ can be obtained.

1. Orthotropic Core. The "frequency equation" form of equation (13) (orthotropic core) is cubic in $\bar{\omega}^2$. However, for $\chi = 0$ (rotary inertia neglected) simplification occurs and the bending frequency of the m, n mode is given by

$$\bar{\omega}^2 = \left[\left(\frac{m}{\eta}\right)^2 + n^2\right]^2\left(\tau + \frac{1}{1+\zeta}\right) - \left[\left(\frac{m}{\eta}\right)^2 k_x + n^2 k_y\right] \tag{18a}$$

where

$$\zeta = \left[r_x\left(\frac{m}{\eta}\right)^2 + n^2 r_y\right] \frac{\left\{1 + \left(\frac{1-\mu}{2}\right) r_x r_y \frac{[(m/\eta)^2 + n^2]^2}{[r_x(m/\eta)^2 + n^2 r_y]}\right\}}{\left\{1 + \left(\frac{1-\mu}{2}\right)\left[r_y\left(\frac{m}{\eta}\right)^2 + n^2 r_x\right]\right\}} \tag{18b}$$

Equation (18a) includes the effects of length-width ratio, face sheet bending stiffness, orthotropic core shear flexibility, and in-plane stress. For $\tau = 0$ (face bending stiffness neglected) and $r_x = r_y$ (isotropic core) the above result reduces to equation (C4) of reference 5.

2. Isotropic Core. For the isotropic core, equations (14a) and (14b) yield *two* frequency equations (if both the rotary inertia and shear flexibility terms χ and r, respectively, are retained). Replacing z_j^2 with $-m^2$ in equation (14b) yields

$$\bar{\omega}^2 = \frac{1}{\chi}\left[\frac{1}{r} + \left(\frac{1-\mu}{2}\right)\left(\frac{m^2}{\eta^2} + n^2\right)\right] \tag{19}$$

This equation gives the frequencies of the "thickness-twist" modes. These are free modes of vibration which, for a *simply supported* panel with an *isotropic* core, occur without any transverse deflection [w(x,y,t) = 0]. The frequencies (ω, not $\bar{\omega}$) given by equation (19) are

independent of the in-plane loads (k_x and k_y), the face bending stiffness (τ) and the mass per unit surface area (ρ_m). The reason is that the transverse forces arising from the in-plane loads, face bending deformations, and lateral inertia are zero when $w(x,y,t) = 0$ for all x and y (see eq. (1a)).

Except for differences in notation and interpretation of stiffnesses, equation (19) agrees with the second of equations (10) in reference 6. (The stiffnesses must be interpreted differently because reference 6 deals with a homogeneous plate in a manner analogous to the Timoshenko beam theory.) Sketches of thickness-twist mode shapes for $\eta = 1$ and $\eta = 0$ are shown in figures 3(a) and 3(b), respectively. As pointed out in reference 6, the two shear angles Q_x/D_Q and Q_y/D_Q are so related as to cause the panel ($\eta > 0$) to twist about a normal to its surface. The equations for these mode shapes have been derived for $\lambda \geq 0$ (eqs. (61) and (81)) and are found to be independent of the airflow. This is because $w(x,y,t) = 0$; hence, on the basis of the aerodynamic theory employed, no aerodynamic forces are produced. (This is not necessarily so for other boundary conditions or for a panel having an orthotropic core.)

The second in-vacuo frequency equation for the isotropic core is obtained from the bracketed portion of equation (14a) by setting $\lambda' = 0$ and $z_j^2 = -m^2$. This equation is quadratic in $\bar{\omega}^2$ and yields

$$\bar{\omega}^2 = \frac{2[\bar{\beta}^2+(\tau\bar{\beta}^2-\bar{\rho})(1+r\bar{\beta})]}{[1+(r+\chi)\bar{\beta}+r\chi(\tau\bar{\beta}^2-\bar{\rho})] \pm \sqrt{[1+(r-\chi)\bar{\beta}-r\chi(\tau\bar{\beta}^2-\bar{\rho})]^2+4\chi\bar{\beta}}} \tag{20a}$$

where

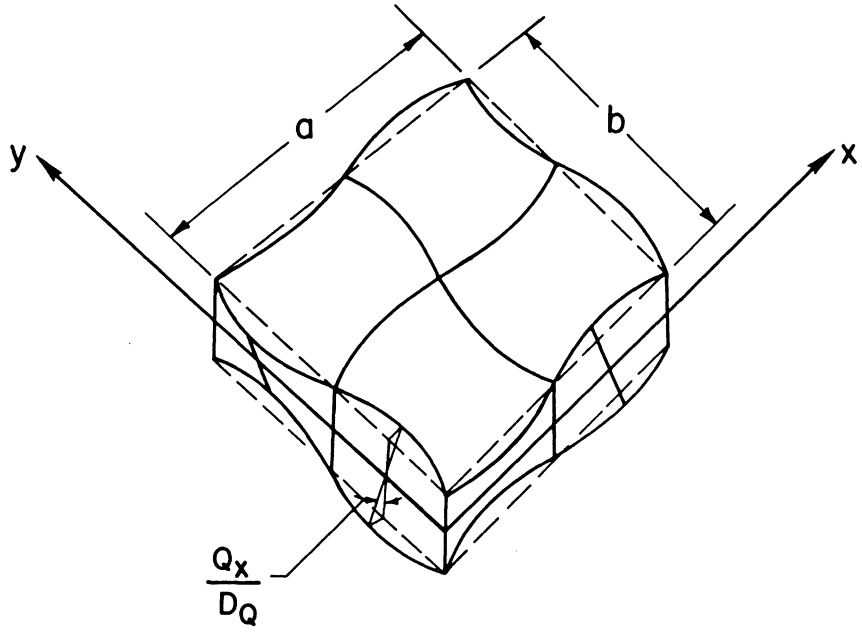

(a) Thickness-twist mode; square panel, isotropic core, m = n = 2.

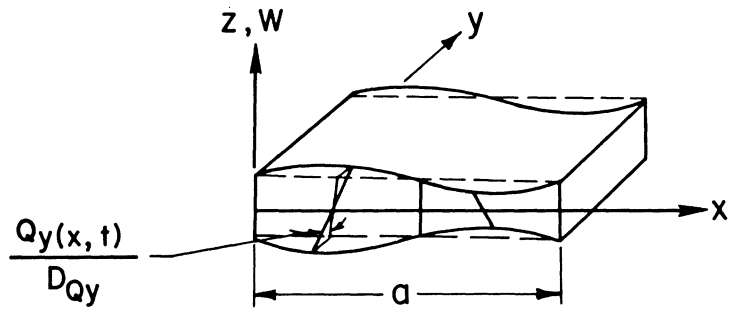

(b) Thickness-twist mode; section of infinitely wide panel, m = 2.

Figure 3.- In-vacuo mode shapes for simply supported edges.

$$\left.\begin{aligned} \overline{\beta} &= \left(\frac{m}{\eta}\right)^2 + n^2 \\ \overline{\rho} &= \left(\frac{m}{\eta}\right)^2 k_x + n^2 k_y \end{aligned}\right\} \tag{20b}$$

It is shown in appendix B that both sets of mode shapes corresponding to these two sets of frequencies involve bending and shearing deformations for which $w(x,y,t) \neq 0$. Thus, both sets of modes induce an aerodynamic loading that may lead to flutter.

For convenience, the frequencies given by the smaller solution for $\overline{\omega}^2$ (i.e., $+\sqrt{\quad}$) are referred to as the "bending" set of frequencies because for $r = X = 0$ (shear flexibility and rotary inertia neglected) they reduce to the frequencies of the pure bending solution given by classical plate theory. The larger solution for $\overline{\omega}^2$ (i.e., $-\sqrt{\quad}$) gives the frequencies of the "thickness-shear" set of modes (described in ref. 6 for $k_x = k_y = 0$).

Additional information on these two sets of modes is given in appendix B where approximate bounds on the ratio of shear angle to total slope ($\gamma_x/w_{,x}$) are derived for a simply supported beam. The results indicate that the shear angle γ_x is larger than the slope $w_{,x}$ for the thickness-shear modes, whereas for the bending modes γ_x is less than $w_{,x}$. The resulting forms for the bending and thickness-shear mode shapes are illustrated in figures 3(c) and 3(d), respectively.

The in-vacuo frequency equations given by (18), (19), and (20) are extremely useful for the rapid estimation of frequency ranges of interest in the numerical computation of frequency loops (variation in

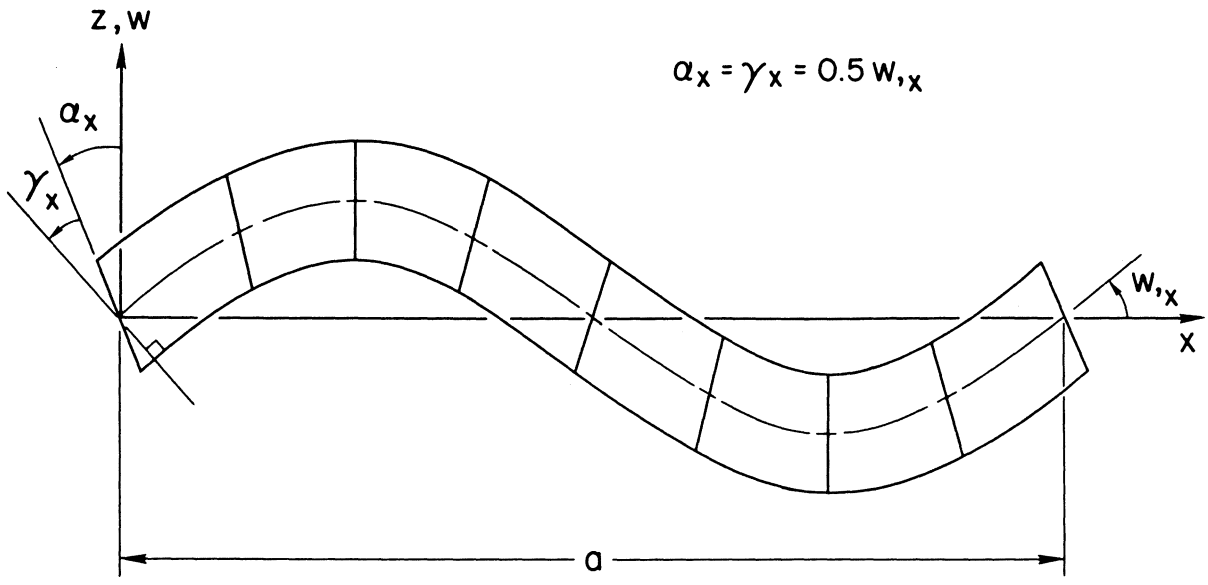

(c) Bending mode of sandwich beam; m = 2.

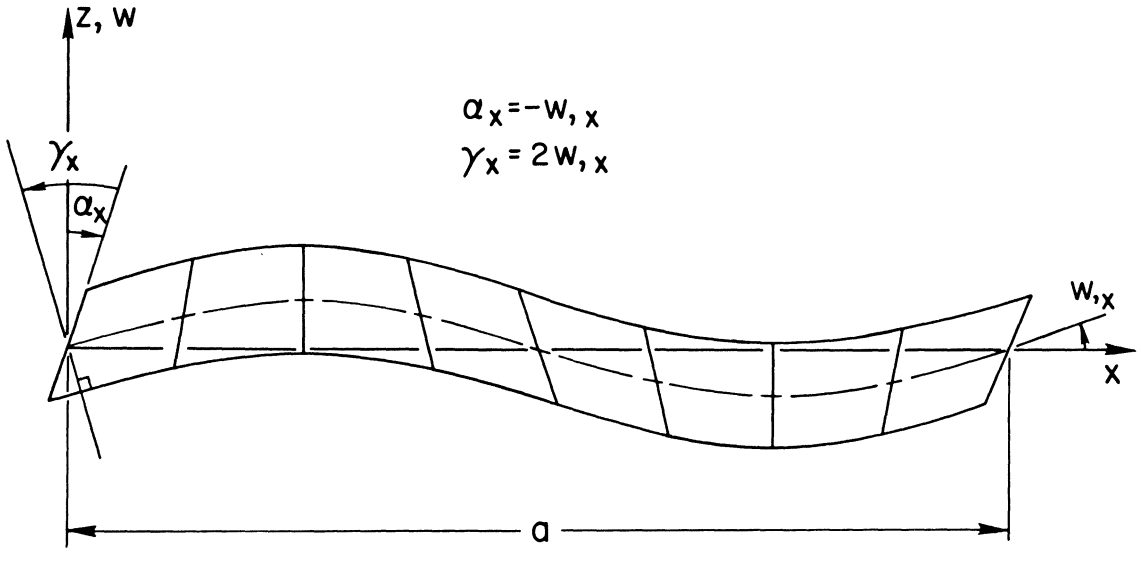

(d) Thickness-shear mode of a sandwich beam; m = 2.

Figure 3.- Concluded.

λ with $\overline{\omega}^2$). These equations can also be used for the in-vacuo beam frequencies by rewriting them in terms of the primed parameters (see eqs. (10)) and letting $\eta = 0$.

Equations (19) and (20) reveal that neither the thickness-twist nor the thickness-shear frequencies are predicted if either of the rotary inertia or shear flexibility terms (χ and r, respectively) is neglected. The existence of the motions associated with these frequencies is due to the combined influence of the shear deformations and the inertia moments caused by rotational acceleration.

E. Expansion of Characteristic Equations in Powers of z_j

In order to determine the roots z_j from the characteristic equations it is necessary to expand these equations in powers of z_j. This is done in the following sections.

1. Orthotropic Core. This case is obtained by expanding equation (13) which results in the following eighth-order polynomial in z_j (j = 1 to 8)

$$c_8 z_j^8 + c_6 z_j^6 + c_5 z_j^5 + c_4 z_j^4 + c_3 z_j^3 + c_2 z_j^2 + c_1 z_j + c_o = 0 \qquad (21)$$

The coefficients c_j are given below in terms of the primed and unprimed parameters for $\eta \geq 1$ and $0 < \eta \leq 1$, respectively.

For $\eta \geq 1$

$$
\left.
\begin{aligned}
c_8 &= \frac{-\tau r_x r_y}{\eta^4}\left(\frac{1-\mu}{2}\right) \\
c_6 &= \frac{1}{\eta^2}\left[\tau s - r_x r_y\left(\frac{1-\mu}{2}\right)(k_x - 2n^2\tau) + r_y\left(\frac{1-\mu}{2}\right)\right] \\
c_5 &= \frac{-r_x r_y}{\eta}\left(\frac{1-\mu}{2}\right)\left(\frac{\lambda}{\pi^3}\right) \\
c_4 &= (k_x - 2n^2\tau)s - \tau(1+gr_x)(1+hr_y) - (1+gr_y) + \left(\frac{1-\mu}{2}\right)(\phi r_x r_y - hr_y - n^2 r_x) \\
c_3 &= \eta s\left(\frac{\lambda}{\pi^3}\right) \\
c_2 &= -\eta^2\left\{\phi s + (k_x - 2n^2\tau)(1+gr_x)(1+hr_y) - \left[n^2(1+gr_x) + h(1+gr_y) + n^2 r_x h\left(\frac{1-\mu}{2}\right)\right]\right\} \\
c_1 &= -\eta^3(1+gr_x)(1+hr_y)\left(\frac{\lambda}{\pi^3}\right) \\
c_0 &= \eta^4(1+gr_x)[\phi(1+hr_y) - n^2 h]
\end{aligned}
\right\} \quad (22a)
$$

For $0 < \eta \leq 1$

$$
\left.
\begin{aligned}
c_8 &= -\tau r_x' r_y'\left(\frac{1-\mu}{2}\right) \\
c_6 &= \tau s' - r_x' r_y'\left(\frac{1-\mu}{2}\right)(k_x' - 2n^2\eta^2\tau) + r_y'\left(\frac{1-\mu}{2}\right) \\
c_5 &= -r_x' r_y'\left(\frac{1-\mu}{2}\right)\left(\frac{\lambda'}{\pi^3}\right) \\
c_4 &= (k_x' - 2n^2\eta^2\tau)s' - \tau(1+g'r_x')(1+h'r_y') - (1+g'r_y') + \left(\frac{1-\mu}{2}\right)(\phi' r_x' r_y' - h' r_y' - n^2\eta^2 r_x') \\
c_3 &= s'\left(\frac{\lambda'}{\pi^3}\right) \\
c_2 &= -\left\{\phi' s' + (k_x' - 2n^2\eta^2\tau)(1+g'r_x')(1+h'r_y') \right. \\
&\quad \left. - \left[n^2\eta^2(1+g'r_x') + h'(1+g'r_y') + n^2\eta^2 r_x' h'\left(\frac{1-\mu}{2}\right)\right]\right\} \\
c_1 &= -(1+g'r_x')(1+h'r_y')\left(\frac{\lambda'}{\pi^3}\right) \\
c_0 &= (1+g'r_x')[\phi'(1+h'r_y') - n^2\eta^2 h']
\end{aligned}
\right\} \quad (22b)
$$

The quantities appearing in the coefficients are given by

$$\left.\begin{aligned} \phi &= \bar{\omega}^2+n^2k_y-n^4\tau & \phi' &= \bar{\omega}'^2+n^2\eta^2k_y'-n^4\eta^4\tau \\ g &= n^2\left(\frac{1-\mu}{2}\right) - \chi\bar{\omega}^2 & g' &= n^2\eta^2\left(\frac{1-\mu}{2}\right) -\chi'\bar{\omega}'^2 \\ h &= n^2 - \chi\bar{\omega}^2 & h' &= n^2\eta^2-\chi'\bar{\omega}'^2 \\ s &= (1+gr_y)r_x+(1+hr_x)r_y\left(\frac{1-\mu}{2}\right) & s' &= (1+g'r_y')r_x'+(1+h'r_x')r_y'\left(\frac{1-\mu}{2}\right) \end{aligned}\right\} \quad (22c)$$

and the remaining parameters are defined by equations (9) and (10).

2. Isotropic Core. For this case, six of the eight roots are obtained from the bracketed portion of equation (14a) and must satisfy (j = 1 to 6)

$$c_6z_j^6 + c_4z_j^4 + c_3z_j^3 + c_2z_j^2 + c_1z_j + c_o = 0 \quad (23)$$

For $\eta \geq 1$

$$\left.\begin{aligned} c_6 &= \frac{-r\tau}{\eta^2} \\ c_4 &= 1 - rk_x + \tau(1 + 3n^2r - r\chi\bar{\omega}^2) \\ c_3 &= -\eta r\left(\frac{\lambda}{\pi^3}\right) \\ c_2 &= \eta^2\{k_x-2n^2(1+\tau)+r[n^2(k_x+k_y)+\bar{\omega}^2-3n^4\tau]+\chi\bar{\omega}^2(1-rk_x+2n^2r\tau)\} \\ c_1 &= \eta^3(1 + n^2r - r\chi\bar{\omega}^2)\left(\frac{\lambda}{\pi^3}\right) \\ c_0 &= -\eta^4\{(\bar{\omega}^2 + n^2k_y - n^4\tau)(1 + n^2r - r\chi\bar{\omega}^2) - n^2(n^2 - \chi\bar{\omega}^2)\} \end{aligned}\right\} \quad (24a)$$

For $0 < \eta \leq 1$

$$\left.\begin{aligned}
c_6 &= -r'\tau \\
c_4 &= 1 - r'k_x' + \tau(1 + 3n^2\eta^2 r' - r'\chi'\bar{\omega}'^2) \\
c_3 &= -r'\left(\frac{\lambda'}{\pi^3}\right) \\
c_2 &= k_x' - 2n^2\eta^2(1+\tau) + r'[n^2\eta^2(k_x'+k_y') + \bar{\omega}'^2 - 3n^4\eta^4\tau] + \chi'\bar{\omega}'^2(1 - r'k_x' + 2n^2\eta^2 r'\tau) \\
c_1 &= (1 + n^2\eta^2 r' - r'\chi'\bar{\omega}'^2)\left(\frac{\lambda'}{\pi^3}\right) \\
c_0 &= -\{(\bar{\omega}'^2 + n^2\eta^2 k_y' - n^4\eta^4\tau)(1 + n^2\eta^2 r' - r'\chi'\bar{\omega}'^2) - n^2\eta^2(n^2\eta^2 - \chi'\bar{\omega}'^2)\}
\end{aligned}\right\} \tag{24b}$$

The other two roots are given by the term y_j' of equation (14b) and are

$$z_{\substack{7\\8}} = \pm\sqrt{n^2\eta^2 + \frac{(1 - r\chi\bar{\omega}^2)}{\left(\frac{1-\mu}{2}\right)\left(\frac{r}{\eta^2}\right)}} = \pm\sqrt{n^2\eta^2 + \frac{(1 - r'\chi'\bar{\omega}'^2)}{\left(\frac{1-\mu}{2}\right) r'}} \tag{25}$$

3. Beam. This is a special case of either the orthotropic or isotropic panel solutions and is most directly obtained from equation (16). Six of the eight roots are determined from (j = 1 to 6)

$$c_6 z_j^6 + c_4 z_j^4 + c_3 z_j^3 + c_2 z_j^2 + c_1 z_j + c_o = 0 \tag{26}$$

where

$$\left.\begin{aligned}
c_6 &= -r_x'\tau & c_2 &= k_x' + r_x'\bar{\omega}'^2 + \chi'\bar{\omega}'^2(1 - r_x'k_x') \\
c_4 &= 1 - r_x'k_x' + \tau(1 - r_x'\chi'\bar{\omega}'^2) & c_1 &= (1 - r_x'\chi'\bar{\omega}'^2)\left(\frac{\lambda'}{\pi^3}\right) \\
c_3 &= -r_x'\left(\frac{\lambda'}{\pi^3}\right) & c_0 &= -\bar{\omega}'^2(1 - r_x'\chi'\bar{\omega}'^2)
\end{aligned}\right\} \tag{27}$$

The roots z_7 and z_8 are given by

$$z_{\substack{7\\8}} = \pm \sqrt{\frac{1 - r_y' \chi' \overline{\omega}'^2}{\left(\frac{1-\mu}{2}\right) r_y'}} \tag{28}$$

F. Relationships Between A_j, B_j, and C_j

The coefficients A_j, B_j, and C_j appearing in equations (5) are not independent quantities. The relationships between them are determined by equation (7). As shown below, these relationships differ according to whether the panel has an orthotropic or isotropic core, or whether the length-width ratio (η) is zero.

1. Panel. From the third of equation (11), which is just another form of equation (7), the quantities B_j and C_j are related as

$$z_j y_j' C_j - n\eta x_j' B_j = 0 \tag{29}$$

where x_j' and y_j' are defined by equations (12). For an *isotropic* core, $x_j' = y_j'$ so that equation (29) becomes

$$[z_j C_j - n\eta B_j] y_j' \Big|_{r_x'=r_y'=r'} = 0 \tag{30}$$

From equation (14b) it is seen that $y_j'|_{r_x'=r_y'=r'} = 0$ only for $j = 7$ or 8 so that the bracketed term of equation (30) must be zero for values of j from 1 through 6. Thus, for the *isotropic* core,

$$C_j = \frac{n\eta}{z_j} B_j \qquad j = 1 \rightarrow 6 \tag{31}$$

where the z_j are the six roots of equation (23). For the *orthotropic* core, equation (29) gives

$$C_j = \frac{n\eta}{z_j} \frac{x'_j}{y'_j} B_j \qquad j = 1 \to 8 \tag{32}$$

where the z_j are the eight roots of equation (21).

In terms of the primed parameters, the third of equation (7) is

$$-n\eta(-n^2\eta^2 + \chi'\bar{\omega}'^2 + z_j^2)A_j + z_j n\eta\left(\frac{1+\mu}{2}\right) r'_x \left(\frac{a^3}{\pi^3 D_s}\right) B_j$$

$$-\left[1 - r'_y\left(z_j^2 \frac{1-\mu}{2} + \chi'\bar{\omega}'^2 - n^2\eta^2\right)\right]\left(\frac{a^3}{\pi^3 D_s}\right) C_j = 0 \tag{33}$$

Then, using equations (31) and (32), the relation between A_j and B_j is found to be, for the *isotropic* core

$$A_j = \left[r' + \frac{1}{(n^2\eta^2 - z_j^2 - \chi'\bar{\omega}'^2)}\right]\left(\frac{B_j}{z_j}\right)\left(\frac{a^3}{\pi^3 D_s}\right) \qquad j = 1 \to 6 \tag{34}$$

and for the *orthotropic* core

$$A_j = \frac{\left[1 + r'_y\left(n^2\eta^2 - z_j^2 \frac{1-\mu}{2} - \chi'\bar{\omega}'^2\right)\right]\frac{x'_j}{y'_j} - z_j^2\left(\frac{1+\mu}{2}\right) r'_x}{(n^2\eta^2 - \chi'\bar{\omega}'^2 - z_j^2)} \left(\frac{B_j}{z_j}\right)\left(\frac{a^3}{\pi^3 D_s}\right) \qquad j = 1 \to 8 \tag{35}$$

To determine A_j and C_j in terms of B_j when $j = 7$ or 8 (for the *isotropic* core), the second of equation (11) is used

$$-z_j^2\left(z_j^2 - n^2\eta^2 + \chi'\bar{\omega}'^2 + \frac{1+\mu}{2} r'_y a'_{11}\right)A_j + \left[-x'_j + z_j^2\left(\frac{1+\mu}{2}\right)(r'_x - r'_y)\right]\left(\frac{a^3}{\pi^3 D_s}\right) B_j = 0 \tag{36}$$

But for an isotropic core, $r'_x = r'_y = r'$, and $x'_j = y'_j = 0$ for $j = 7$ or 8. Since the coefficient of A_j is not zero in general, it follows that

$$A_j = 0 \qquad j = 7, 8 \tag{37}$$

for the *isotropic* core. The first of equation (11) then gives

$$C_j = \frac{z_j}{n\eta} B_j \qquad j = 7, 8 \tag{38}$$

for the *isotropic* core. Except for the term $\chi'\bar{\omega}'^2$ in A_j, the above relations between A_j, B_j, and C_j, for the isotropic core, are the same as in references 4 and 5.

2. Beam. If equation (7) is rewritten in terms of the primed parameters (so that the column matrix does not contain the width $b = \infty$), the result for $\eta = 0$ is

$$\left[\begin{array}{cc:c} a'_{11}\big|_{\eta=0} & z_j & 0 \\ -z_j(z_j^2+\chi'\bar{\omega}'^2) & -[1-r'_x(z_j^2+\chi'\bar{\omega}'^2)] & 0 \\ \hdashline 0 & 0 & y'_j\big|_{\eta=0} \end{array}\right] \left\{\begin{array}{c} A_j \\ \dfrac{a^3B_j}{\pi^3D_s} \\ \dfrac{a^3C_j}{\pi^3D_s} \end{array}\right\} = \left\{\begin{array}{c} 0 \\ 0 \\ 0 \end{array}\right\} \tag{39}$$

The third of equation (39) gives

$$\frac{a^3C_j}{\pi^3D_s}\, y'_j\big|_{\eta=0} = 0$$

But, from equation (16),

$$y'_j\big|_{\eta=0} = 1 - r'_y\left[z_j^2\left(\frac{1-\mu}{2}\right) + \chi'\bar{\omega}'^2\right] = 0$$

only for $j = 7$ or 8. Therefore,

$$C_j = 0 \qquad j = 1 \to 6 \tag{40}$$

Thus, the only nonzero C_j are C_7 and C_8, and, as seen from equation (39), they are independent of A_j and B_j.

It is only for values of j from 1 through 6 that the determinant of coefficients of A_j and B_j is equal to zero (giving eq. (26)).

Thus, A_j and B_j must be zero for $j = 7$ or 8.

$$A_j = B_j = 0 \qquad j = 7, 8 \tag{41}$$

For $j = 1\text{-}6$, the second of equation (39) gives

$$A_j = \left(r_x' - \frac{1}{z_j^2 + \chi'\overline{\omega}'^2}\right)\left(\frac{B_j}{z_j}\right)\left(\frac{a^3}{\pi^3 D_s}\right) \qquad j = 1 \to 6 \tag{42}$$

G. Satisfaction of Leading- and Trailing-Edge Boundary Conditions, and Corresponding Frequency Determinants

Since the relationships between the coefficients A_j, B_j, and C_j have been determined, w, Q_x and Q_y can be expressed in terms of one set of coefficients. The boundary conditions can then be applied to obtain the frequency equations for the case of the orthotropic core, isotropic core, or beam.

1. Orthotropic Core. When equations (32) and (35) are used, equations (5) become, for $n \geq 1$ and omitting $\begin{matrix}\sin\\ \cos\end{matrix}\left\{\frac{n\pi y}{b}\right\} e^{i\omega t}$

$$\left.\begin{aligned} w(x) &= \frac{\eta b^3}{\pi^3 D_s} \sum_{j=1}^{8} \frac{a_j}{b_j} \frac{e^{\overline{m}_j (x/a)}}{z_j} B_j \\ Q_x(x) &= \sum_{j=1}^{8} e^{\overline{m}_j (x/a)} B_j \\ Q_y(x) &= n\eta \sum_{j=1}^{8} \frac{x_j}{y_j} \frac{e^{\overline{m}_j (x/a)}}{z_j} B_j \end{aligned}\right\} \tag{43}$$

where x_j, x_j', y_j, y_j' are given by equations (12) and a_j, a_j', b_j, b_j' are defined as

$$\left.\begin{aligned} a_j &= \left\{1 + r_y\left[n^2 - \left(\frac{z_j}{\eta}\right)^2\left(\frac{1-\mu}{2}\right) - \chi\bar{\omega}^2\right]\right\}\left(\frac{x_j}{y_j}\right) - \left(\frac{z_j}{\eta}\right)^2\left(\frac{1+\mu}{2}\right) r_x \\ a_j' &= \left\{1 + r_y'\left[(n\eta)^2 - z_j^2\left(\frac{1-\mu}{2}\right) - \chi'\bar{\omega}'^2\right]\right\}\left(\frac{x_j'}{y_j'}\right) - z_j^2\left(\frac{1+\mu}{2}\right) r_x' \end{aligned}\right\} \tag{44a}$$

$$\left.\begin{aligned} b_j &= n^2 - \chi\bar{\omega}^2 - \left(\frac{z_j}{\eta}\right)^2 \\ b_j' &= (n\eta)^2 - \chi'\bar{\omega}'^2 - z_j^2 \end{aligned}\right\} \tag{44b}$$

(The primed quantities are to be used for $\eta \leq 1$.)

Application of the eight boundary conditions (eqs. (4)) to equations (43) gives the following set of eight homogeneous equations

$$\sum_{j=1}^{8} c_{ij} B_j = 0 \qquad i = 1, 2, \ldots, 8 \tag{45}$$

where for $\eta \geq 1$ the coefficients c_{ij} are:

	Clamped Edges at x = 0 and x = a	Simply Supported Edges at x = 0 and x = a
$c_{1j} =$	$\frac{a_j}{b_j}\frac{1}{z_j}$	$\frac{a_j}{b_j}\frac{1}{z_j}$
$c_{2j} =$	$\frac{a_j}{b_j}\frac{e^{\bar{m}_j}}{z_j}$	$\frac{a_j}{b_j}\frac{e^{\bar{m}_j}}{z_j}$
$c_{3j} =$	1	z_j
$c_{4j} =$	$e^{\bar{m}_j}$	$z_j e^{\bar{m}_j}$
$c_{5j} =$	$\frac{a_j}{b_j}$	$\frac{a_j}{b_j} z_j$
$c_{6j} =$	$\frac{a_j}{b_j} e^{\bar{m}_j}$	$\frac{a_j}{b_j} z_j e^{\bar{m}_j}$
$c_{7j} =$	$\frac{x_j}{y_j}\frac{1}{z_j}$	$\frac{x_j}{y_j}\frac{1}{z_j}$
$c_{8j} =$	$\frac{x_j}{y_j}\frac{e^{\bar{m}_j}}{z_j}$	$\frac{x_j}{y_j}\frac{e^{\bar{m}_j}}{z_j}$

(46)

If $0 < \eta < 1$, a_j, b_j, x_j, and y_j are replaced with a_j', b_j', x_j', and y_j', respectively. If the determinant of the coefficients of B_j is set equal to zero, the frequency equation for the panel with an orthotropic core is obtained.

$$\left|c_{ij}\right|^{8\times 8} = 0 \tag{47}$$

2. *Isotropic Core.* When equations (31), (34), and (38) are used, equations (5) become, omitting the terms $\begin{matrix}\sin \\ \cos\end{matrix}\left\{\frac{n\pi y}{b}\right\} e^{i\omega t}$

$$\left.\begin{aligned} w(x) &= \frac{\eta b^3}{\pi^3 D_s}\sum_{j=1}^{6}\left(r + \frac{1}{b_j}\right)\frac{e^{\bar{m}_j(x/a)}}{z_j}B_j \\ Q_x(x) &= \sum_{j=1}^{8} e^{\bar{m}_j(x/a)}B_j \\ Q_y(x) &= n\eta\sum_{j=1}^{6}\frac{e^{\bar{m}_j(x/a)}}{z_j}B_j + \frac{1}{n\eta}\sum_{j=7}^{8} z_j e^{\bar{m}_j(x/a)}B_j \end{aligned}\right\} \tag{48}$$

Application of the eight boundary conditions (eqs. (4)) to equations (48) gives the following set of eight homogeneous equations

$$\sum_{j=1}^{8}\bar{c}_{ij}B_j = 0 \qquad i = 1, 2, \ldots, 8 \tag{49}$$

where the $\bar{c}_{ij}$ are not the same as the c_{ij} used in equation (45). For $\eta \geq 1$, the coefficients $\bar{c}_{ij}$ are:

	Clamped Edges at x = 0 and a		Simply Supported Edges at x = 0 and a	
	$j = 1 \to 6$	$j = 7, 8$	$j = 1 \to 6$	$j = 7, 8$
$\bar{c}_{1j} =$	$\left(r + \frac{1}{b_j}\right)\frac{1}{z_j}$	0	$\left(r + \frac{1}{b_j}\right)\frac{1}{z_j}$	0
$\bar{c}_{2j} =$	$\left(r + \frac{1}{b_j}\right)\frac{e^{\bar{m}_j}}{z_j}$	0	$\left(r + \frac{1}{b_j}\right)\frac{e^{\bar{m}_j}}{z_j}$	0
$\bar{c}_{3j} =$	1	1	z_j	z_j
$\bar{c}_{4j} =$	$e^{\bar{m}_j}$	$e^{\bar{m}_j}$	$z_j e^{\bar{m}_j}$	$z_j e^{\bar{m}_j}$
$\bar{c}_{5j} =$	$\left(r + \frac{1}{b_j}\right)$	0	$\left(r + \frac{1}{b_j}\right) z_j$	0
$\bar{c}_{6j} =$	$\left(r + \frac{1}{b_j}\right) e^{\bar{m}_j}$	0	$\left(r + \frac{1}{b_j}\right) z_j e^{\bar{m}_j}$	0
$\bar{c}_{7j} =$	$\frac{n\eta}{z_j}$	$\frac{z_j}{n\eta}$	$\frac{n\eta}{z_j}$	$\frac{z_j}{n\eta}$
$\bar{c}_{8j} =$	$n\eta \frac{e^{\bar{m}_j}}{z_j}$	$\frac{z_j e^{\bar{m}_j}}{n\eta}$	$n\eta \frac{e^{\bar{m}_j}}{z_j}$	$\frac{z_j e^{\bar{m}_j}}{n\eta}$

(50)

If $0 < \eta < 1$, r and b_j are replaced with r' and b_j', respectively. If the determinant of the coefficients of B_j is set equal to zero, the frequency equation for the panel with an isotropic core is obtained.

$$\left|\bar{c}_{ij}\right|_{8\times 8} = 0 \tag{51}$$

3. Beam. In this case, w, Q_x, and Q_y are independent of the y-coordinate, and equations (5) are replaced with

$$\left.\begin{aligned} w(x,t) &= \sum_j A_j e^{\overline{m}_j(x/a)} e^{i\omega t} \\ Q_x(x,t) &= \sum_j B_j e^{\overline{m}_j(x/a)} e^{i\omega t} \\ Q_y(x,t) &= \sum_j C_j e^{\overline{m}_j(x/a)} e^{i\omega t} \end{aligned}\right\} \tag{52}$$

It is recalled from the discussion of equation (16) that the above expressions for w and Q_x correspond to the "beam" solution and lead to a sixth-order polynomial in $z_j = m_j/\pi$ (given by eq. (26)). For $w = Q_x = 0$ the above expression for Q_y, when substituted into equations (1), yields the bracketed term of equation (16). The two roots of this term were called z_7 and z_8 (eq. (28)) and, as will be seen, correspond to the thickness-twist solution for an infinitely wide panel.

When equations (40), (41), and (42) are used, the above expressions become (omitting $e^{i\omega t}$)

$$\left.\begin{aligned} w(x) &= \frac{a^3}{\pi^3 D_s} \sum_{j=1}^{6} \left(r_x' + \frac{1}{b_j'}\right) \frac{e^{\overline{m}_j(x/a)}}{z_j} B_j \\ Q_x(x) &= \sum_{j=1}^{6} e^{\overline{m}_j(x/a)} B_j \\ Q_y(x) &= \sum_{j=7}^{8} e^{\overline{m}_j(x/a)} C_j \end{aligned}\right\} \tag{53}$$

where

$$b_j' = -(z_j^2 + \chi'\overline{\omega}'^2)$$

Application of the boundary conditions (eqs. (4)) gives two sets of homogeneous equations

$$\sum_{j=1}^{6} \tilde{c}_{ij} B_j = 0 \qquad i = 1, 2, \ldots, 6 \tag{54a}$$

$$\sum_{j=7}^{8} \hat{c}_{ij} C_j = 0 \qquad i = 7, 8 \tag{54b}$$

Of the eight roots for z_j (given by eqs. (26) and (28)) the coefficients $\tilde{c}_{ij}$ depend only on z_1 through z_6. These coefficients are given by:

	Clamped Edges at x = 0 and a	Simply Supported Edges at x = 0 and a
$\tilde{c}_{1j} =$	$\left(r_x' + \frac{1}{b_j'}\right)\frac{1}{z_j}$	$\left(r_x' + \frac{1}{b_j'}\right)\frac{1}{z_j}$
$\tilde{c}_{2j} =$	$\left(r_x' + \frac{1}{b_j'}\right)\frac{e^{\overline{m}_j}}{z_j}$	$\left(r_x' + \frac{1}{b_j'}\right)\frac{e^{\overline{m}_j}}{z_j}$
$\tilde{c}_{3j} =$	1	z_j
$\tilde{c}_{4j} =$	$e^{\overline{m}_j}$	$z_j e^{\overline{m}_j}$
$\tilde{c}_{5j} =$	$\left(r_x' + \frac{1}{b_j'}\right)$	$\left(r_x' + \frac{1}{b_j'}\right) z_j$
$\tilde{c}_{6j} =$	$\left(r_x' + \frac{1}{b_j'}\right) e^{\overline{m}_j}$	$\left(r_x' + \frac{1}{b_j'}\right) z_j e^{\overline{m}_j}$

(55)

The coefficients $\hat{c}_{ij}$ are the same for both sets of boundary conditions and are:

$$\left.\begin{aligned} \hat{c}_{77} &= \hat{c}_{78} = 1 \\ \hat{c}_{87} &= e^{\overline{m}_7}, \qquad \hat{c}_{88} = e^{\overline{m}_8} \end{aligned}\right\} \tag{56}$$

These coefficients depend only on z_7 and z_8.

The frequency equation obtained by setting the determinant of the coefficients of C_j equal to zero is simply

$$|\hat{c}_{ij}| = \begin{vmatrix} 1 & 1 \\ e^{\overline{m}_7} & e^{\overline{m}_8} \end{vmatrix} = e^{\overline{m}_8} - e^{\overline{m}_7} = 0 \tag{57}$$

From equation (28), $\overline{m}_7$ and $\overline{m}_8$ are given by

$$\frac{\overline{m}_j}{\pi} = z_j = \pm\sqrt{\frac{1 - r_y'\chi'\overline{\omega}'^2}{\left(\frac{1-\mu}{2}\right) r_y'}} \qquad j = 7, 8 \tag{58}$$

For nonrepeated roots[2] equation (57) can be satisfied only if $1 - r_y'\chi'\overline{\omega}'^2 < 0$, so that

$$z_j = \frac{\overline{m}_j}{\pi} = \pm i\delta, \qquad \delta = +\sqrt{\frac{r_y'\chi'\overline{\omega}'^2 - 1}{\left(\frac{1-\mu}{2}\right) r_y'}} > 0 \qquad j = 7, 8$$

Then equation (57) becomes

$$e^{-i\pi\delta} - e^{i\pi\delta} = -2i \sin \pi\delta = 0$$

---

[2]For repeated roots ($z_7 = z_8 = 0$) the functional form of the solution changes to $Q_y(x) = [C_7 + C_8(x/a)]e^{0(x/a)}$. Application of $Q_y(0) = Q_y(a) = 0$ gives $\begin{vmatrix} 1 & 0 \\ 1 & 1 \end{vmatrix} \neq 0$, proving that $z_7 = z_8 = 0$ is not a solution.

so that

$$\overline{m}_j = \pm i\pi\delta = \pm im\pi \qquad \begin{matrix} m = 1, 2, \ldots \\ j = 7, 8 \end{matrix} \tag{59}$$

By squaring both sides of equation (58), the use of equation (59) yields

$$\overline{\omega}'^2 = \frac{1}{\chi'}\left(\frac{1}{r'} + \frac{1 - \mu}{2} m^2\right) \qquad m = 1, 2, \ldots \tag{60}$$

which is a special case ($\eta = 0$) of the thickness-twist frequency equation. (See eq. (19).) Note that these frequencies are independent of the airflow. The mode shape corresponding to equation (60) is

$$\left.\begin{aligned} w(x) &= Q_x(x) = 0 \\ \frac{Q_y(x)}{D_{Q_y}} &= \left(\frac{2iC_7}{D_{Q_y}}\right) \sin\left[m\pi\left(\frac{x}{a}\right)\right] \end{aligned}\right\} \tag{61}$$

and is sketched in figure 3(b) for $m = 2$.

The frequency equation for the bending and thickness-shear modes of the beam is obtained from equation (54a) and is

$$\left|\tilde{c}_{ij}\right|^{6\times6} = 0 \tag{62}$$

The airflow does affect these frequencies since the z_j, $j = 1 \rightarrow 6$, do depend on λ'.

H. Uncoupled Solution for Simply Supported, Isotropic Panel

The frequency determinants obtained for the panels ($\eta > 0$) determine the frequencies of the bending, thickness-shear, and thickness-twist modes. For the simply supported isotropic panel, the information

describing the thickness-twist motion uncouples from that describing the bending and thickness-shear motions. These uncoupled results are presented in the following sections.

1. Frequency Determinant. The frequency determinant for the isotropic panel is given by equation (51). For the simply supported edge condition this determinant can be simplified, by manipulating its rows and columns, to yield

$$(1-r\chi\bar{\omega}^2)^2 \begin{vmatrix} 1 & 1 & 1 & 1 & 1 & 1 & 0 & 0 \\ e^{\bar{m}_1} & e^{\bar{m}_2} & e^{\bar{m}_3} & e^{\bar{m}_4} & e^{\bar{m}_5} & e^{\bar{m}_6} & 0 & 0 \\ z_1^2 & z_2^2 & z_3^2 & z_4^2 & z_5^2 & z_6^2 & 0 & 0 \\ z_1^2 e^{\bar{m}_1} & z_2^2 e^{\bar{m}_2} & z_3^2 e^{\bar{m}_3} & z_4^2 e^{\bar{m}_4} & z_5^2 e^{\bar{m}_5} & z_6^2 e^{\bar{m}_6} & 0 & 0 \\ z_1^4 & z_2^4 & z_3^4 & z_4^4 & z_5^4 & z_6^4 & 0 & 0 \\ z_1^4 e^{\bar{m}_1} & z_2^4 e^{\bar{m}_2} & z_3^4 e^{\bar{m}_3} & z_4^4 e^{\bar{m}_4} & z_5^4 e^{\bar{m}_5} & z_6^4 e^{\bar{m}_6} & 0 & 0 \\ \hline 0 & 0 & 0 & 0 & 0 & 0 & 1 & 1 \\ 0 & 0 & 0 & 0 & 0 & 0 & e^{\bar{m}_7} & e^{\bar{m}_8} \end{vmatrix} = 0 \qquad (63)$$

or

$$(1 - r\chi\bar{\omega}^2)^2 \times |6 \times 6| \times (e^{\bar{m}_8} - e^{\bar{m}_7}) = 0 \qquad (64)$$

where $|6 \times 6|$ is the 6×6 subdeterminant of equation (63). Note that it does not depend on the roots $z_7(\bar{m}_7)$ and $z_8(\bar{m}_8)$.

From the first term of equation (63) it appears that the boundary conditions are satisfied for any values of the roots z_j when the frequency is such that $1 - r\chi\bar{\omega}^2 = 1 - r'\chi'\bar{\omega}'^2 = 0$. However, when $1 - r\chi\bar{\omega}^2 = 0$ the characteristic equation (eq. (14a)), from which the roots z_j are determined, becomes

$$r'\left(\frac{1-\mu}{2}\right)\left[a'_{11}r' + \left(z_j^2 - n^2\eta^2 + \frac{1}{r'}\right)\right](z_j^2 - n^2\eta^2)^2 = 0$$

which is seen to have two pairs of *repeated* roots ($z_5 = z_7 = n\eta$, $z_6 = z_8 = -n\eta$). The form of the solutions for w, Q_x and Q_y given by equations (5) is valid only for *distinct* roots of the characteristic equation. Thus, equation (64) is not valid at the frequency $\overline{\omega}^2 = 1/(r\chi)$. For $\overline{\omega}^2 \gtrless 1/(r\chi)$ equation (64) is valid and becomes

$$|6 \times 6| = 0 \tag{65a}$$

$$(e^{\overline{m}_8} - e^{\overline{m}_7}) = 0 \tag{65b}$$

The frequencies associated with equation (65b) are the thickness-twist frequencies. This is shown by considering equation (25)

$$z_j = \frac{\overline{m}_j}{\pi} = \pm\sqrt{(n\eta)^2 + \frac{1 - r'\chi'\overline{\omega}'^2}{\left(\frac{1-\mu}{2}\right)r'}} \qquad j = 7, 8 \tag{66}$$

For nonrepeated values of z_7 and z_8, equation (65b) can be satisfied only if

$$n^2\eta^2 + \frac{1 - r'\chi'\overline{\omega}'^2}{\left(\frac{1-\mu}{2}\right)r'} = -\delta^2$$

is a negative number (i.e., $z_7 = -i\delta$, $z_8 = +i\delta$). If such is the case, equation (65b) becomes

$$e^{+i\pi\delta} - e^{-i\pi\delta} = 2i \sin \pi\delta = 0$$

which is satisfied by

$$\delta = m \qquad m = 1, 2, \ldots$$

so

$$z_j = \pm im \qquad \begin{matrix} j = 7, 8 \\ m = 1, 2, \ldots \end{matrix}$$

Squaring both sides of equation (66) and using the above solution for z_j yields

$$\overline{\omega}^2 = \frac{1}{\chi}\left[\frac{1}{r} + \left(\frac{1 - \mu}{2}\right)\left(\frac{m^2}{\eta^2} + n^2\right)\right] \tag{67}$$

which is the thickness-twist frequency equation. The original derivation of this equation (see eq. (19)) was based on $\lambda' = 0$ (no airflow), whereas the derivation above is valid for $\lambda' \geq 0$. Note that these frequencies are independent of λ (dynamic pressure) and therefore cannot coalesce with the bending or thickness-shear frequencies. (This is not necessarily so for other boundary conditions or for a panel having an orthotropic core.)

Numerical results (ch. III) show that as λ approaches zero the frequencies determined from equation (65a) approach the frequencies given by equation (20a). Thus, equation (65a) gives the frequencies of the bending and thickness-shear motions.

2. *Mode Shapes.* For all edges simply supported, equation (49) can be written as[3]

---

[3]For the first six columns of equation (68), the elements of column j are obtained from the corresponding elements of column one by replacing the subscript 1 with the subscript j.

$$
\begin{array}{c}
\begin{matrix} j=1 & 2 & 3 & 4 & 5 & 6 & 7 & 8 \end{matrix} \\
\left[\begin{array}{cccccc:cc}
\left(r+\frac{1}{b_1}\right)\frac{1}{z_1} & . & . & . & . & \left(r+\frac{1}{b_6}\right)\frac{1}{z_6} & 0 & 0 \\
\left(r+\frac{1}{b_1}\right)\frac{e^{\bar{m}_1}}{z_1} & . & . & . & . & . & 0 & 0 \\
\left(r+\frac{z_1^2}{n^2\eta^2 b_1}\right)\frac{n^2\eta^2}{z_1} & . & . & . & . & . & 0 & 0 \\
\left(r+\frac{z_1^2}{n^2\eta^2 b_1}\right)\frac{n^2\eta^2 e^{\bar{m}_1}}{z_1} & . & . & . & . & . & 0 & 0 \\
\left(r+\frac{1}{b_1}\right) z_1 & . & . & . & . & . & 0 & 0 \\
\left(r+\frac{1}{b_1}\right) z_1 e^{\bar{m}_1} & . & . & . & . & \left(r+\frac{1}{b_6}\right) z_6 e^{\bar{m}_6} & 0 & 0 \\
\hdashline
\frac{n\eta}{z_1} & . & . & . & . & \frac{n\eta}{z_6} & \frac{z_7}{n\eta} & \frac{z_8}{n\eta} \\
\frac{n\eta e^{\bar{m}_1}}{z_1} & . & . & . & . & \frac{n\eta e^{\bar{m}_6}}{z_6} & \frac{z_7 e^{\bar{m}_7}}{n\eta} & \frac{z_8 e^{\bar{m}_8}}{n\eta}
\end{array}\right]
\left\{\begin{array}{c} B_1 \\ B_2 \\ B_3 \\ B_4 \\ B_5 \\ B_6 \\ - \\ B_7 \\ B_8 \end{array}\right\}
=
\left\{\begin{array}{c} 0 \\ 0 \\ 0 \\ 0 \\ 0 \\ 0 \\ \\ 0 \\ 0 \end{array}\right\}
\end{array}
\tag{68}
$$

Use of the relation between A_j and B_j for $j = 1 \rightarrow 6$ (eq. (34)) enables the above equation to be expressed as

$$
\begin{array}{c}
\begin{matrix} j=1 & 2 & 3 & 4 & 5 & 6 & 7 & 8 \end{matrix} \\
\left[\begin{array}{cccccc:cc}
1 & . & . & . & . & 1 & 0 & 0 \\
e^{\bar{m}_1} & . & . & . & . & . & 0 & 0 \\
\dfrac{[1-(z_j/n\eta)^2]}{(1+rb_1)} & . & . & . & . & . & 0 & 0 \\
\dfrac{[1-(z_j/n\eta)^2]e^{\bar{m}_1}}{(1+rb_1)} & . & . & . & . & . & 0 & 0 \\
z_1^2 & . & . & . & . & . & 0 & 0 \\
z_1^2 e^{\bar{m}_1} & . & . & . & . & . & 0 & 0 \\
\hdashline
\dfrac{n\eta k}{r+(1/b_1)} & . & . & . & . & \dfrac{n\eta k}{r+(1/b_6)} & \dfrac{z_7}{n\eta} & \dfrac{z_8}{n\eta} \\
\dfrac{n\eta k e^{\bar{m}_1}}{r+(1/b_1)} & . & . & . & . & \dfrac{n\eta k e^{\bar{m}_6}}{r+(1/b_6)} & \dfrac{z_7 e^{\bar{m}_7}}{n\eta} & \dfrac{z_8 e^{\bar{m}_8}}{n\eta}
\end{array}\right]
\left\{\begin{array}{c} A_1 \\ A_2 \\ A_3 \\ A_4 \\ A_5 \\ A_6 \\ \hdashline B_7 \\ B_8 \end{array}\right\}
=
\left\{\begin{array}{c} 0 \\ 0 \\ 0 \\ 0 \\ 0 \\ 0 \\ \hdashline 0 \\ 0 \end{array}\right\}
\end{array}
\tag{69}
$$

where $k = \pi^3 D_s/\eta b^3$. Equation (69) is of the form

$$
\underset{6\times 6}{[K_{11}]}\ \underset{6\times 2}{[K_{12}]}\ \underset{6\times 1}{\{A_j\}} = \{0\}
$$

$$
\underset{2\times 6}{[K_{21}]}\ \underset{2\times 2}{[K_{22}]}\ \underset{2\times 1}{\{B_j\}} = \{0\}
$$

so that

$$
[K_{11}]\{A_j\} + [K_{12}]\{B_j\} = \{0\} \tag{70a}
$$

$$
[K_{21}]\{A_j\} + [K_{22}]\{B_j\} = \{0\} \tag{70b}
$$

Replacing b_j with $n^2 - \chi\bar{\omega}^2 - (z_j/\eta)^2$ (see eq. (44b)) and noting that all elements of $[K_{12}]$ are zero reduces equation (70a) to

$$\begin{bmatrix} 1 & 1 & 1 & 1 & 1 & 1 \\ e^{\overline{m}_1} & e^{\overline{m}_2} & e^{\overline{m}_3} & e^{\overline{m}_4} & e^{\overline{m}_5} & e^{\overline{m}_6} \\ \psi_1 & \psi_2 & \psi_3 & \psi_4 & \psi_5 & \psi_6 \\ \psi_1 e^{\overline{m}_1} & \psi_2 e^{\overline{m}_2} & \psi_3 e^{\overline{m}_3} & \psi_4 e^{\overline{m}_4} & \psi_5 e^{\overline{m}_5} & \psi_6 e^{\overline{m}_6} \\ z_1^2 & z_2^2 & z_3^2 & z_4^2 & z_5^2 & z_6^2 \\ z_1^2 e^{\overline{m}_1} & z_2^2 e^{\overline{m}_2} & z_3^2 e^{\overline{m}_3} & z_4^2 e^{\overline{m}_4} & z_5^2 e^{\overline{m}_5} & z_6^2 e^{\overline{m}_6} \end{bmatrix} \begin{Bmatrix} A_1 \\ A_2 \\ A_3 \\ A_4 \\ A_5 \\ A_6 \end{Bmatrix} = \begin{Bmatrix} 0 \\ 0 \\ 0 \\ 0 \\ 0 \\ 0 \end{Bmatrix} \tag{71}$$

where

$$\psi_j = \left[\frac{1}{\dfrac{1 - r\chi\overline{\omega}^2}{1 - \left(\dfrac{z_j}{n\eta}\right)^2} + n^2 r} \right] \tag{72}$$

The mode shape for w is then

$$w(x,y,t) = \sin \frac{n\pi y}{b} e^{i\omega t} \sum_{j=1}^{6} A_j e^{\overline{m}_j (x/a)} \tag{73}$$

where, for $j = 1$ (ref. 16, p. 34)

$$A_{j=1} = (-1)^{j+1} c \begin{vmatrix} 1 & 1 & 1 & 1 & 1 \\ e^{\overline{m}_2} & e^{\overline{m}_3} & e^{\overline{m}_4} & e^{\overline{m}_5} & e^{\overline{m}_6} \\ \psi_2 & \psi_3 & \psi_4 & \psi_5 & \psi_6 \\ \psi_2 e^{\overline{m}_2} & \psi_3 e^{\overline{m}_3} & \psi_4 e^{\overline{m}_4} & \psi_5 e^{\overline{m}_5} & \psi_6 e^{\overline{m}_6} \\ z_2^2 & z_3^2 & z_4^2 & z_5^2 & z_6^2 \end{vmatrix}$$

and so on, where c is an arbitrary constant.

By setting the determinant of the square matrix in equation (71) to zero, one obtains, with manipulation of both rows and *columns*,

$$(1 - r\chi\bar{\omega}^2)^2 \begin{vmatrix} 1 & 1 & 1 & 1 & 1 & 1 \\ e^{\bar{m}_1} & e^{\bar{m}_2} & e^{\bar{m}_3} & e^{\bar{m}_4} & e^{\bar{m}_5} & e^{\bar{m}_6} \\ z_1^2 & z_2^2 & z_3^2 & z_4^2 & z_5^2 & z_6^2 \\ z_1^2 e^{\bar{m}_1} & z_2^2 e^{\bar{m}_2} & z_3^2 e^{\bar{m}_3} & z_4^2 e^{\bar{m}_4} & z_5^2 e^{\bar{m}_5} & z_6^2 e^{\bar{m}_6} \\ z_1^4 & z_2^4 & z_3^4 & z_4^4 & z_5^4 & z_6^4 \\ z_1^4 e^{\bar{m}_4} & z_2^4 e^{\bar{m}_2} & z_3^4 e^{\bar{m}_3} & z_4^4 e^{\bar{m}_4} & z_5^4 e^{\bar{m}_5} & z_6^4 e^{\bar{m}_6} \end{vmatrix} = 0 \qquad (74)$$

Except for the "missing" term $(e^{\bar{m}_7} - e^{\bar{m}_8})$, equation (74) is the same frequency equation as given by equation (63).

Since equation (74) was obtained by altering *columns* (as well as rows) in the determinant of the coefficients of A_j, it is important to note that

$$(1-r\chi\bar{\omega}^2)^2 \begin{bmatrix} 1 & 1 & 1 & 1 & 1 & 1 \\ e^{\bar{m}_1} & e^{\bar{m}_2} & e^{\bar{m}_3} & e^{\bar{m}_4} & e^{\bar{m}_5} & e^{\bar{m}_6} \\ z_1^2 & z_2^2 & z_3^2 & z_4^2 & z_5^2 & z_6^2 \\ z_1^2 e^{\bar{m}_1} & z_2^2 e^{\bar{m}_2} & z_3^2 e^{\bar{m}_3} & z_4^2 e^{\bar{m}_4} & z_5^2 e^{\bar{m}_5} & z_6^2 e^{\bar{m}_6} \\ z_1^4 & z_2^4 & z_3^4 & z_4^4 & z_5^4 & z_6^4 \\ z_1^4 e^{\bar{m}_4} & z_2^4 e^{\bar{m}_2} & z_3^4 e^{\bar{m}_3} & z_4^4 e^{\bar{m}_4} & z_5^4 e^{\bar{m}_5} & z_6^4 e^{\bar{m}_6} \end{bmatrix} \begin{Bmatrix} A_1 \\ A_2 \\ A_3 \\ A_4 \\ A_5 \\ A_6 \end{Bmatrix} \neq \begin{Bmatrix} 0 \\ 0 \\ 0 \\ 0 \\ 0 \\ 0 \end{Bmatrix} \qquad (75)$$

If one used equation (75), with an equal sign, the correct frequency equation for simple support boundary conditions would be obtained (see eq. (74)). However, the mode shape for w would be incorrect (see eq. (71)).

The "missing" term $(e^{\bar{m}_7} - e^{\bar{m}_8})$ alluded to after equation (74) can be obtained from equation (70b), which is rewritten below.

$$\underset{[K_{21}]}{2\times 6}\begin{Bmatrix} A_1 \\ A_2 \\ A_3 \\ A_4 \\ A_5 \\ A_6 \end{Bmatrix} + \begin{bmatrix} \frac{z_7}{n\eta} & \frac{z_8}{n\eta} \\ \frac{z_7 e^{\bar{m}_7}}{n\eta} & \frac{z_8 e^{\bar{m}_8}}{n\eta} \end{bmatrix} \begin{Bmatrix} B_7 \\ B_8 \end{Bmatrix} = \begin{Bmatrix} 0 \\ 0 \end{Bmatrix} \tag{76}$$

Consider the possibility that $w = 0$ for all values of the x-coordinate; then $A_j = 0$ for $j = 1 \rightarrow 6$ (in addition to $A_7 = A_8 = 0$ by eq. (37)). Then, the above equation becomes simply

$$\begin{bmatrix} z_7 & z_8 \\ z_7 e^{\bar{m}_7} & z_8 e^{\bar{m}_8} \end{bmatrix} \begin{Bmatrix} B_7 \\ B_8 \end{Bmatrix} = \begin{Bmatrix} 0 \\ 0 \end{Bmatrix} \tag{77}$$

giving a frequency equation

$$z_7 z_8 (e^{\bar{m}_8} - e^{\bar{m}_7}) = 0 \tag{78}$$

Although equation (78) is satisfied by z_7 or z_8 equal to zero, this solution cannot be considered valid since, by equation (25), $z_7 = -z_8$ which makes $z_7 = z_8 = 0$ a repeated root. Thus, for distinct roots, equation (78) reduces to equation (65b) which is satisfied by $\bar{m}_{7,8} = \pm im\pi$, $m = 1, 2, 3, \ldots$ and again leads to the thickness-twist frequency equation (eq. (67)).

Because $A_j = 0$ for $j = 1 \rightarrow 6$, equations (34) and (31) show that $B_j = C_j = 0$ for $j = 1 \rightarrow 6$. The mode shapes given by equations (48) then reduce to

$$\left.\begin{aligned} w(x) &= 0 \\ Q_x(x) &= e^{\overline{m}_7(x/a)}B_7 + e^{\overline{m}_8(x/a)}B_8 \\ Q_y(x) &= \frac{z_7}{n\eta}\, e^{\overline{m}_7(x/a)}B_7 + \frac{z_8}{n\eta}\, e^{\overline{m}_8(x/a)}B_8 \end{aligned}\right\} \tag{79}$$

Since $z_7 = -z_8 \neq 0$, equation (77) gives

$$B_7 - B_8 = 0 \tag{80}$$

The use of equations (5), (79), and (80) together with $\overline{m}_{7,8} = \pm im\pi$, $m = 1, 2, 3, \ldots$, then yields

$$\left.\begin{aligned} w(x,y,t) &= 0 \\ Q_x(x,y,t) &= 2B_7 \cos\frac{m\pi x}{a} \sin\frac{n\pi y}{b}\, e^{i\omega t} \\ Q_y(x,y,t) &= \frac{-2B_7}{(n\eta/m)} \sin\frac{m\pi x}{a} \cos\frac{n\pi y}{b}\, e^{i\omega t} \end{aligned}\right\} \tag{81}$$

as the mode shape for the thickness-twist motion. (See fig. 3(a).)

I. Single Differential Equation Approaches and Comparison with Smirnov's Results

It is seen from equations (21), (23), and (25) that the characteristic equations for both the orthotropic and isotropic cores correspond to an eighth-order system of differential equations. In reference 8, Smirnov obtained flutter solutions for sandwich panels having *isotropic* cores; these solutions were derived from a sixth-, rather than an eighth-order differential equation. The sixth-order equation is an incomplete description of the panel motion, but for *simply supported* edges it does happen to lead to the correct bending and thickness-shear solutions. This occurrence is related to the uncoupled frequency determinant given by equation (63). The connection between

the sixth-order solution for the simply supported, isotropic panel and the uncoupled eighth-order solution given by equation (63) is brought out in the following sections.

1. Uncoupled Solution. In general, the solutions for w, Q_x, and Q_y depend on all eight roots ($\overline{m}_j$) of the characteristic equation (see discussion after eq. (5)). For a panel having an *isotropic* core, however, equation (37) shows that $A_7 = A_8 = 0$ even though B_j and C_j are all nonzero. Thus, in this special case, the solution for w depends on only six of the eight roots while the complete solution (i.e., for w, Q_x, and Q_y) still depends on all eight roots (as shown by eqs. (48)).

With $A_7 = A_8 = 0$, half the elements in columns 7 and 8 of the frequency determinant are zero ($\overline{c}_{1j} = \overline{c}_{2j} = \overline{c}_{5j} = \overline{c}_{6j} = 0$ in eqs. (50), $j = 7$ and 8). Furthermore, for *simply supported* edges the elements $\overline{c}_{3j}$ and $\overline{c}_{4j}$ of columns 7 and 8 are proportional to elements $\overline{c}_{7j}$ and $\overline{c}_{8j}$, respectively. This leads to the uncoupled frequency determinant (eq. (63)) wherein $\overline{m}_7$ and $\overline{m}_8$ are associated with the thickness-twist frequencies and $\overline{m}_1$ through $\overline{m}_6$ are associated with the bending and thickness-shear frequencies.

The uncoupling of the thickness-twist solution from the bending and thickness-shear solution is seen to be caused by two conditions. The condition $A_7 = A_8 = 0$ is a result of the factorable characteristic equation, (14a), and is due to the isotropic core. The proportionality of elements in the frequency determinant is due to the simple support boundary conditions. A change in either of these conditions prevents the solution from becoming uncoupled. Thus, a clamped isotropic panel will not have uncoupled solutions, nor will a simply supported orthotropic panel.

The fact that $A_7 = A_8 = 0$ arises from the factorable characteristic equation suggests that the eighth-order system of differential equations given by (1a), (1b), and (1c) also has a factorable form. This is shown next.

2. Eighth-Order Differential Equation. The three differential equations (1a), (1b), and (1c) can be written in the form

$$\begin{bmatrix} L_{11} & L_{12} & L_{13} \\ L_{21} & L_{22} & L_{23} \\ L_{31} & L_{32} & L_{33} \end{bmatrix} \begin{Bmatrix} w \\ Q_x \\ Q_y \end{Bmatrix} = \begin{Bmatrix} 0 \\ 0 \\ 0 \end{Bmatrix} \tag{82}$$

where

$$\left.\begin{aligned}
L_{11} &= -(D_{f_1} + D_{f_2})\nabla^4 - N_x \frac{\partial^2}{\partial x^2} - N_y \frac{\partial^2}{\partial y^2} + p \\
L_{12} &= \frac{\partial}{\partial x} \\
L_{13} &= \frac{\partial}{\partial y} \\
L_{21} &= -\frac{\partial^3}{\partial x\, \partial y^2} - \frac{\partial^3}{\partial x^3} + \frac{I_o}{D_s} \frac{\partial^3}{\partial x\, \partial t^2} \\
L_{22} &= -\frac{1}{D_s} - \frac{I_o}{D_s} \frac{1}{D_{Q_x}} \frac{\partial^2}{\partial t^2} + \frac{1}{D_{Q_x}} \left[\frac{\partial^2}{\partial x^2} + \left(\frac{1 - \mu}{2} \right) \frac{\partial^2}{\partial y^2} \right] \\
L_{23} &= \frac{1}{D_{Q_y}} \left(\frac{1 + \mu}{2} \right) \frac{\partial^2}{\partial x\, \partial y} \\
L_{31} &= -\frac{\partial^3}{\partial y\, \partial x^2} - \frac{\partial^3}{\partial y^3} + \frac{I_o}{D_s} \frac{\partial^3}{\partial y\, \partial t^2} \\
L_{32} &= \frac{1}{D_{Q_x}} \left(\frac{1 + \mu}{2} \right) \frac{\partial^2}{\partial x\, \partial y} \\
L_{33} &= -\frac{1}{D_s} - \frac{I_o}{D_s} \frac{1}{D_{Q_y}} \frac{\partial^2}{\partial t^2} + \frac{1}{D_{Q_y}} \left[\frac{\partial^2}{\partial y^2} + \left(\frac{1 - \mu}{2} \right) \frac{\partial^2}{\partial x^2} \right]
\end{aligned}\right\} \tag{83}$$

and p is given by equation (2).

A single differential equation in w, Q_x, or Q_y is obtained by expanding the determinant of the matrix $[L_{ij}]$, treating the operational coefficients as algebraic quantities (ref. 16, p. 117). The general result is an eighth-order differential operator, D_8, operating on w, Q_x, or Q_y. For an isotropic core ($D_{Q_x} = D_{Q_y} = D_Q$) the operators L_{23} and L_{32} are equal and the operator D_8 factors into the product

$$D_8 = D_2 D_6 \tag{84}$$

where D_2 and D_6 are the second- and sixth-order differential operators given by

$$D_2 = \frac{-1}{D_s}\left(1 + \frac{I_o}{D_Q}\frac{\partial^2}{\partial t^2}\right) + \frac{1 - \mu}{2}\frac{1}{D_Q}\nabla^2 \tag{85a}$$

$$D_6 = L_{11}\frac{1}{D_s}\left[\frac{D_s}{D_Q}\nabla^2 - \left(1 + \frac{I_o}{D_Q}\frac{\partial^2}{\partial t^2}\right)\right] + \left(\nabla^2 - \frac{I_o}{D_s}\frac{\partial^2}{\partial t^2}\right)\nabla^2 \tag{85b}$$

When the operators D_2 and D_6 are applied to any one of equations (5) and the results set equal to zero, equations (25) and (23) are reobtained, respectively, giving the *eight* roots z_j. This approach has no particular advantage over the method of working directly with equations (82) since the three simultaneous equations must still be used to determine the relations between A_j, B_j, and C_j. The formal expansion of the determinant of $[L_{ij}]$, although lengthy,[4] does give the complete *eighth*-order differential equation. If, however, the two shear angles (Q_x/D_{Q_x}, Q_y/D_{Q_y}) are eliminated from equations (82) by

[4]This expansion is given in reference 14 for the case of an orthotropic panel, but with the face sheet bending stiffness and rotary inertia neglected.

differentiation, only a *sixth*-order equation in w is obtained. This is shown in the next section.

3. Sixth-Order Differential Equation. For an isotropic core ($D_{Q_x} = D_{Q_y} = D_Q$), the sixth-order differential equation in w is obtained by first differentiating equation (1b) with respect to x, differentiating equation (1c) with respect to y, and adding the resulting equations together to obtain

$$\nabla^2 w = \left(1 + \frac{I_o}{D_Q}\frac{\partial^2}{\partial t^2} - \frac{D_s}{D_Q}\nabla^2\right)\Phi \tag{86}$$

where

$$\Phi = \left(w_{,x} - \frac{Q_x}{D_Q}\right)_{,x} + \left(w_{,y} - \frac{Q_y}{D_Q}\right)_{,y} \tag{87}$$

Equation (1a) can be written as

$$(D_{f_1} + D_{f_2})\nabla^4 w + N_x w_{,xx} + N_y w_{,yy} + D_Q(\Phi - \nabla^2 w) - p = 0 \tag{88}$$

by noting the identity

$$D_Q(\Phi - \nabla^2 w) \equiv -(Q_{x,x} + Q_{y,y})$$

The solution for Φ in terms of w is easily obtained from equation (88) and when substituted into equation (86) leads to a sixth-order differential equation in w

$$D_s\left[1 + \frac{D_{f_1}+D_{f_2}}{D_s}\left(1 + \frac{I_o}{D_Q}\frac{\partial^2}{\partial t^2}\right)\right]\nabla^4 w + \left(1 + \frac{I_o}{D_Q}\frac{\partial^2}{\partial t^2}\right)\left[N_x w_{,xx} + N_y w_{,yy} - p\right]$$

$$-I_o\frac{\partial^2}{\partial t^2}\nabla^2 w - \frac{D_s}{D_Q}\left[(D_{f_1} + D_{f_2})\nabla^6 w + N_x\frac{\partial^2}{\partial x^2}\nabla^2 w + N_y\frac{\partial^2}{\partial y^2}\nabla^2 w - \nabla^2 p\right] = 0 \tag{89}$$

Equation (89) corresponds to $D_6(w) = 0$ (eq. (85b)) since when p and w are replaced with equations (2) and (5), respectively, equation (23), giving *six* of the roots z_j, is again obtained. The factor D_2 (eq. (85a)) is missing from equation (89) and hence the roots z_7 and z_8, given by equation (25), are not obtained. Also, since equation (89) is a sixth-order equation, only three boundary conditions per edge can be specified. Thus, the sixth-order differential equation is seen to be incomplete, and solutions derived from it alone are, in general, incorrect.

4. Solutions Based on Sixth-Order Equation. For simply supported edges the incomplete sixth-order system does happen to lead to the correct frequency equation for the bending and thickness-shear modes. This can be shown by introducing a function $\overline{\chi}$ defined by[5]

$$\Phi = \nabla^2\overline{\chi} \tag{90}$$

(The function $\overline{\chi}$ is used to express the boundary conditions in terms of a single variable.) Comparison of this result with equation (86) shows that

$$w = \left(1 + \frac{I_o}{D_Q}\frac{\partial^2}{\partial t^2} - \frac{D_s}{D_Q}\nabla^2\right)\overline{\chi} \tag{91}$$

If equation (2) is written as

$$p = -\rho_m \frac{\partial^2 w}{\partial t^2} + \overline{q} \tag{92}$$

---

[5]The symbol $\overline{\chi}$ corresponds to Smirnov's χ (ref. 8) and is distinct from the χ used herein for the rotary inertia parameter.

where $\overline{q}$ is the aerodynamic loading, equations (88), (90), (91), and (92) can be combined to give a sixth-order differential equation in $\overline{\chi}$.

$$D_s\left[1+\tau-\tau\left(\frac{-I_o}{D_Q}\frac{\partial^2}{\partial t^2}+\frac{D_s}{D_Q}\nabla^2\right)\right]\nabla^4\overline{\chi}+\left(N_x\frac{\partial^2}{\partial x^2}+N_y\frac{\partial^2}{\partial y^2}\right)\left(1+\frac{I_o}{D_Q}\frac{\partial^2}{\partial t^2}-\frac{D_s}{D_Q}\nabla^2\right)\overline{\chi}$$

$$-I_o\frac{\partial^2}{\partial t^2}\nabla^2\overline{\chi}+\rho_m\frac{\partial^2}{\partial t^2}\left(1+\frac{I_o}{D_Q}\frac{\partial^2}{\partial t^2}-\frac{D_s}{D_Q}\nabla^2\right)\overline{\chi}-\overline{q}=0 \qquad (93)$$

When the rotary inertia terms $[I_o(\partial^2/\partial t^2)]$ are dropped, and τ is neglected with respect to one, equation (93) reduces to the differential equation used by Smirnov (ref. 8). Replacing $\overline{q}$ with the aerodynamic loading term $[(-2q/\beta)(\partial w/\partial x)]$ and setting

$$\overline{\chi}=\sum_{j=1}^{6}\overline{A}_j e^{\overline{m}_j(x/a)}\sin\frac{n\pi y}{b}\,e^{i\omega t} \qquad (94)$$

in equation (93), once more leads to equation (23) for *six* of the roots z_j; again, z_7 and z_8 are not obtained.

If, for simply supported edges, boundary conditions (4b) and (4d) are combined (so as to have three rather than four boundary conditions), the following modified boundary equations are obtained.

at x = 0 and a	at y = 0 and b	
$w = 0$	$w = 0$	(95a)
$w_{,xx} = 0$	$w_{,yy} = 0$	(95b)
$\frac{1}{D_Q}(Q_{x,x}+Q_{y,y})=0$	$\frac{1}{D_Q}(Q_{y,y}+Q_{x,x})=0$	(95c)

These *three* boundary conditions per edge are satisfied along the panel boundary provided the function $\overline{X}$ is required to satisfy

$$\overline{X} = \nabla^2\overline{X} = \nabla^4\overline{X} = 0 \tag{96}$$

along the boundary.[6]

Applying equations (96) to equation (94) yields the following relationships between the six $\overline{A}_j$.

$$\begin{bmatrix} 1 & 1 & 1 & 1 & 1 & 1 \\ e^{\overline{m}_1} & e^{\overline{m}_2} & e^{\overline{m}_3} & e^{\overline{m}_4} & e^{\overline{m}_5} & e^{\overline{m}_6} \\ z_1^2 & z_2^2 & z_3^2 & z_4^2 & z_5^2 & z_6^2 \\ z_1^2 e^{\overline{m}_1} & z_2^2 e^{\overline{m}_2} & z_3^2 e^{\overline{m}_3} & z_4^2 e^{\overline{m}_4} & z_5^2 e^{\overline{m}_5} & z_6^2 e^{\overline{m}_6} \\ z_1^4 & z_2^4 & z_3^4 & z_4^4 & z_5^4 & z_6^4 \\ z_1^4 e^{\overline{m}_1} & z_2^4 e^{\overline{m}_2} & z_3^4 e^{\overline{m}_3} & z_4^4 e^{\overline{m}_4} & z_5^4 e^{\overline{m}_5} & z_6^4 e^{\overline{m}_6} \end{bmatrix} \begin{Bmatrix} \overline{A}_1 \\ \overline{A}_2 \\ \overline{A}_3 \\ \overline{A}_4 \\ \overline{A}_5 \\ \overline{A}_6 \end{Bmatrix} = \begin{Bmatrix} 0 \\ 0 \\ 0 \\ 0 \\ 0 \\ 0 \end{Bmatrix} \tag{97}$$

Note that the determinant of the square matrix in equation (97) is identical to the uncoupled 6 × 6 subdeterminant of equation (63).

The relation between $\overline{A}_j$ (corresponding to $\overline{X}$) and A_j (corresponding to w) is determined by equation (91) and is found to be

$$A_j = (1 + rb_j)\overline{A}_j \qquad j = 1 \rightarrow 6 \tag{98}$$

---

[6]Equations (95c) are satisfied because of the identity

$$\frac{1}{D_Q}\left[\omega^2 I_o \nabla^2\overline{X} + D_s\nabla^4\overline{X} + (Q_{x,x} + Q_{y,y})\right] \equiv 0$$

where equation (44b) has been used. By employing equation (98), it is possible to manipulate the rows of equation (97) so as to reobtain equation (71) which was originally derived from the complete eighth-order system.

Equation (97) depends on only six roots, and these are the same roots as are given by equation (23). Thus, the sixth-order equation, used with the modified simple support boundary conditions, does predict the correct solution for the bending and thickness-shear motion. (Note that the sixth-order equation does not predict the thickness-twist solution.) For other boundary conditions, however, (several of which are considered in ref. 8) the bending and thickness-shear motions will not, in general, be independent of the other two roots given by the second-order equation (i.e., eq. (85a)). In such cases the sixth-order system will not give the correct frequency equation. In reference 17, several other instances are noted where the assumption of core isotropy has led to the erroneous use of differential equations that are two orders less than is appropriate.

Another instance in which the characteristic equation factors is when $\eta = 0$ (beam behavior). In this case A_j and B_j are related but are independent of C_j (eqs. (40), (41), and (42)). This reflects the fact that the "cylindrical bending" of the sandwich beam is governed by a sixth-order rather than an eighth-order differential equation (see discussion after eq. (16)).

The bending and thickness-shear frequency equation for the simply supported beam ($\eta = 0$) is given by equations (55) and (62) as

$$\left|\tilde{c}_{ij}\right|_{6\times6} = 0$$

By manipulation of the rows, this determinant can be reduced to the determinant obtained from equation (97). Thus, the sixth-order system correctly predicts the bending and thickness-shear frequencies for both the simply supported beam and the panel.

For the *clamped beam* ($\eta = 0$) the sixth-order differential equation also predicts the correct frequency equation. In this case

$$\overline{\chi} = \sum_{j=1}^{6} \tilde{A}_j e^{\overline{m}_j (x/a)} e^{i\omega t} \tag{99}$$

and application of

$$\left(1 + \frac{I_o}{D_Q}\frac{\partial^2}{\partial t^2} - \frac{D_s}{D_Q}\frac{d^2}{dx^2}\right)\overline{\chi} = \frac{d\overline{\chi}}{dx} = \frac{d^3\overline{\chi}}{dx^3} = 0 \tag{100}$$

yields,[7]

$$\sum_{j=1}^{6} d_{ij}\tilde{A}_j = 0 \qquad i = 1, 2, \ldots, 6 \tag{101}$$

where

$$\left.\begin{aligned} d_{1j} &= 1 - r'\chi'\overline{\omega}'^2 - r'z_j^2 & d_{2j} &= (1 - r'\chi'\overline{\omega}'^2 - r'z_j^2)e^{\overline{m}_j} \\ d_{3j} &= z_j & d_{4j} &= z_j e^{\overline{m}_j} \\ d_{5j} &= z_j^3 & d_{6j} &= z_j^3 e^{\overline{m}_j} \end{aligned}\right\} \tag{102}$$

---

[7]Except for the term $(I_o/D_Q)(\partial^2/\partial t^2)$ (rotary inertia) these boundary conditions are the same as used by Smirnov in reference 7.

Hence, the corresponding frequency equation predicted by the sixth-order system is

$$\left|d_{ij}\right|_{6\times 6} = 0 \tag{103}$$

From the eighth-order system the bending and thickness-shear frequency determinant for the beam solution is

$$\left|\tilde{c}_{ij}\right|_{6\times 6} = 0 \tag{104}$$

(See eqs. (54a), (55), and (62).) The elements $\tilde{c}_{ij}$ are given by equations (55) and depend on only six of the eight roots for z_j. For the clamped beam these elements are seen to be different from the elements d_{ij} predicted by the sixth-order system (eqs. (102)). By using equation (98) and by manipulating the rows of equation (104), however, it is possible to reduce the elements of $|\tilde{c}_{ij}|$ to the corresponding elements of $|d_{ij}|$. Thus, for the beam ($\eta = 0$), the sixth-order system predicts the same clamped bending and thickness-shear frequency solution as the eighth-order system. (Note that the sixth-order system does not give the thickness-twist solution.) For $\eta > 0$ (panel rather than beam) the clamped eighth-order solution depends on all eight roots of the corresponding characteristic equation (see eqs. (49), (50), and (51)); in this case the sixth-order system does not adequately describe the motion.

The above results show that for the simply supported *isotropic* panel and the simply supported or clamped beam, the solution from the eighth-order system of differential equations uncouples and can be expressed as a sixth- plus a second-order system. The solution is

uncoupled in the sense that the sixth-order system predicts the bending and thickness-shear frequencies while the second-order system independently predicts the thickness-twist frequencies. In the approach used by Smirnov a single differential equation in w corresponding to the sixth-order system only is obtained. This approach is therefore not applicable to the general case where the eighth-order system does not uncouple.

III. COMPUTATIONAL PROCEDURE FOR OBTAINING NUMERICAL RESULTS

For the type of aerodynamic-force approximation used herein, pairs of panel frequencies coalesce at certain dynamic pressures, thus forming "frequency loops" in the λ, $\bar{\omega}^2$ plane. (See fig. 4.) Below the peak of a particular loop the two frequencies forming the loop are real and distinct. In this case the motion of the corresponding modes is stable. At the peak (i.e., where $\partial\lambda/\partial\omega = 0$) the two frequencies have coalesced; they are still real at this point but are on the verge of becoming complex. Above the peak the pair of frequencies exist as complex quantities and produce an oscillatory diverging motion termed flutter (ref. 18, p. 245). The value of λ corresponding to the peak of the lowest loop corresponds to the critical (minimum) flutter condition and is designated λ_{cr}. (See fig. 4.)

Points on the frequency loops are combinations of λ and $\bar{\omega}^2$ for which the roots z_j of the characteristic equation also cause the corresponding frequency determinant to equal zero. A practical procedure for determining the frequency loops is to fix $\bar{\omega}^2$ and vary λ between prescribed limits, computing first the roots z_j and then the frequency determinant D for each λ. These steps can be repeated until a value of λ is found that differs from the correct value (i.e., $D = 0$) by only an acceptable amount. (An allowable error in λ of 0.01 percent was accepted in calculating the numerical results presented herein.) By incrementing $\bar{\omega}^2$ and repeating the above process one can systematically obtain the frequency loops. Of course, the same procedure can be used by holding λ fixed and iterating to solutions for $\bar{\omega}^2$.

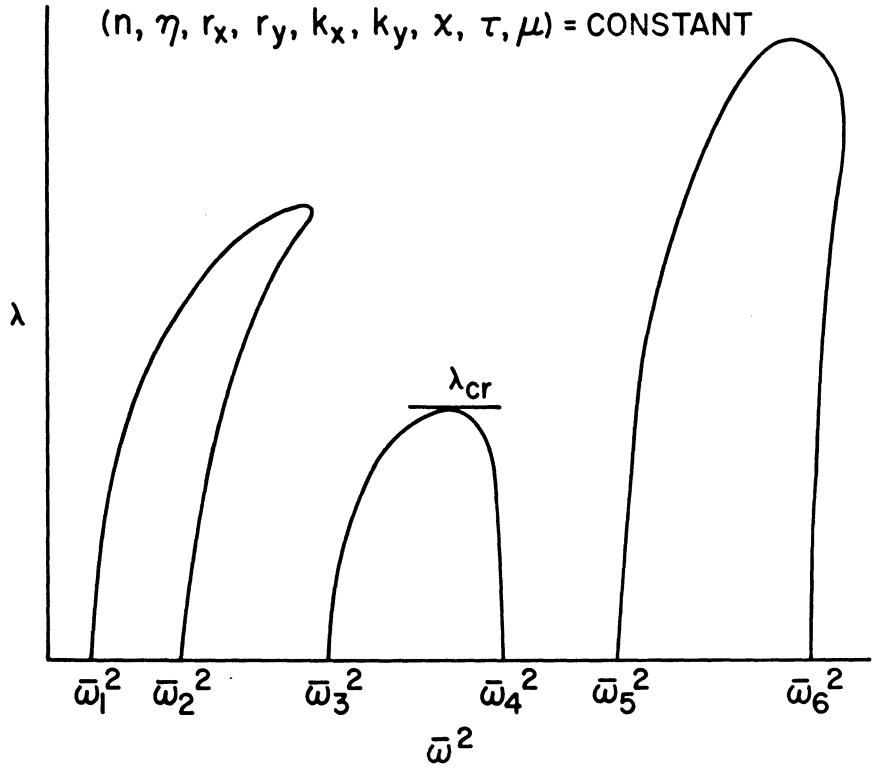

Figure 4.- Frequency coalescence behavior illustrating critical value of the dynamic pressure parameter.

A. Roots of the Characteristic Equations

In references 4 and 5 the characteristic equation was a fourth-order polynomial whose roots could be computed analytically. The characteristic equations obtained herein are eighth- and sixth-order polynomials (eqs. (21), (23), and (26)) and their roots were computed numerically, using Bairstow's method as programmed in reference 19. As a check on the accuracy of the computations, the coefficients of the polynomial as computed from the roots were compared with the input coefficients; the coefficients generally agreed to 12 digits or better. (All computations were performed in double precision arithmetic.)

There is no guarantee that the array of roots returned from the root finding subroutine will be ordered in a consistent, systematic manner. For example, when $\lambda = \lambda_1$ the two roots stored in z(1) and z(2) may be the most negative and the second most negative roots, respectively. On the next trial value of λ, $\lambda = \lambda_1 + \Delta\lambda$, the roots stored in z(1) and z(2) may be the second most negative and the most negative roots, respectively, with the remaining roots ordered in the same sequence as for $\lambda = \lambda_1$ (see fig. 5). Computing the frequency determinants $D(\lambda)$ and $D(\lambda + \Delta\lambda)$ with the names (i.e., z_1 and z_2) of the two most negative roots interchanged when $\lambda = \lambda_1 + \Delta\lambda$ is equivalent to interchanging columns 1 and 2 of $D(\lambda_1 + \Delta\lambda)$, hence producing a false change of sign. Since a sign change indicates the existence of a solution in the interval $\Delta\lambda$, a consistent, systematic procedure for ordering the roots must be incorporated in the programming to prevent the occurrence of false changes in the sign of the frequency determinant.

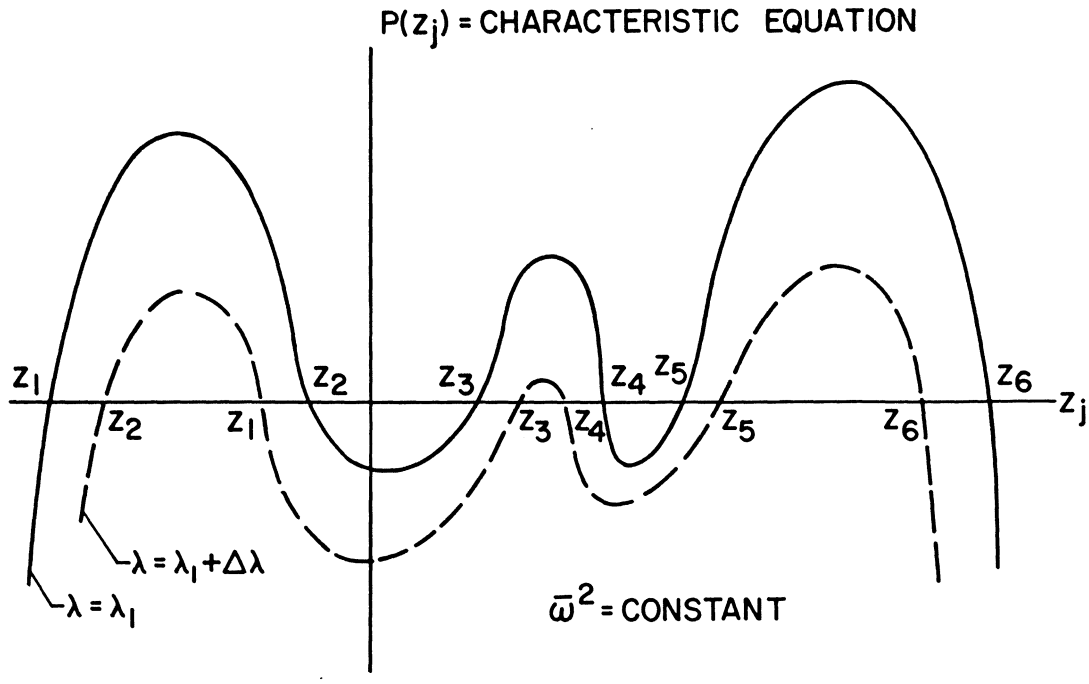

Figure 5.- Schematic of characteristic equation for two values of λ with fixed $\bar{\omega}^2$.

The approach used herein was to identify the real and complex roots and then to sort and name them according to the magnitude and sign of their real and imaginary parts.

B. Frequency Determinant

Some of the roots z_j will usually be complex, thus causing elements of columns j of the frequency determinant to be complex also. Since the coefficients appearing in the characteristic equation $P(z_j) = 0$ are real, however, complex roots will occur in complex conjugate pairs. This allows the frequency determinant to be computed from a matrix of *real* numbers. To show this, consider the 4×4 determinant

$$D = \begin{vmatrix} E_1 & E_2 & E_3 & E_4 \\ E_1 e^{\overline{m}_1} & E_2 e^{\overline{m}_2} & E_3 e^{\overline{m}_3} & E_4 e^{\overline{m}_4} \\ F_1 & F_2 & F_3 & F_4 \\ F_1 e^{\overline{m}_1} & F_2 e^{\overline{m}_2} & F_3 e^{\overline{m}_3} & F_4 e^{\overline{m}_4} \end{vmatrix} \tag{105}$$

where $E_j = E(z_j)$ and $F_j = F(z_j)$ are analytic functions of $z_j = \overline{m}_j/\pi = (\alpha_j/\pi) + i(\delta_j/\pi)$ that are real when z_j is real. (Eq. (105) is of the same form as the frequency determinants derived herein.) Then if z_1 and z_2 are complex conjugates, let

$$\pi z_1 = \alpha_1 + i\delta_1 = \overline{m}_1$$

$$\pi z_2 = \pi z_1^* = \alpha_1 - i\delta_1 = \overline{m}_1^*$$

so D becomes

$$D = \begin{vmatrix} E(z_1) & E(z_1^*) & E_3 & E_4 \\ E(z_1)e^{\overline{m}_1} & E(z_1^*)e^{\overline{m}_1^*} & E_3e^{\overline{m}_3} & E_4e^{\overline{m}_4} \\ F(z_1) & F(z_1^*) & F_3 & F_4 \\ F(z_1)e^{\overline{m}_1} & F(z_1^*)e^{\overline{m}_1^*} & F_3e^{\overline{m}_3} & F_4e^{\overline{m}_4} \end{vmatrix}$$

By the principle of reflection (ref. 20), $E(z_1^*) = [E(z_1)]^*$, and so on, giving

$$D = \begin{vmatrix} E(z_1) & [E(z_1)]^* & E_3 & E_4 \\ E(z_1)e^{\overline{m}_1} & [E(z_1)e^{\overline{m}_1}]^* & E_3e^{\overline{m}_3} & E_4e^{\overline{m}_4} \\ F(z_1) & [F(z_1)]^* & F_3 & F_4 \\ F(z_1)e^{\overline{m}_1} & [F(z_1)e^{\overline{m}_1}]^* & F_3e^{\overline{m}_3} & F_4e^{\overline{m}_4} \end{vmatrix}$$

If column 2 is added to column 1, the quantity 2 factored from the new column 1, and the resulting column 1 subtracted from column 2, the above expression for D simplifies to

$$D = -2i \begin{vmatrix} R[E_1] & I[E_1] & E_3 & E_4 \\ R[E_1e^{i\delta_1}]e^{\alpha_1} & I[E_1e^{i\delta_1}]e^{\alpha_1} & E_3e^{\overline{m}_3} & E_4e^{\overline{m}_4} \\ R[F_1] & I[F_1] & F_3 & F_4 \\ R[F_1e^{i\delta_1}]e^{\alpha_1} & I[F_1e^{i\delta_1}]e^{\alpha_1} & F_3e^{\overline{m}_3} & F_4e^{\overline{m}_4} \end{vmatrix} \tag{106}$$

where R and I denote the real and imaginary parts, respectively, of the bracketed expressions and where $\overline{m}_1 = \alpha_1 + i\delta_1$ has been used. Note that D is purely *imaginary* when z_3 and z_4 are real. If z_3 and z_4 are also a complex conjugate pair ($\pi z_3 = \overline{m}_3 = \alpha_3 + i\delta_3$, $z_4 = z_3^*$), then columns 3 and 4 can be manipulated in the same manner to give

$$D = (-2i)^2 \begin{vmatrix} R[E_1] & I[E_1] & R[E_3] & I[E_3] \\ R[E_1 e^{i\delta_1}]e^{\alpha_1} & I[E_1 e^{i\delta_1}]e^{\alpha_1} & R[E_3 e^{i\delta_3}]e^{\alpha_3} & I[E_3 e^{i\delta_3}]e^{\alpha_3} \\ R[F_1] & I[F_1] & R[F_3] & I[F_3] \\ R[F_1 e^{i\delta_1}]e^{\alpha_1} & I[F_1 e^{i\delta_1}]e^{\alpha_1} & R[F_3 e^{i\delta_3}]e^{\alpha_3} & I[F_3 e^{i\delta_3}]e^{\alpha_3} \end{vmatrix}$$

which is a *real* number.

The above procedure applies to an $n \times n$ determinant whose elements are of the form of equation (105). Thus, the frequency determinants considered herein can be computed from determinants whose elements are real rather than complex. This result is useful since it gives one access to a wider range of available methods for evaluating the determinants.

The terms e^{α_j} and $e^{\overline{m}_j}$ appearing in the frequency determinants can cause a computer overflow condition for large positive exponents (i.e., $e^{\overline{m}_j}$ may be too large a number for the computer to represent). A simple way to avoid this problem is to write the elements of the determinants so that no positive real exponents occur. For example, consider equation (106) with $\alpha_1 > 0$, $\overline{m}_3 < 0$, and $\overline{m}_4 - \alpha_1 > 0$. Then, equation (106) can be written

$$D = -2i \begin{vmatrix} R[E_1] & I[E_1] & E_3 & E_4 e^{-(\overline{m}_4 - \alpha_1)} \\ R[E_1 e^{i\delta_1}] & I[E_1 e^{i\delta_1}] & E_3 e^{\overline{m}_3 - \alpha_1} & E_4 \\ R[F_1] & I[F_1] & F_3 & F_4 e^{-(\overline{m}_4 - \alpha_1)} \\ R[F_1 e^{i\delta_1}] & I[F_1 e^{i\delta_1}] & F_3 e^{\overline{m}_3 - \alpha_1} & F_4 \end{vmatrix} e^{\alpha_1} e^{\alpha_1} e^{\overline{m}_4 - \alpha_1}$$

or

$$D = -2i e^{\overline{m}_4 + \alpha_1} \Delta$$

where Δ is the determinant of the 4×4 matrix in the above equation. Since it is only the sign of the frequency determinant that is of interest (as D passes through zero), it is only necessary to compute Δ, which contains no elements having e raised to a positive real power.

It should be noted that some of the elements of the frequency determinants derived herein involve terms where b_j, y_j, and z_j appear in the denominator. If one of these quantities passes through zero (as λ or $\overline{\omega}^2$ is being incremented) the frequency determinant D will change sign by passing through plus and minus infinity, rather than by passing through zero. Thus, the form of the frequency determinant should be modified so as to prevent D from becoming infinite. This can be done by multiplying the elements of column j by the appropriate products of b_j, y_j, and z_j so that none of these three quantities appear in the denominator of any element.

IV. NUMERICAL RESULTS AND DISCUSSION

The procedure discussed in chapter III has been used to compute frequency loops and flutter boundaries for a selected range of parameters. These results, which are discussed in the following sections, indicate the effects and importance of the face sheet bending stiffness, rotary inertia, and orthotropic core shear stiffnesses.

A. Effects of Face Sheet Bending Stiffness

The influence of the two face sheet bending stiffnesses D_{f_1} and D_{f_2} is felt through the parameter $\tau = (D_{f_1} + D_{f_2})/D_s$. If both face sheets are identical this parameter becomes $\tau = (1/3)\{(f/c)/[1+(f/c)]\}^2$ which depends only on the face sheet to core thickness ratio (f = face thickness and c = core thickness).

In reference 4, flutter boundaries were calculated for sandwich panels having clamped or simply supported leading and trailing edges and simply supported side edges. These results, which were from an analysis that neglected the face sheet bending stiffness, predicted that for both a square panel ($\eta = 1$) and an infinitely wide panel ($\eta = 0$, i.e., a beam) the clamped edge condition gives a lower flutter speed than the simply supported edge condition when the shear flexibility parameter, r', exceeds a value of about 0.2.[8]

---

[8]For an isotropic core and identical face sheets

$$r' = \left[\frac{\pi^2}{2(1 - \mu^2)}\right]\left(\frac{c}{a}\right)^2\left(\frac{f}{c}\right)\left(\frac{E_f}{G_c}\right)$$

where E_f and G_c are Young's and the shear modulus of face and core, respectively.

That an increase in boundary restraint could lower the flutter speed was an unexpected result. Indeed, Smirnov's flutter analysis of the sandwich beam (ref. 7) showed that for "large" values of f/c and r' ($f/c = 0.632$, $r' = \pi^2$) the clamped edge condition does give a higher flutter speed than the simply supported edge condition. Since Smirnov did not present results corresponding to smaller values of f/c, it was not possible to determine whether the difference in the effect of the boundary conditions predicted by reference 7 (where $\tau > 0$) and reference 4 (where $\tau = 0$) was due to the "largeness" of the f/c chosen by Smirnov (ref. 7), or whether it was the neglect of τ in reference 4. Neglecting τ lowers the order of the beam differential equations from sixth to fourth order (see eq. (26)) and raises the possibility that $\lim_{f/c \to 0} \lambda'_{cr}(f/c) \neq \lambda'_{cr}(0)$ (refs. 21 and 22).[9]

To investigate this possibility, flutter boundaries were computed from the solutions to the sixth-order beam equations derived herein for clamped and simply supported edges, and for f/c ranging from 0.01 to 0.632. These results are shown in figure 6 where the variation in λ'_{cr} with f/c is presented for $r' = 0$, 0.4, and 2.0 (with $k'_x = \chi' = 0$, i.e., no in-plane load, and rotary inertia neglected). The curves labeled $r' = 0$ correspond to panels having an infinite shear modulus, and in this case the only effect of τ is to increase the values of λ'_{cr} computed from the $\tau = 0$ analysis by the factor $(1 + \tau)$ (see eq. (26)). (Note that $D_s(1 + \tau)$ equals the total panel bending stiffness.) For $r' = 0.4$, the clamped beam has a lower flutter boundary than

[9]By $(f/c) \to 0$ it is understood that (f/c) goes to zero only in the expression for τ.

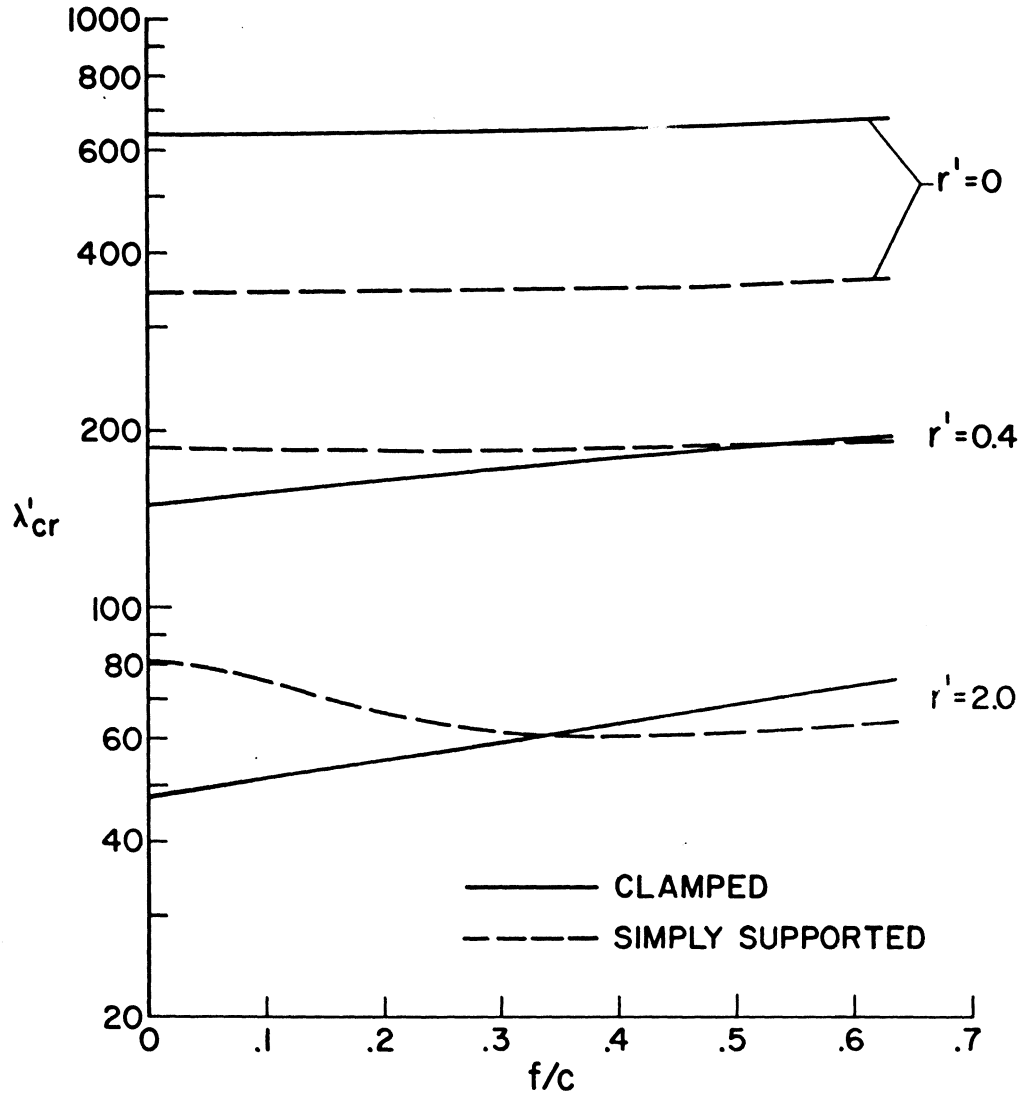

Figure 6.- Effect of face sheet to core thickness ratio on flutter boundaries of sandwich beams; $\eta = k'_x = \chi' = 0$.

the simply supported beam until $f/c \approx 0.53$ where the boundaries cross. The same situation exists for $r' = 2.0$ except that the boundaries cross at a smaller value of f/c. In all cases $\lim_{f/c \to 0} \lambda'_{cr}(f/c) = \lambda'_{cr}(0)$ indicating that the flutter solutions to the fourth-order beam equation presented in reference 4 correctly describe the beam bending behavior for sufficiently small values of f/c. For values of f/c greater than zero the face bending stiffness is seen to increase in importance as the shear flexibility parameter (r') increases.

The behavior of the frequency loops for four points on the $r' = 2.0$ flutter boundaries of figure 6 are shown in figure 7. These loops are formed by the lowest two natural frequencies of the beam. The third and fourth, fifth, and sixth, and presumably all higher frequencies coalesce at larger values of λ'. For $\lambda' = 0$ (no airflow) the frequencies behave in the "usual" manner, namely that their values are increased by an increase in boundary restraint. Also, an increase in panel stiffness (due to increasing f/c) causes an increase in these frequencies. Comparison of figures 7(a) and 7(d) indicates that f/c has a larger effect on the clamped beam frequencies than on those of the simply supported beam.

For $\lambda' > 0$ the beam vibrational motion induces an aerodynamic loading which subjects the beam to a nonconservative force distribution (ref. 18). The stability of such a nonconservative elastic system is not necessarily increased with an increase in the forces of restraint. In reference 23, for example, the destabilizing effect of increasing deflectional spring support stiffness at panel boundaries was noted for certain panel configurations. In figure 7 this same type of behavior is

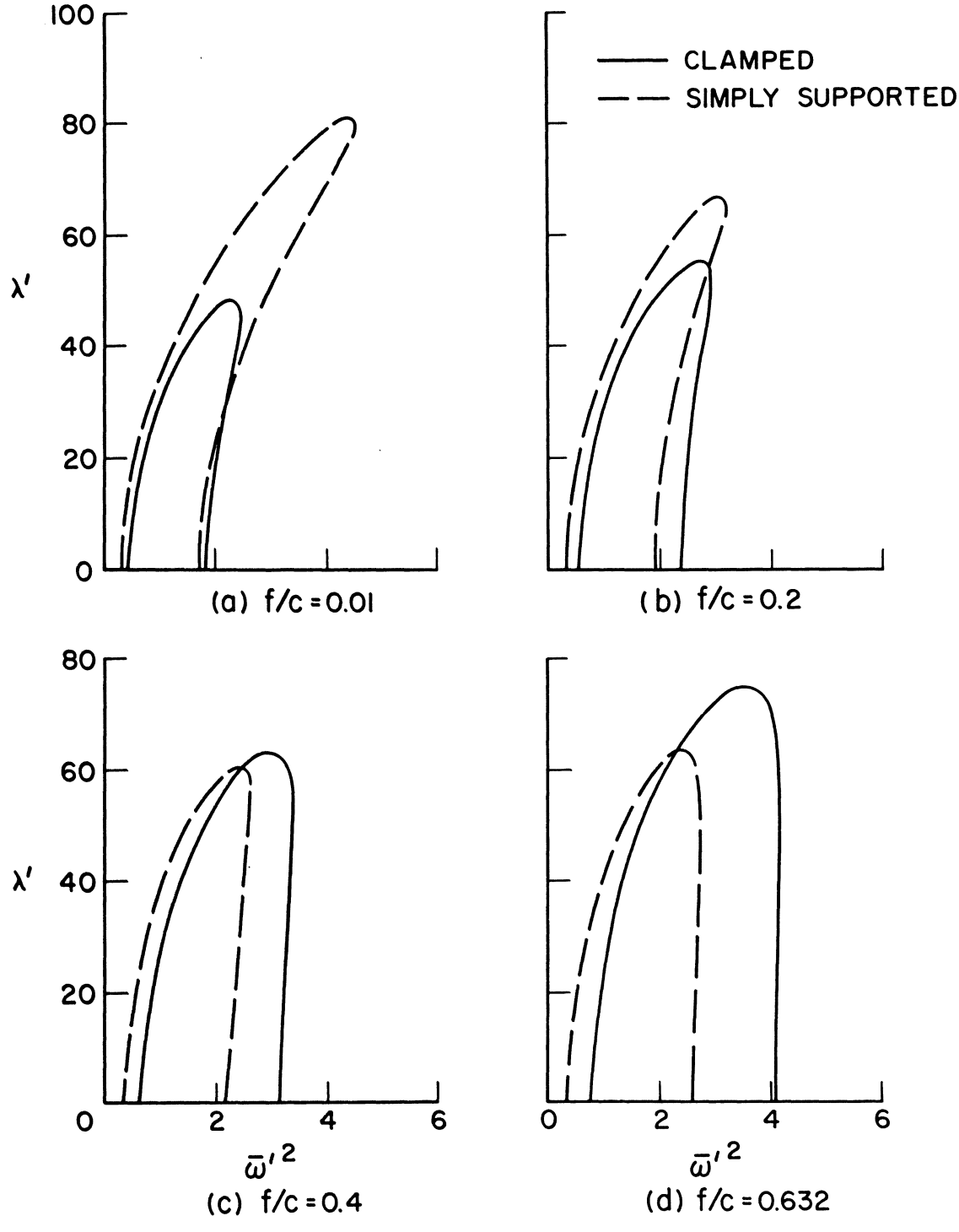

Figure 7.- Effect of face sheet bending stiffness on frequency loops; $r' = 2.0$, $\eta = k_x' = \chi' = 0$.

observed for $f/c = 0.01$ and $f/c = 0.20$ where an increase in boundary restraint from the simply supported (zero moment) to the clamped (nonzero moment) edge condition is destabilizing.

The variation in λ'_{cr} with r' is shown in figures 8(a) and 8(b) for $f/c = 0.01$ and $f/c = 0.632$, respectively ($\eta = k'_x = \chi' = 0$). For $f/c = 0.01$, the clamped edge condition gives a higher flutter boundary than the simply supported edge condition when r' is less than about 0.2. For $0.2 < r' < 10$ the simply supported beam is more stable than the clamped beam. The flutter boundaries presented in reference 4, for $0 \leq r' \leq 2$ and $\tau = 0$ ($f/c = 0$), are essentially identical to the $r' \leq 2$ portion of the curves in figure 8(a). In figure 8(b), f/c is equal to 0.632 and in this case the clamped boundary is never lower than the simply supported boundary, although in the range $0.5 < r' < 0.8$, they do coincide. At $r' = \pi^2$, the curves pass through the solutions obtained by Smirnov in reference 7.

In reference 5, the analysis of reference 4 ($\tau = 0$) was used to compute flutter boundaries for a wide range of simply supported panel configurations. For panels supporting an in-plane tension load in the airflow direction the theory predicted that an increase in core shear stiffness (decrease in r) could lower λ_{cr}. This is illustrated in figure 9 (taken from ref. 5) which is for $n = \eta = 1$, $k_y = \tau = \chi = 0$, and $k_x = -4$. (For $r = 0$, the value $k_x = -4$ represents a tensile load with a magnitude equal to the buckling load of the panel at zero dynamic pressure.) It is seen that λ_{cr} for $r = 2$ is more than a third larger than λ_{cr} at $r = 0$ (infinite shear stiffness). To determine whether the face bending stiffness affects this behavior (decrease in

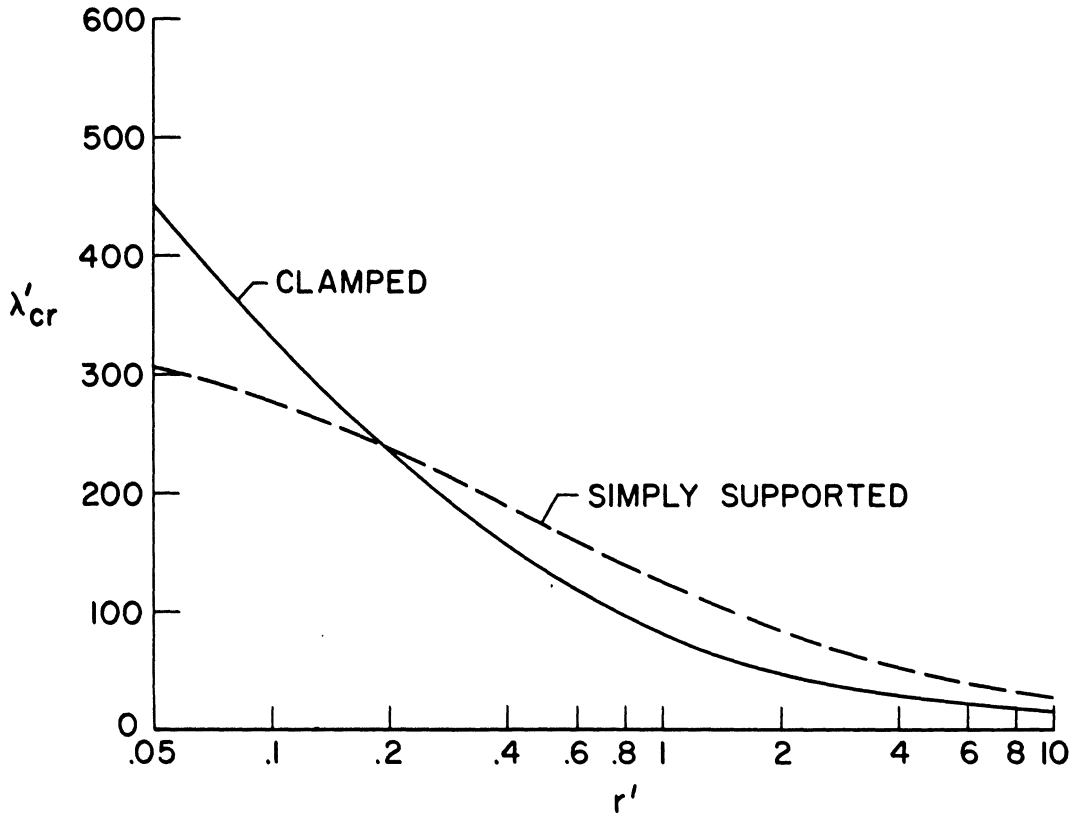

(a) f/c = 0.01

Figure 8.- Effect of shear flexibility on flutter boundaries of sandwich beams; $\eta = k'_x = \chi' = 0$.

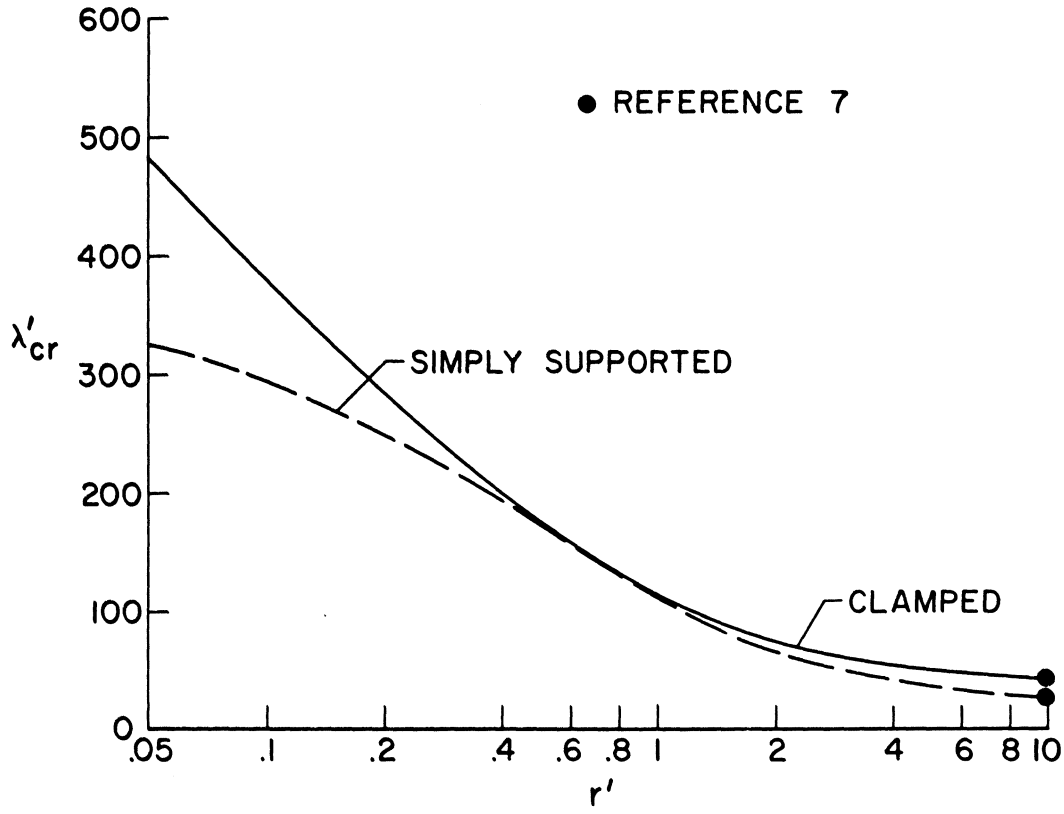

(b) f/c = 0.632

Figure 8.- Concluded.

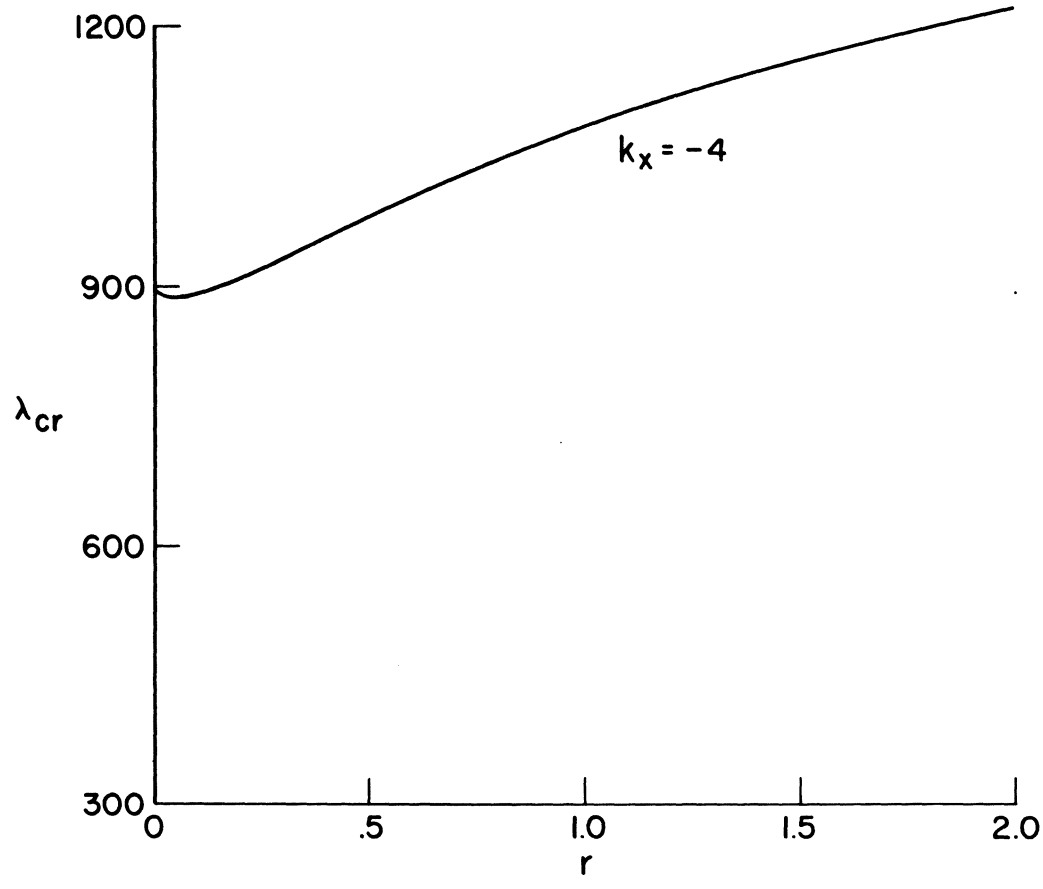

Figure 9.- Effect of transverse shear flexibility and in-plane tension load on λ_{cr} for simply supported edges (ref. 5); $n = \eta = 1$, $k_y = \chi = \tau = 0$.

flutter speed with increase in core shear stiffness), the first seven frequency loops for the point $r = 2$, of figure 9, were computed from the analysis herein for $f/c = 0.01$. These results are presented in figure 10 where it is seen that the first two bending frequencies (B1 and B2) coalesce at $\lambda_{cr} = 1231$. This is the same value for λ_{cr} obtained with $\tau = 0$. Thus, the flutter boundary in figure 9 appears to be unaffected by small, but nonzero, values of f/c (or τ).

B. Effects of Rotary Inertia

In the preceding section the flutter condition corresponded to the coalescence of the lowest two bending mode frequencies as illustrated in figure 10. It was mentioned in the discussion of equations (19) and (20) that the inclusion of both rotary inertia and shear flexibility in the analysis admits the two additional motions termed the thickness-shear and thickness-twist modes. In general, both of these motions produce transverse deflections $w(x,y,t)$ perpendicular to the panel's undeformed middle surface. In such cases there is the possibility of frequency coalescence from all three types of motion since a transverse deflection from any of the possible modes will influence the aerodynamic loading which in turn may change the panel response.

For a simply supported panel with an isotropic core there is no transverse motion associated with the thickness-twist modes (see eqs. (81)). In this case, only the bending and thickness-shear modes interact with the aerodynamics. The typical variation of the in-vacuo ($\lambda = 0$) values of these bending and thickness-shear frequencies with the

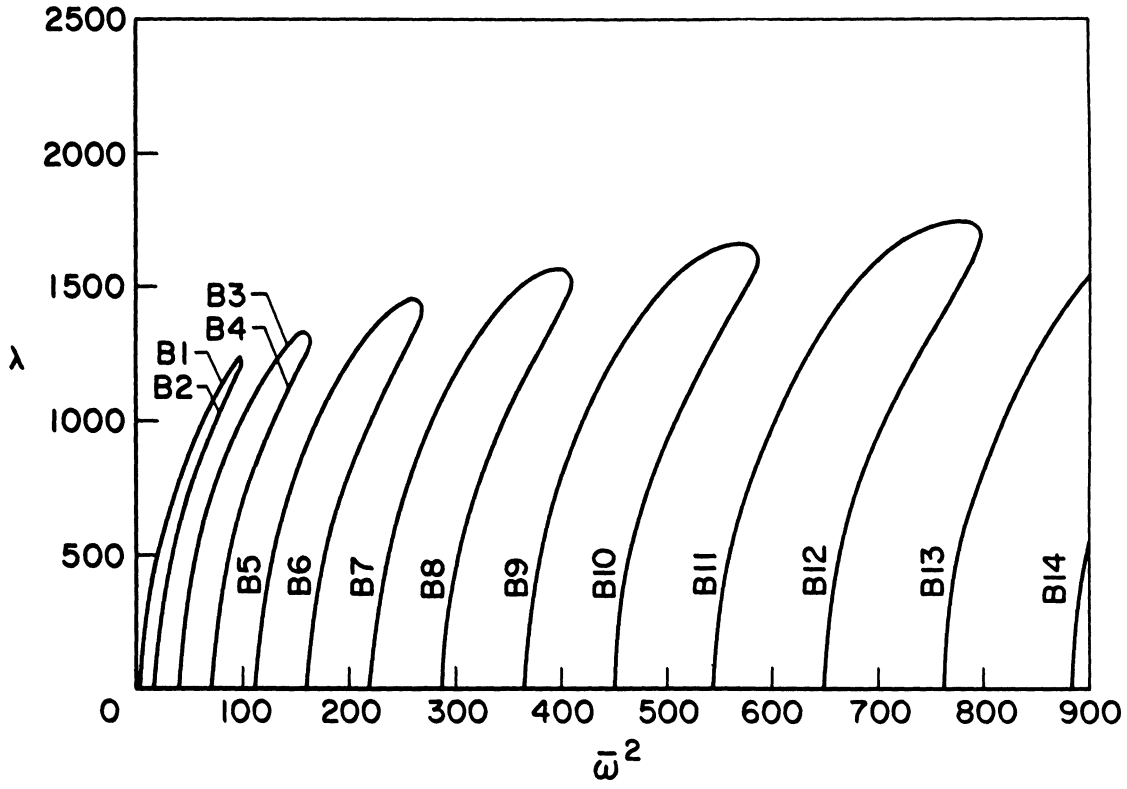

Figure 10.- Frequency loops corresponding to r = 2 of figure 9 but with f/c = 0.01; n = η = 1, r = 2, k_x = -4, k_y = 0, χ = 0; simply supported edges.

rotary inertia parameter, χ, is shown in figure 11.[10] The first 14 bending frequencies, labeled B1 through B14, are nearly independent of χ whereas the first two thickness-shear frequencies, labeled TS1 and TS2, are approximately inversely proportional to χ. (These bending and thickness-shear frequencies were computed from eqs. (20).)

Except for χ, the panel parameters used to compute the frequency curves in figure 11 are the same as used in figure 10, where $\chi = 0$. Thus, the $\chi = 0$ values for the bending frequencies of figure 11 correspond to the intersection of the frequency loops with the $\lambda = 0$ line in figure 10. For $\chi > 0$, the frequency loops of figure 10 are altered as a result of the thickness-shear modes. This is illustrated in figures 12(a) to 12(e).

The most striking feature of figure 12(a) ($\chi = 0.002$) is that the fifth bending frequency (B5) has broken away from the sixth bending frequency (B6). The B6 frequency now coalesces with B7 while B5 presumably coalesces with some higher frequency mode. Note that for $\chi = 0$ (fig. 10), the first frequency loop determines λ_{cr} since each succeeding loop coalesces at successively larger values of λ. Of the first six frequency loops shown for $\chi = 0.002$ (fig. 12(a)) the first loop still coalesces at a smaller λ than the others. However, each

---

[10]For panels having identical faces, and cores which are light compared to the face sheet weight, the rotary inertia parameter is given, approximately, by

$$\chi \approx \left(\frac{\pi}{2}\right)^2 \left(\frac{c}{b}\right)^2 \left(1 + \frac{f}{c}\right)^2$$

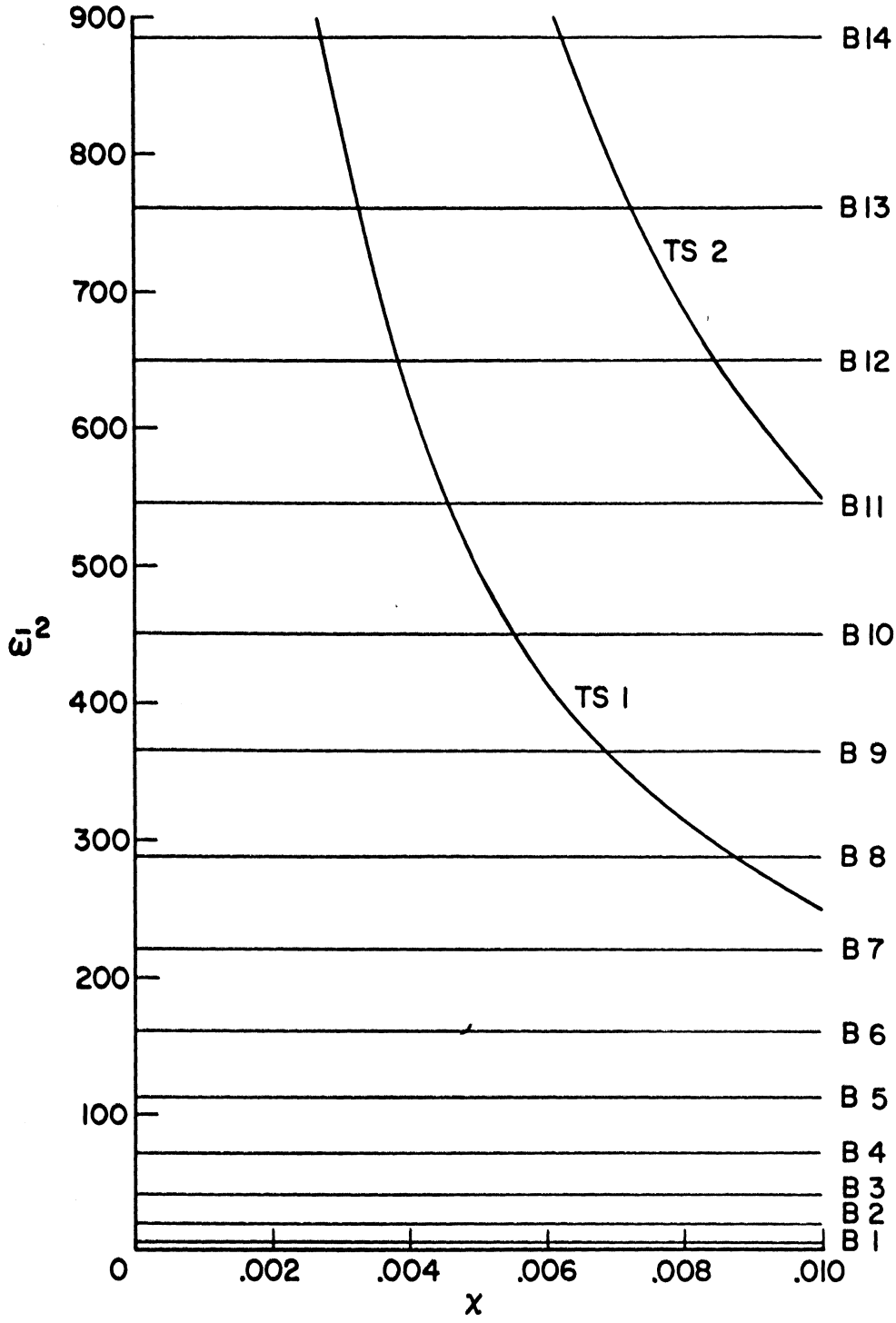

Figure 11.- Variation of in-vacuo bending and thickness-shear frequencies with rotary inertia parameter; $n = \eta = 1$, $r = 2$, $k_x = -4$, $k_y = 0$, $f/c = 0.01$, $\lambda = 0$; simply supported edges.

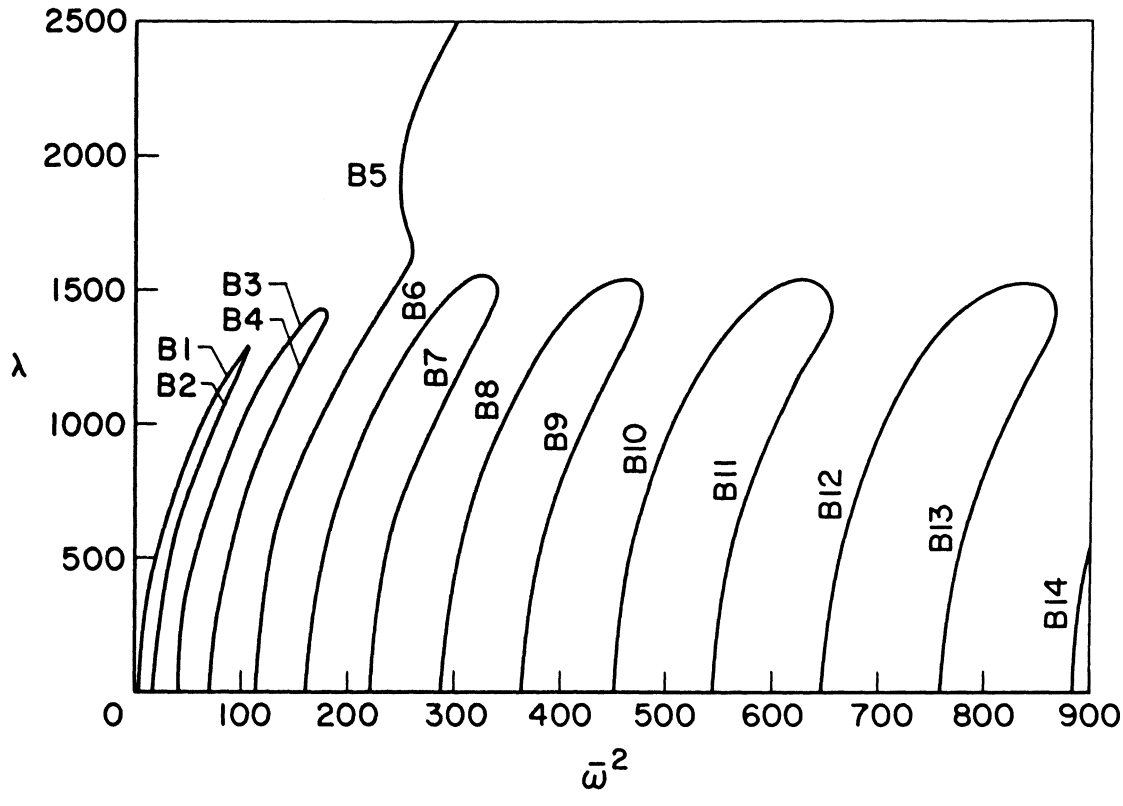

(a) $\chi = 0.002$

Figure 12.- Effect of rotary inertia on frequency loops of figure 10; $n = \eta = 1$, $r = 2$, $k_x = -4$, $k_y = 0$, $f/c = 0.01$; simply supported edges.

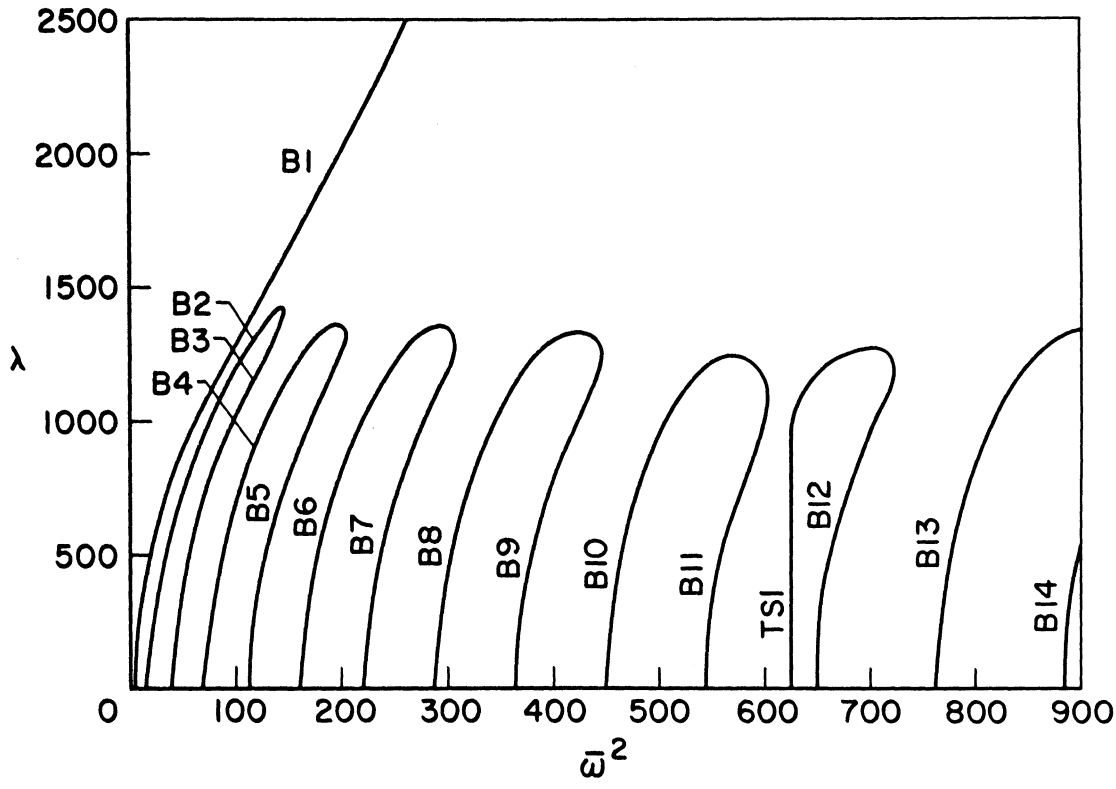

(b) $\chi = 0.004$

Figure 12.- Continued.

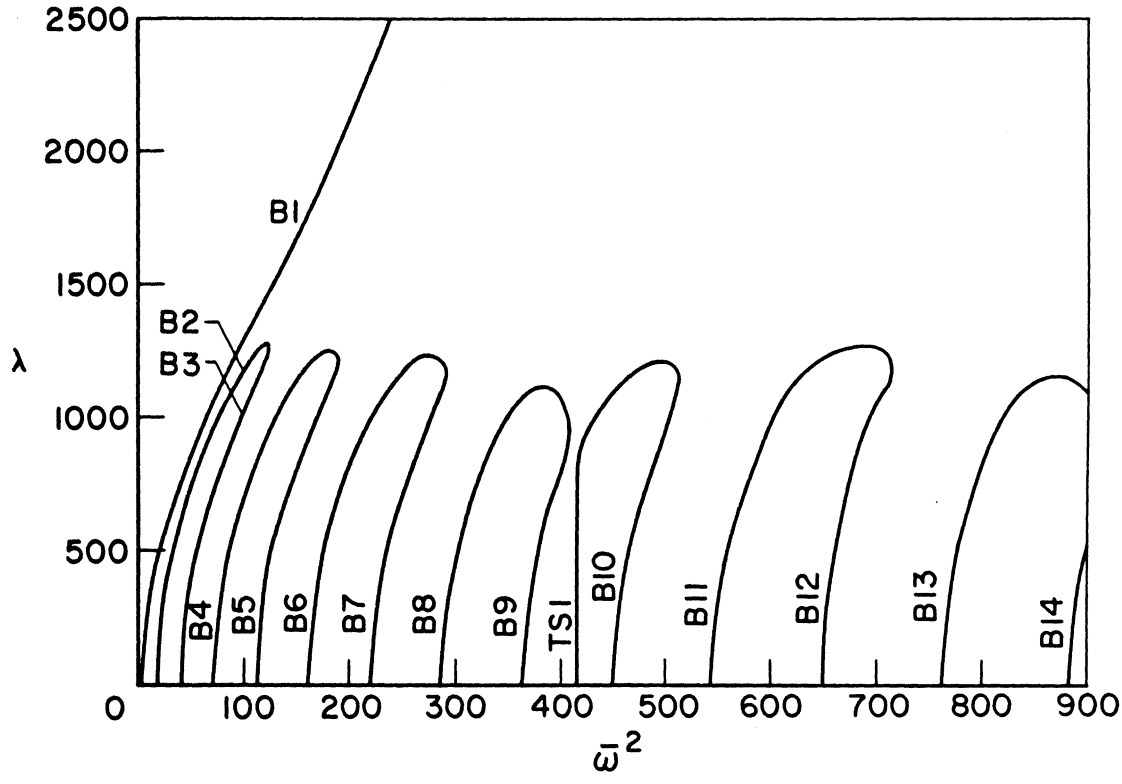

(c) $\chi = 0.006$

Figure 12.- Continued.

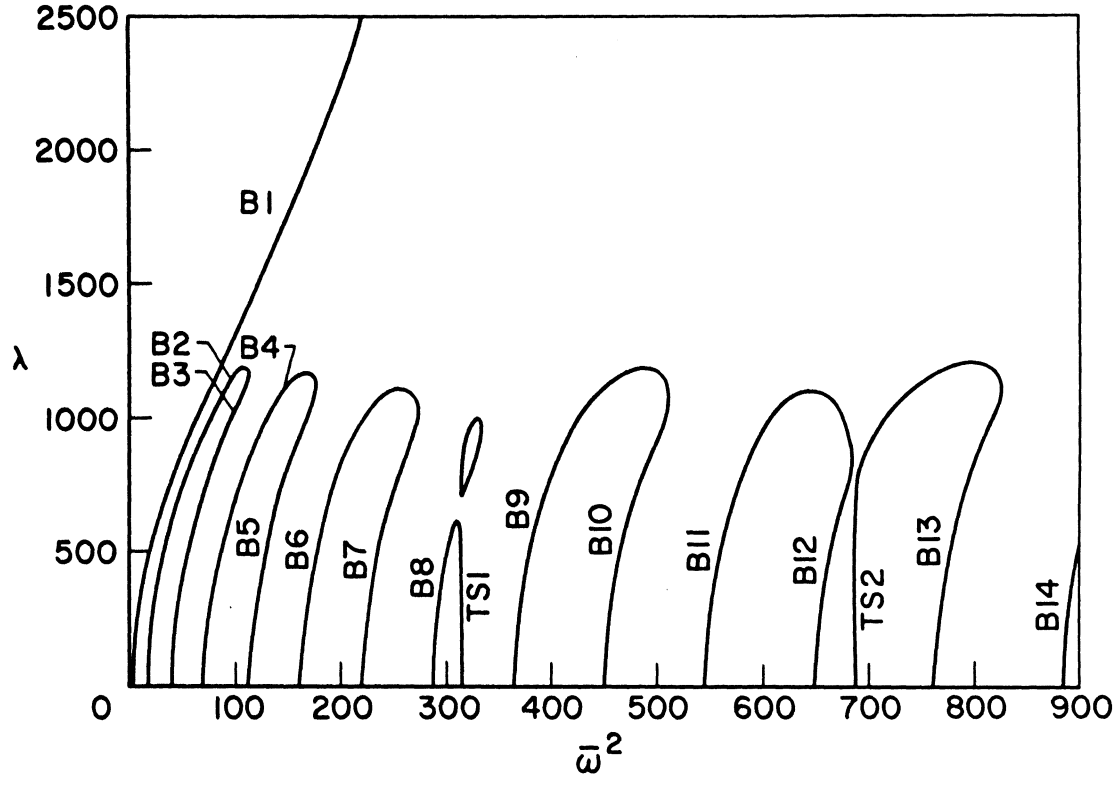

(d) X = 0.008

Figure 12.- Continued.

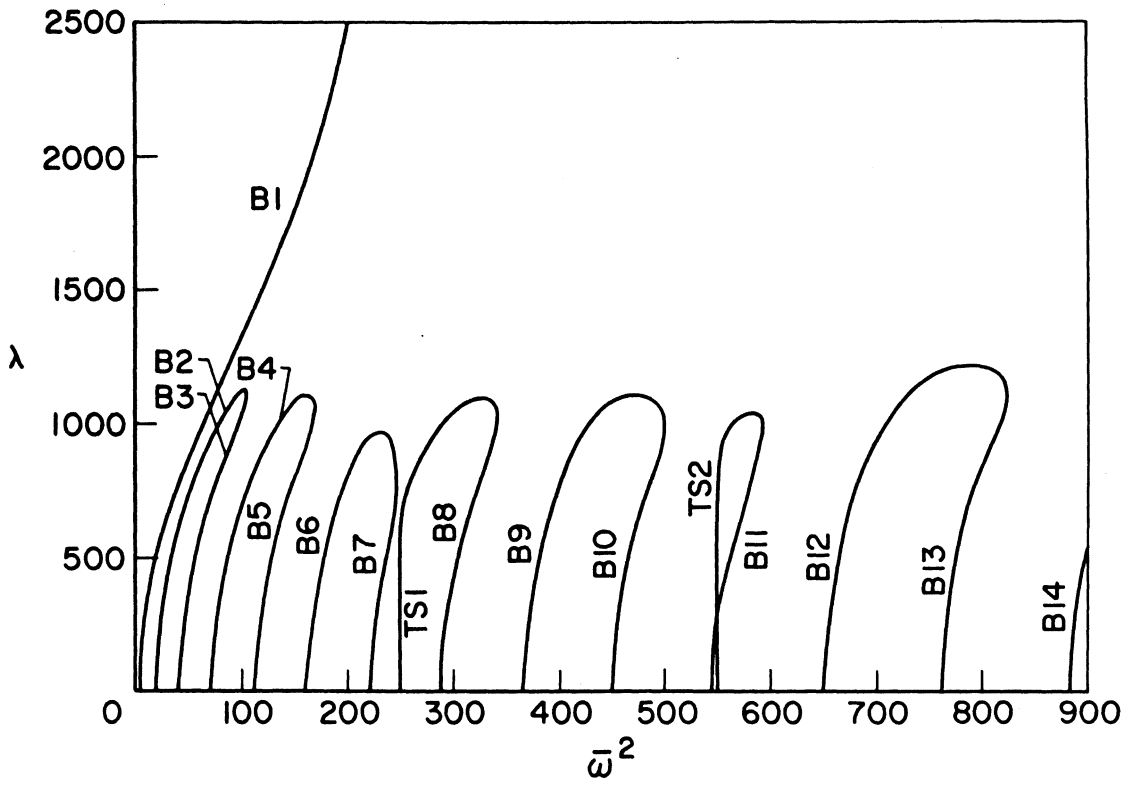

(e) $\chi = 0.010$

Figure 12.- Concluded.

succeeding loop does not coalesce at successively larger λ (note B12-B13). This raises the possibility that λ_{cr} may be determined by some still higher frequency modes.

Increasing χ to 0.004 results in additional changes in the modes which coalesce. As shown in figure 12(b), the B1 mode has now broken away from B2. In addition the first thickness-shear natural frequency (TS1) is near the B12 frequency, with which it coalesces. Of the seven frequency loops shown the fifth loop (formed by B10 and B11) coalesces at a smaller λ than the others. An increase in χ to 0.006 (fig. 12(c)) again changes the pattern and the fourth loop (formed by B8 and B9) coalesces at the smallest λ.

When χ is increased to 0.008 (fig. 12(d)) the B8 and TS1 frequencies coalesce and become complex at $\lambda = 616$. Note that this is 50 percent less than λ_{cr} for $\chi = 0$ (fig. 10). However, when λ is increased to 709, these frequencies become real again, making the motion of the corresponding modes stable. The motion remains stable until a second instability region is reached at $\lambda = 995$. This type of behavior (region of stability bounded above and below by unstable regions) was also noted in reference 23 for orthotropic panels mounted on deflectional spring supports.

For $\chi = 0.010$ (fig. 12(e)) the in-vacuo values of the B11 and TS2 frequencies are nearly equal. As λ increases to about 320 they become equal but remain real (i.e., the corresponding modes vibrate at the same frequency but are stable). The vibrations of these modes remain stable until λ is increased to 1042 where their frequencies finally coalesce.

This frequency crossover behavior, with the frequencies remaining real, is similar to results obtained in reference 24 for panels covering an enclosed cavity.

Another effect of the rotary inertia is that it makes the solution for λ_{cr} dependent on k_y. This differs from the solution of reference 4 where the frequency and crossflow loading terms always grouped in the characteristic equation as $\overline{\omega}^2 + n^2 k_y$, a change in k_y merely shifting the frequency loops along the $\overline{\omega}^2$ axis. This unique grouping does not occur for $\chi > 0$ (see eqs. (22c), (24), and (27)).

The sensitivity of the frequency loops to k_y for $\chi = 0.010$ is indicated by comparing figure 12(e) with figure 13. The only difference in the parameters selected for these figures is that $k_y = 0$ in figure 12(e) whereas $k_y = -4$ (tension load) in figure 13. One effect of the change from $k_y = 0$ to $k_y = -4$ is that the in-vacuo bending frequencies are increased from $\overline{\omega}^2$ to approximately $\overline{\omega}^2 + 4$. The in-vacuo thickness-shear frequencies, however, are essentially unaffected by this change in k_y. The frequency loops for both values of k_y are quite similar, being formed by the same frequency pairs and coalescing at corresponding values of λ that differ by less than 2 percent. Thus, at least for the parameters considered, the crossflow loading term k_y has only a minor effect on frequency coalescence.

C. Effects of an Orthotropic Core

One of the effects of an orthotropic core ($r_x \neq r_y$) is illustrated in figure 14, where $r_x = 2.0$ and $r_y = 0.5$ (all other conditions are the same as in fig. 12(d)). It is seen that the thickness-twist frequencies (TT1, TT2, and TT3) are no longer independent of λ and that

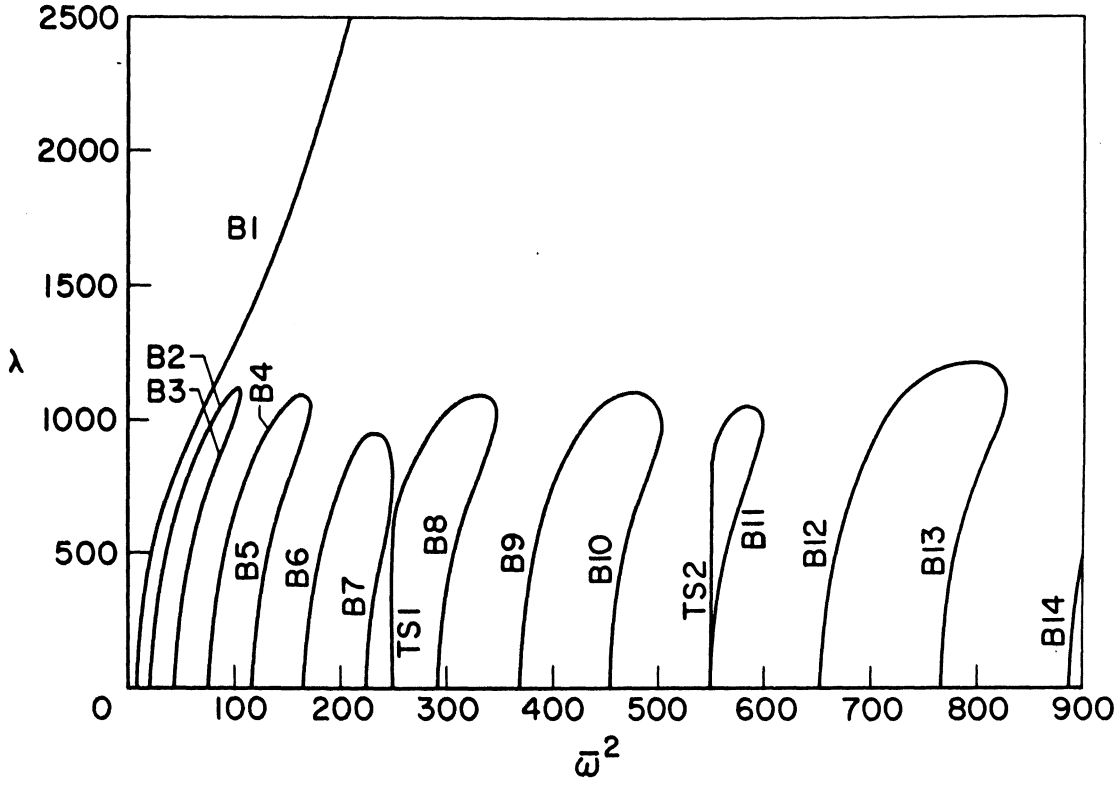

Figure 13.- Effect of crossflow loading on frequency loops of figure 12(e); $n = \eta = 1$, $r = 2$, $k_x = -4$, $k_y = -4$, $f/c = 0.01$, $\chi = 0.010$; simply supported edges.

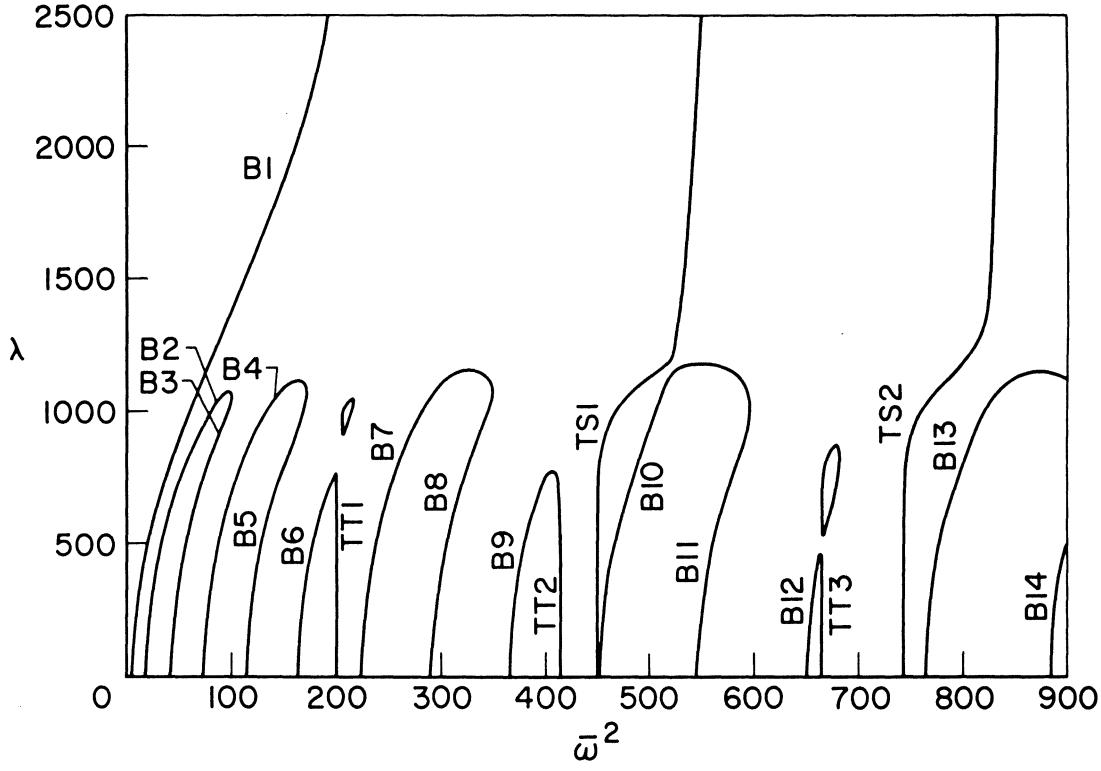

Figure 14.- Illustration of thickness-twist frequency coalescence; orthotropic core and simply supported edges; $n = \eta = 1$, $r_x = 2$, $r_y = 0.5$, $k_x = -4$, $k_y = 0$, $f/c = 0.01$, $\chi = 0.008$, $\mu = 0.3$.

they now coalesce with the bending frequencies. For this particular choice of parameters it is also seen that the first two thickness-shear frequencies (TS1 and TS2) do not coalesce with their adjacent bending frequencies. Their behavior is now similar to the first bending frequency.

In the remaining examples of panels having orthotropic cores the rotary inertia has been neglected ($\chi = 0$) and λ_{cr} is determined from the coalescence of the lowest two bending frequencies. This facilitates the determination of λ_{cr} so that the general effects of changes in core orthotropy can be made with much less numerical computation.

Figure 15 shows the variation in the flutter dynamic pressure parameter (λ_{cr} or λ'_{cr}) with length-width ratio ($\eta = a/b$) for three values of the shear flexibility parameter r_y (or r'_y) and with r_x (or r'_x) held constant. All results are presented in terms of parameters defined by the shortest panel dimension (length or width). Thus, for $a/b \leq 1$ the primed parameters (defined by a) must be used whereas for $a/b \geq 1$ the unprimed parameters (defined by b) must be used. The solid curves are from the exact solutions derived herein and were computed with $f/c = 0.01$ in the equation for τ. For the isotropic core ($r_x = r_y$, $r'_x = r'_y$) the flutter boundary coincides with the results of references 4 and 5 wherein the face sheet bending stiffness was neglected ($\tau = f/c = 0$). The flutter boundaries for the orthotropic cores ($r_y \gtrless r_x$) bracket the boundary for the isotropic core except at $a/b = 0$ where the solution is independent of r_y (see eqs. (26), (42), and (53)). The dashed curves in figure 15 are from the two-mode

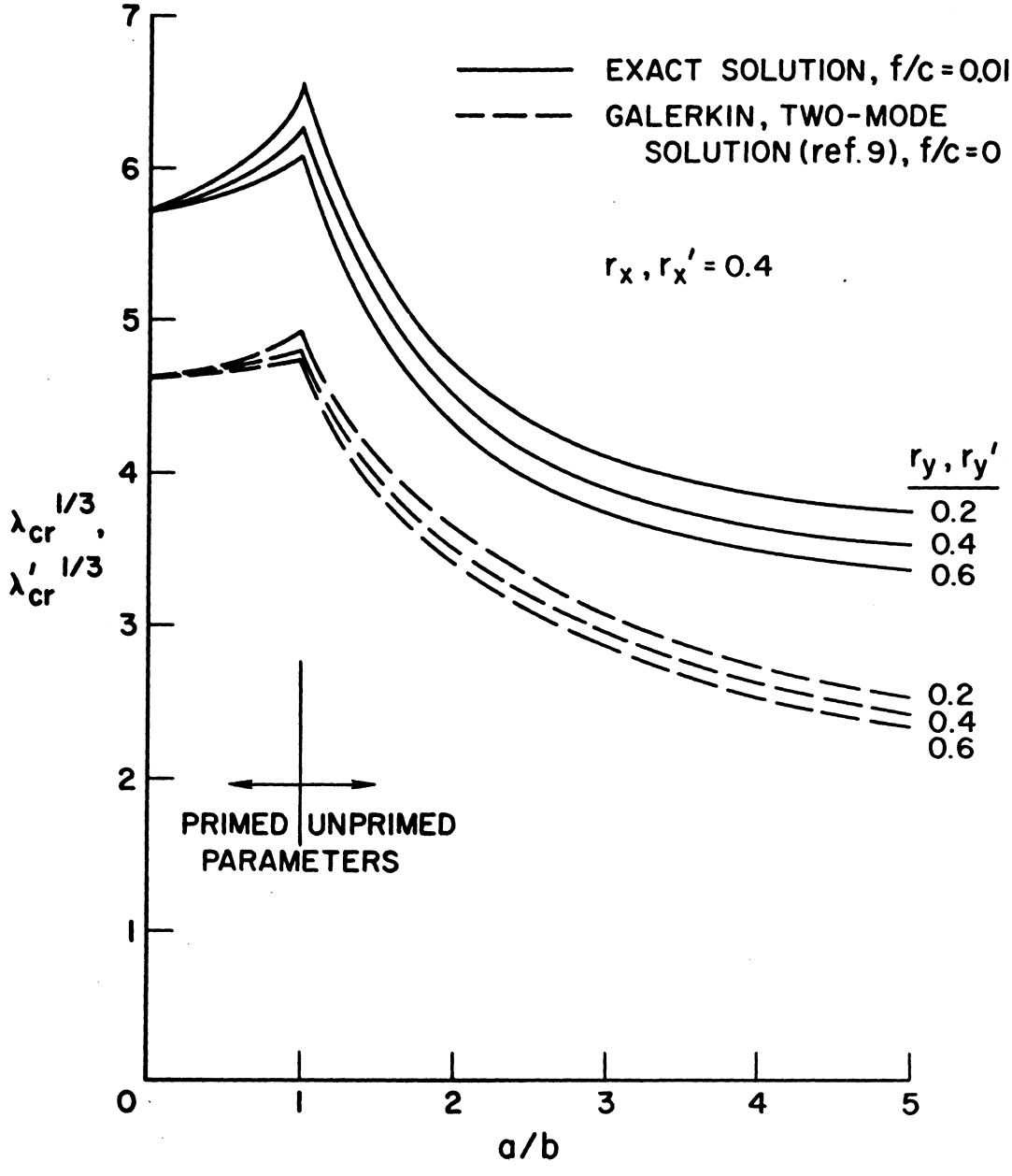

Figure 15.- Comparison of flutter boundaries for simply supported panels as predicted by two-mode Galerkin solution and exact solution; $k_x = k_y = \chi = 0$, $n = 1$, $\mu = 0.3$.

Galerkin solution of reference 9.[11] This approximate solution predicts the correct trends for the range of parameters shown but underestimates the exact solutions by a considerable amount.

The frequency loops for the square panel having $r_x = 0.4$ and $r_y = 0.2$ (peak of solid and dashed boundaries in fig. 15) are shown in figure 16. The loop predicted by the two-mode Galerkin solution is symmetric about a line midway between the two in-vacuo frequencies ($\lambda = 0$), whereas the exact loop leans to the right and coalesces at a considerably larger value of λ. Note that the Galerkin solution correctly predicts the in-vacuo frequencies because the two modes used in the Galerkin solution are the exact mode shapes for $\lambda = 0$.

Figure 17 indicates the variation in λ_{cr} with changes in the core shear flexibilities (r_x, r_y) for a square panel. The solid and dashed curves are for clamped and simply supported leading and trailing edges, respectively. These curves show the variation in λ_{cr} with r_y for $r_x = 0.4$. The circular symbols locate solutions for isotropic cores and indicate changes in λ_{cr} with changes in r_x for r_y = constant. By noting the changes that occur in λ_{cr} as r_x and r_y are varied, from initial equal values to final equal values, one can determine the relative importance of r_x and r_y.

---

[11] In reference 9 this two-mode solution was derived for the more general case of a panel having both orthotropic bending and orthotropic shear stiffnesses. The results shown in figure 15 are for isotropic bending stiffness and the corresponding two-mode solution, in terms of the notation used herein, is given in appendix C.

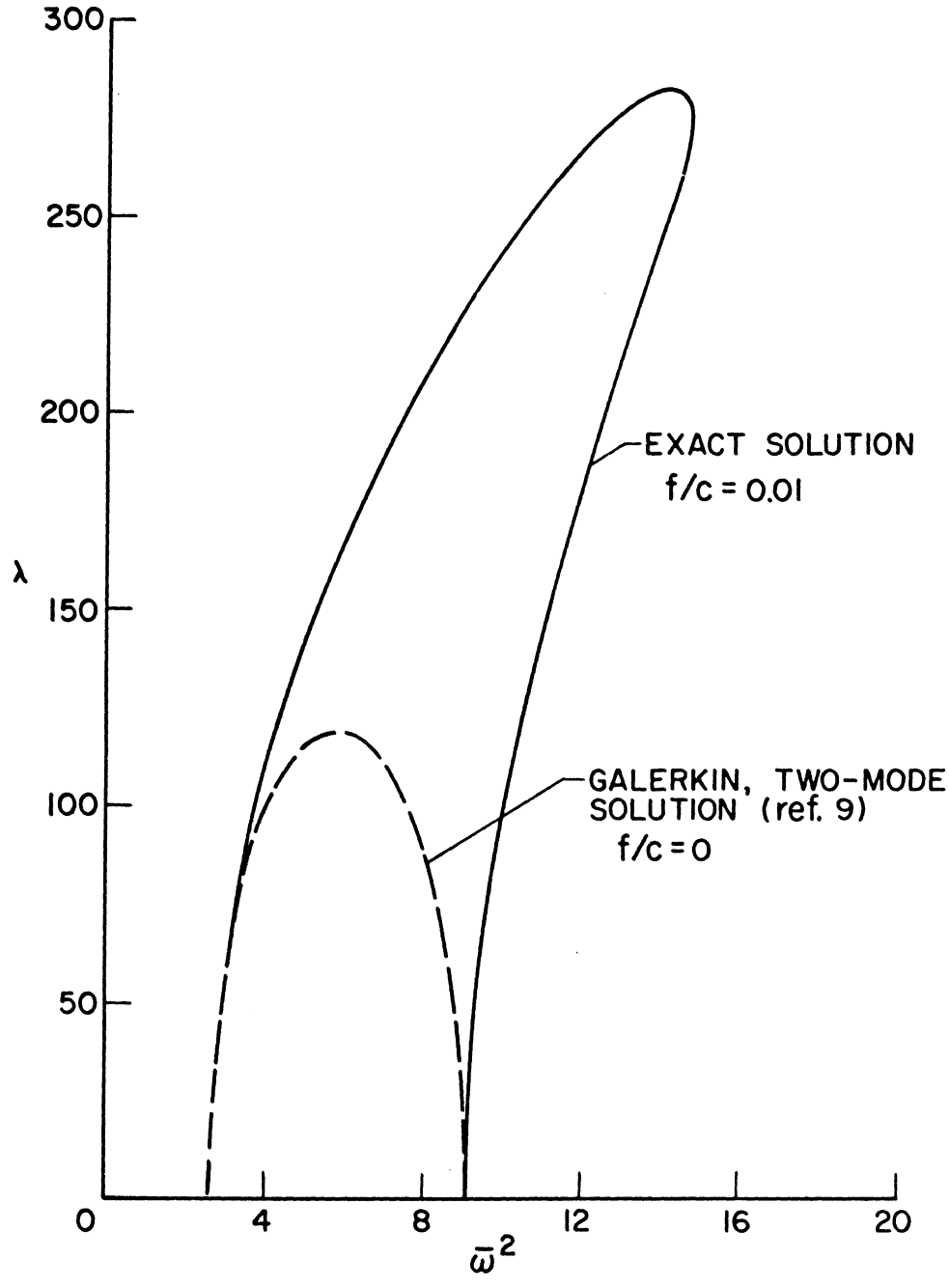

Figure 16.- Comparison of frequency loops for a simply supported panel having an orthotropic core, as predicted by two-mode Galerkin and exact solutions; $n = \eta = 1$, $r_x = 0.4$, $r_y = 0.2$, $k_x = k_y = \chi = 0$, $\mu = 0.3$.

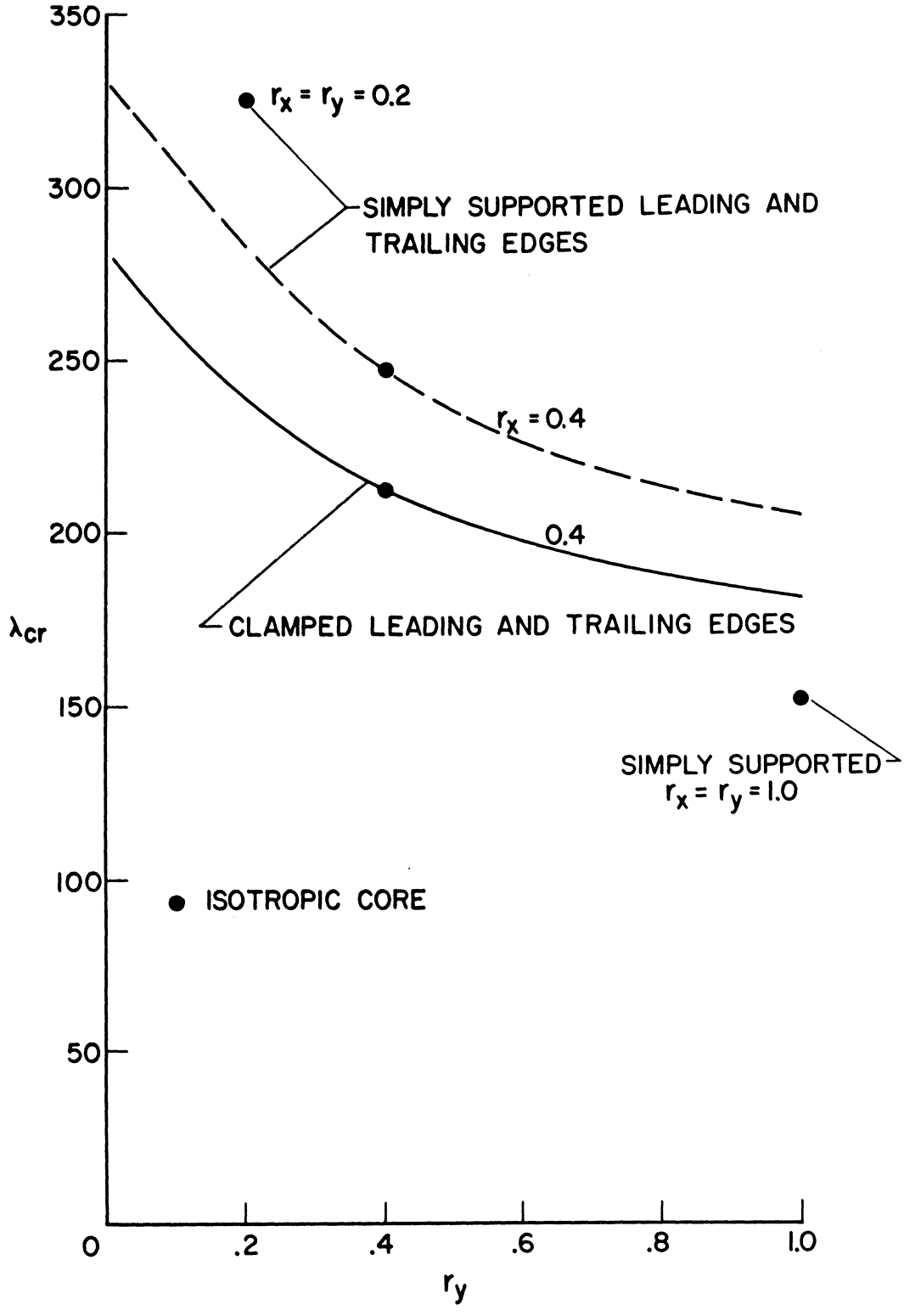

Figure 17.- Variation in λ_{cr} with crossflow shear flexibility; $n = \eta = 1$, $k_x = k_y = \chi = 0$, $f/c = 0.01$, $\mu = 0.3$; side edges simply supported.

For example, consider the simply supported panel. Starting at $r_x = r_y = 0.2$, λ_{cr} equals 325. If one follows the path r_y = constant to $r_x = 0.4$, $r_y = 0.2$ to $r_y = 1.0$ (along the $r_x = 0.4$ curve), and finally r_y = constant (i.e., 1.0) to $r_x = 1.0$, λ_{cr} ends up at 153, a change in λ_{cr} of 172 (53 percent). Of this amount, 29 percent is due to the change in r_x and 24 percent is due to the change in r_y. Thus, for a square panel, the two shear flexibility parameters appear to be of comparable importance.

There is apparently no experimental flutter data for sandwich type panels available for comparison with the results predicted by the theory presented herein. The validity of the theory's representation of orthotropic cores such as honeycomb, however, appears to be established by the comparison between experimental and theoretical vibration results reported in reference 25.

V. CONCLUDING REMARKS

On the basis of static aerodynamic theory, an exact solution is obtained for the supersonic flutter of flat rectangular, biaxially stressed sandwich panels. The airflow is assumed to be parallel to simply supported side edges. The leading and trailing edges are either simply supported or clamped. The mathematical model describing the panel motion includes terms which account for rotary inertia, face sheet bending deformations, and transverse shear deformations of an orthotropic core, such as honeycomb. Numerical results are presented in graphical form to illustrate the effects of these physical properties on the flutter solution. For the range of parameters considered, the following conclusions are noted.

The face sheet bending stiffness has a negligible effect on flutter if the faces are thin compared to the core thickness. In such cases flutter boundaries can be adequately predicted by somewhat simpler theories that treat the face sheets as membranes. The face sheet bending stiffness becomes more important as the face to core thickness ratio increases. This is especially true for panels having relatively flexible cores.

The combined influences of rotary inertia and core shear flexibility can markedly change the frequency coalescence behavior. Failure to account for this combined effect can lead to significant overestimates of flutter dynamic pressure values. The rotary inertia also causes the flutter solution to be slightly dependent on the crossflow in-plane loading.

The directional shear stiffness properties of the core are of comparable importance for square panels. As the panel width increases, the importance of the shear stiffness in the crossflow direction decreases.

A two-mode Galerkin solution gives the correct trends for the flutter boundary of a panel having an orthotropic core but significantly underestimates the exact solution. Also, an existing exact solution for panels having isotropic cores is shown to be correct only for certain restricted cases, the solution having been obtained from a differential equation and boundary conditions which are incomplete.

VI. APPENDIXES

The following appendixes include explanatory information concerning the panel theories of references 14 and 15, the in-vacuo mode shapes, and the Galerkin solution of reference 9.

A. Stiffness and Inertia Properties

The sandwich panel theory of reference 14 was developed in terms of orthotropic stiffnesses that are defined by the ratios of various internal forces and distortions. For example, the bending stiffness D_x is defined as the ratio of moment M_x to curvature $w_{,xx}$ when no other forces or moments are acting. This approach is applicable to a wide variety of panel constructions (e.g., honeycomb core, corrugation stiffened) but requires a separate evaluation of the stiffnesses.

The sandwich panel theory of reference 15 applies to an isotropic panel construction for which the form of the face sheet and core deformations are specified. The strain energy of the structure is expressed in terms of the assumed deformations so that differential equations of equilibrium and their corresponding boundary conditions can be obtained by a variational procedure. The coefficients of the virtual displacements appearing in the boundary condition equations are expressions involving various panel distortions ($w_{,xx}$, for example) and the elastic and geometric properties of the core and faces. Physically, these coefficients are the boundary forces associated with the corresponding virtual displacements. Hence, they can be used to define the panel stiffnesses.

The approach of reference 15 is easily adapted to define the stiffnesses for a panel having isotropic face sheets and a core with

orthotropic shear moduli (G_{c_x}, G_{c_y}). (The extensional stiffnesses of the core are neglected.) The expressions for these stiffnesses, defined in the manner of reference 14, are given in table I.

The sandwich panel theories of references 14 and 15 do not include inertia forces. Inclusion of the transverse inertia loading is straightforward; inclusion of inertia loadings due to longitudinal and rotational motions requires careful consideration of the panel's elastic deformations, the position of its center of mass, and its elastic axis location.

The panel deformations (as considered in ref. 15) occurring in the x, z-plane are illustrated in figure 18. The slope of the panel faces, $\partial w/\partial x$, is comprised of a core shear contribution (γ_{c_x}) and an angular contribution (α_{c_x}). The quantities γ_{c_x} and α_{c_x} are defined with respect to the core orientation given by the line ab. Alternately, $\partial w/\partial x$ is comprised of the angles γ_x and α_x, which are defined with respect to the line cd drawn between the midpoints of the face sheets.

The angle γ_x is related to the transverse shear stiffness D_{Q_x}, as defined in the manner of reference 14, by the equation $\gamma_x = Q_x/D_{Q_x}$. Thus

$$\alpha_x = w_{,x} - \frac{Q_x}{D_{Q_x}} \tag{A1}$$

gives the angle α_x in terms of w and Q_x/D_{Q_x} which are considered to be unknowns in equations (1). From figure 18, α_x is also seen to be related to the x-components of the displacements of the face midpoints (u_1 and u_2) by the relation

TABLE I.- STIFFNESS AND MASS PROPERTIES FOR SANDWICH

PANELS HAVING HONEYCOMB TYPE CORES

	Nonidentical Faces	Identical Faces
D_{f_1}, D_{f_2}	$\frac{E_{f_1} f_1^3}{12(1 - \mu^2)}, \quad \frac{E_{f_2} f_2^3}{12(1 - \mu^2)}$	$\frac{E_f f^3}{12(1 - \mu^2)}$
D_s	$\frac{(E_{f_1} f_1)(E_{f_2} f_2)(c)^2 \left(1 + \frac{f_1 + f_2}{2c}\right)^2}{(E_{f_1} f_1 + E_{f_2} f_2)(1 - \mu^2)}$	$\frac{E_f f c^2 \left(1 + \frac{f}{c}\right)^2}{2(1 - \mu^2)}$
D_{Q_x}, D_{Q_y}	$G_{c_x} c \left(1 + \frac{f_1 + f_2}{2c}\right)^2, \quad G_{c_y} c \left(1 + \frac{f_1 + f_2}{2c}\right)^2$	$G_c c \left(1 + \frac{f}{c}\right)^2$
τ	$\frac{D_{f_1} + D_{f_2}}{D_s}$	$\frac{1}{3}\left(\frac{\frac{f}{c}}{1 + \frac{f}{c}}\right)^2$
ρ_m	$\rho_c c + \rho_{f_1} f_1 + \rho_{f_2} f_2$	$\rho_c c + 2\rho_f f$
I_o	$\rho_{f_1} f_1 d_1^2 + \rho_{f_2} f_2 d_2^2$	$2\rho_f f \left(\frac{c}{2}\right)^2 \left(1 + \frac{f}{c}\right)^2$
d_1, d_2	$\frac{E_{f_2} f_2 c}{E_{f_1} f_1 + E_{f_2} f_2} \left(1 + \frac{f_1 + f_2}{2c}\right), \quad \frac{E_{f_1} f_1 c}{E_{f_1} f_1 + E_{f_2} f_2} \left(1 + \frac{f_1 + f_2}{2c}\right)$	$\frac{c + f}{2}$
$\bar{e}$	$d_1 - \frac{c + f_1}{2}$	0.0

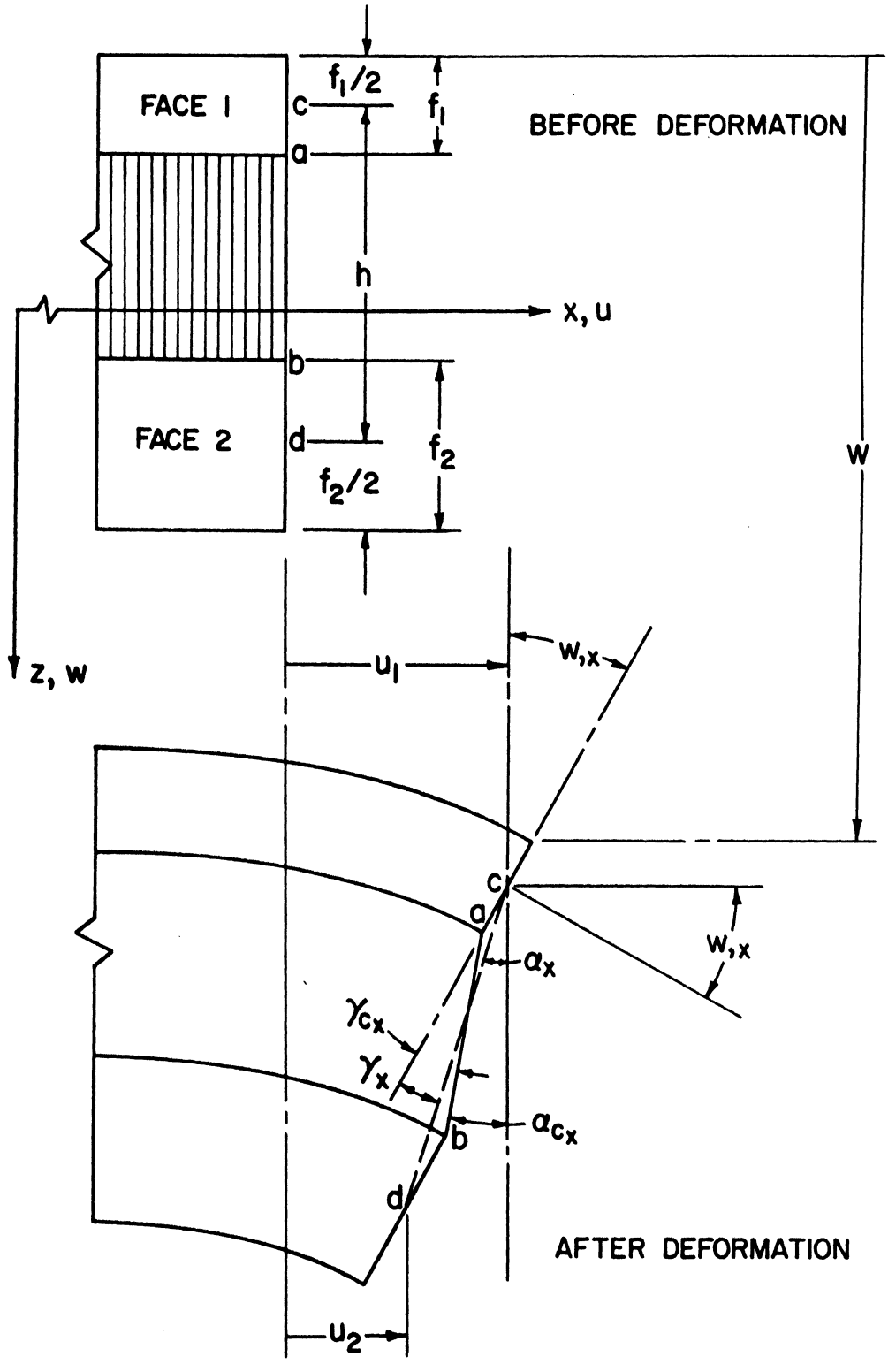

Figure 18.- Deformed panel geometry.

$$\alpha_x = \frac{u_1 - u_2}{h} \tag{A2}$$

where h is the distance between the midpoints of the two faces.

The interpretation of α_x and its relation to the elastic axis can be determined from figure 19. This figure is a plot of the x-components of the displacements shown in figure 18. The midpoint displacement of face i is u_i. It is associated with the axial force N_{x_i} acting on face i. The total axial force is $N_x = N_{x_1} + N_{x_2}$ which is used to define an effective displacement

$$\bar{u} = \frac{u_1 E_{f_1} f_1 + u_2 E_{f_2} f_2}{E_{f_1} f_1 + E_{f_2} f_2} \tag{A3}$$

The use of equation (A3) to eliminate either u_1 or u_2 from equation (A2) gives

$$\left.\begin{aligned} u_1 &= \bar{u} + d_1 \alpha_x \\ u_2 &= \bar{u} - d_2 \alpha_x \end{aligned}\right\} \tag{A4}$$

where

$$\left.\begin{aligned} d_1 &= \left(\frac{E_{f_2} f_2}{E_{f_1} f_1 + E_{f_2} f_2}\right) h \\ d_2 &= \left(\frac{E_{f_1} f_1}{E_{f_1} f_1 + E_{f_2} f_2}\right) h \\ d_1 + d_2 &= h = c + \frac{f_1 + f_2}{2} \\ \alpha_x &= \frac{u_1 - u_2}{h} = w_{,x} - \frac{Q_x}{D Q_x} \end{aligned}\right\} \tag{A5}$$

The virtual work of the axial forces N_{x_i} is

$$\delta W = N_{x_1} \delta u_1 + N_{x_2} \delta u_2$$

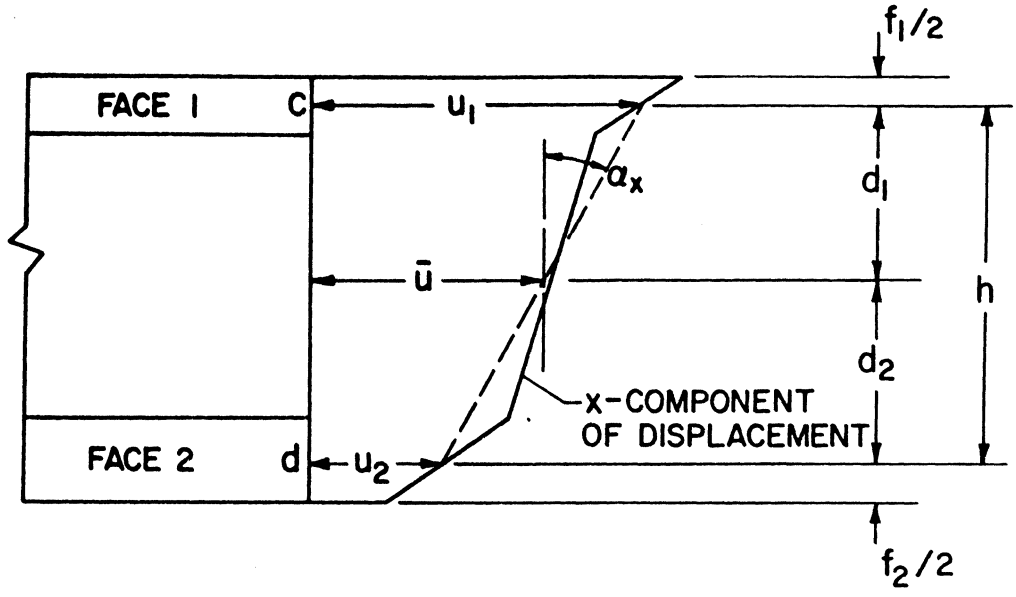

Figure 19.- Elastic axis location and variation of x-component of displacement across the panel thickness.

which, if equations (A4) are used, becomes

$$\delta W = (N_{x_1} + N_{x_2})\delta\bar{u} + (N_{x_1}d_1 - N_{x_2}d_2)\delta\alpha_x \tag{A6}$$

Thus, the work due to the axial face sheet loads N_{x_1} and N_{x_2} is equivalent to the work done by the moment of these forces (about the point defined by d_1 (or d_2)) acting through the angle α_x, plus the work done by the total force $N_{x_1} + N_{x_2}$ acting through the displacement $\bar{u}$. Hence, the term d_1 (or d_2) locates the elastic axis of the panel cross section.

For face i, the virtual work of the inertial forces due to the x and y components of the middle surface displacements (u_i and v_i, respectively) is

$$\delta W_i = -\int_{x=0}^{a}\int_{y=0}^{b} \rho_{f_i} f_i \left(\frac{\partial^2 u_i}{\partial t^2}\,\delta u_i + \frac{\partial^2 v_i}{\partial t^2}\,\delta v_i\right)dx\,dy$$

Inclusion of this term (for both faces) in the analysis of reference 15 yields the following equation of motion for the rotation of a differential element about the elastic axes perpendicular to the xz-plane.

$$D_s\left\{w_{,xxx} + w_{,xyy} + \frac{Q_x}{D_s} - \frac{1}{D_{Q_x}}\left[Q_{x,xx} + \left(\frac{1-\mu}{2}\right)Q_{x,yy}\right] - \left(\frac{1+\mu}{2}\right)\frac{Q_{y,xy}}{D_{Q_y}}\right\}$$

$$= \left(\rho_{f_1} f_1 d_1^2 + \rho_{f_2} f_2 d_2^2\right)\frac{\partial^2\left(w_{,x} - \frac{Q_x}{D_{Q_x}}\right)}{\partial t^2} - \left(\rho_{f_2} f_2 d_2 - \rho_{f_1} f_1 d_1\right)\frac{\partial^2\bar{u}}{\partial t^2} \tag{A7}$$

The left hand side of this equation represents the restoring moment about the elastic axis due to the elastic forces. The first term on the right hand side is the mass moment of inertia (I_o) of the face sheets

about the elastic axis, multiplied by the angular acceleration of the face sheets about the elastic axis; hence this term can be interpreted as the moment due to rotary inertia. The last term on the right hand side arises because the center of mass does not necessarily coincide with the elastic axis. The quantity $(\rho_{f_2} f_2 d_2 - \rho_{f_1} f_1 d_1)$ is equal to $d_{cm}(\rho_{f_1} f_1 + \rho_{f_2} f_2)$ where d_{cm} is the distance from the elastic axis to the center of mass of the two face sheets and $(\rho_{f_1} f_1 + \rho_{f_2} f_2)$ is the total mass of the two faces. The acceleration $\partial^2 \overline{u}/\partial t^2$ is the acceleration of the elastic axis in the x-direction.

It is noted that equation (A7) is a particular case of the general vector equation of motion (ref. 26)

$$\vec{M}_p = \dot{\vec{H}}_p + \vec{\rho}_{cm} \times m\ddot{\vec{r}}_p$$

where $\vec{M}_p$ is the moment of applied forces about an arbitrary point p; $\dot{\vec{H}}_p$ is the time rate of change of angular momentum about p; $\vec{\rho}_{cm}$ is the vector distance from p to the center of mass of a system of mass m; and $\ddot{\vec{r}}_p$ is the acceleration of the point p. In equation (A7), point p corresponds to the elastic axis.

The equation of motion for the x-direction is

$$-N_{x,x} + N_{xy,y} = (\rho_{f_1} f_1 + \rho_{f_2} f_2) \frac{\partial^2}{\partial t^2} (\overline{u} - d_{cm}\alpha_x) \tag{A8}$$

The term $(\overline{u} - d_{cm}\alpha_x)$ is simply the x-component of the center of mass displacement.

It is seen that equations (A7) and (A8) are dynamically coupled (i.e., $\partial^2 \overline{u}/\partial t^2$ and $\partial^2 \alpha_x/\partial t^2$ appear in both equations). However, for the case of identical face sheets, or faces which satisfy the relation

$$\frac{E_{f_1}}{\rho_{f_1}} = \frac{E_{f_2}}{\rho_{f_2}} \tag{A9}$$

the elastic axis and center of mass coincide and the equations uncouple. In this case equation (A7) reduces to equation (1b). Hence, the solutions to equations (1a), (1b), and (1c) that are obtained herein are strictly applicable to panels having identical face sheets, or face sheets satisfying equation (A9). Also, the stipulation that N_x and N_y are constant assumes that the inertia force due to longitudinal acceleration of the center of mass is negligible.

It should also be noted that the inertial forces due to the rotational accelerations of the core and faces about their midpoints have been neglected. For typical sandwich construction of lightweight cores and thin face sheets, these inertia contributions are expected to be negligible compared to the inertia of the face sheets about the elastic axis.

B. In-vacuo Bending and Thickness-Shear Mode Shapes for a Simply Supported Sandwich Beam

The two differential equations governing the beam behavior ($\eta = 0$) are obtained from equation (82).

$$\begin{bmatrix} L_{11} & L_{12} \\ L_{21} & L_{22} \end{bmatrix} \begin{Bmatrix} w \\ Q_x \end{Bmatrix} = \begin{Bmatrix} 0 \\ 0 \end{Bmatrix} \tag{B1}$$

The differential operators L_{ij} are given by equations (83) except that all terms involving derivatives with respect to y are omitted. For simply supported edges at $x = 0$ and $x = a$ the boundary conditions are

$$\left.\begin{aligned} w &= 0 \\ \gamma_{x,x} = (Q_x/D_{Q_x})_{,x} &= 0 \\ w_{,xx} &= 0 \end{aligned}\right\} \tag{B2}$$

Expressions for the transverse deflection w and the shear angle γ_x that satisfy the boundary conditions are

$$\left.\begin{aligned} w(x,t) &= A_m \sin \frac{m\pi x}{a}\, e^{i\omega t} \\ \gamma_x(x,t) &= \frac{Q_x(x,t)}{D_{Q_x}} = \frac{B_m}{D_{Q_x}} \cos \frac{m\pi x}{a}\, e^{i\omega t} \end{aligned}\right\} \tag{B3}$$

The above expressions for w and γ_x also satisfy the differential equations, provided that

$$\begin{bmatrix} -\tau m^4 + m^2 k_x' + \bar{\omega}'^2 & -m \\ m(-m^2 + \chi'\bar{\omega}'^2) & 1 - r_x'(-m^2 + \chi'\bar{\omega}'^2) \end{bmatrix} \begin{Bmatrix} A_m \\ \dfrac{a^3}{\pi^3 D_s} B_m \end{Bmatrix} = \begin{Bmatrix} 0 \\ 0 \end{Bmatrix} \tag{B4}$$

For the nontrivial case, equation (B4) is satisfied by equating the determinant of the square matrix to zero. The resulting equation can be solved for $\bar{\omega}'^2$ and yields the following frequency equation:

$$\bar{\omega}_{\substack{B \\ TS}}'^2 = \frac{2[m^4 + (\tau m^4 - m^2 k_x')(1 + r_x' m^2)]}{[1 + (r_x' + \chi')m^2 + r_x'\chi'(\tau m^4 - m^2 k_x')] \pm \sqrt{[1 + (r_x' - \chi')m^2 - r_x'\chi'(\tau m^4 - m^2 k_x')]^2 + 4\chi' m^2}} \tag{B5}$$

As in the case of the panel ($\eta > 0$, eq. (20a)) the smaller solution for $\bar{\omega}'^2$ ($+\sqrt{\ }$) gives the frequencies of the bending modes ($\bar{\omega}_B'^2$), and the larger solution ($-\sqrt{\ }$) gives the frequencies of the thickness-shear modes ($\bar{\omega}_{TS}'^2$).

The shapes of the bending and thickness-shear modes are obtained from the relation between A_m and B_m. This relation, determined from equation (B4), is

$$\left.\begin{aligned} \frac{\pi}{a}\left(\frac{A_m}{\frac{B_m}{D_{Q_x}}}\right) &= \frac{1}{m}\left[\frac{1 + r_x'\left(m^2 - \chi'\bar{\omega}_B'^2_{TS}\right)}{r_x'\left(m^2 - \chi'\bar{\omega}_B'^2_{TS}\right)}\right] \\ \text{or} \\ \frac{\pi}{a}\left(\frac{A_m}{\frac{B_m}{D_{Q_x}}}\right) &= \frac{m}{r_x'\left(-\tau m^4 + m^2 k_x' + \bar{\omega}_B'^2_{TS}\right)} \end{aligned}\right\} \qquad \text{(B6)}$$

When equations (B6) are used in conjunction with equations (B3), the following relation between the slope of the beam ($w_{,x}$) and the shear angle (γ_x) is obtained

$$\frac{\gamma_x}{w_{,x}} = \frac{r_x'\left(m^2 - \chi'\bar{\omega}_B'^2_{TS}\right)}{1 + r_x'\left(m^2 - \chi'\bar{\omega}_B'^2_{TS}\right)} \qquad \text{(B7)}$$

or

$$\frac{\gamma_x}{w_{,x}} = \frac{r_x'}{m^2}\left(\bar{\omega}_B'^2_{TS} + m^2 k_x' - \tau m^4\right)$$

It is recalled from appendix A that

$$w_{,x} = \alpha_x + \gamma_x \qquad \text{(B8)}$$

where α_x is the beam rotation about the elastic axis. The transverse deflection is thus

$$w = \int (\alpha_x + \gamma_x) dx$$

and is comprised of a contribution due to rotation and a contribution due to shear. The proportion of each contribution is determined as follows:

$$w = \int \left(\frac{\alpha_x}{w_{,x}} + \frac{\gamma_x}{w_{,x}} \right) w_{,x} \, dx$$

$$w = \int \left[\frac{1}{1 + r_x' \left(m^2 - \chi' \overline{\omega}_{B_{TS}}'^2 \right)} + \frac{r_x' \left(m^2 - \chi' \overline{\omega}_{B_{TS}}'^2 \right)}{1 + r_x' \left(m^2 - \chi' \overline{\omega}_{B_{TS}}'^2 \right)} \right] w_{,x} \, dx \qquad \text{(B9)}$$

where equations (B7) and (B8) have been used. Thus, the relative contribution to w (or $w_{,x}$) produced by the rotation is given by the first term in the bracket of equation (B9); the second term gives the relative contribution due to shear. Note that the shear contribution vanishes for $r_x' = 0$ (infinite shear stiffness). Additional information about the shear and rotational contributions is revealed by writing equation (B5) in the following form.

$$\overline{\omega}_{B_{TS}}'^2 = \frac{2[m^4 + (\tau m^4 - m^2 k_x')(1 + r_x' m^2)]}{[1 + (r_x' + \chi')m^2 + r_x' \chi' (\tau m^4 - m^2 k_x')] \left(1 \pm \left\{ 1 - \frac{4 r_x' \chi' [m^4 + (\tau m^4 - m^2 k_x')(1 + r_x' m^2)]}{[1 + (r_x' + \chi')m^2 + r_x' \chi' (\tau m^4 - m^2 k_x')]^2} \right\}^{1/2} \right)} \qquad \text{(B10)}$$

For many practical parameter values[12] the magnitude of the underlined fraction in equation (B10) has a value much less than 1.[13] In such cases equation (B10) can be approximated by

$$\overline{\omega}_{B_{TS}}'^{2} \approx \frac{2[m^4+(\tau m^4-m^2k_x')(1+r_x'm^2)]}{[1+(r_x'+\chi')m^2+r_x'\chi'(\tau m^4-m^2k_x')]\left(1 \pm \left\{1- \frac{2r_x'\chi'[m^4+(\tau m^4-m^2k_x')(1+r_x'm^2)]}{[1+(r_x'+\chi')m^2+r_x'\chi'(\tau m^4-m^2k_x')]^2}\right\}\right)} \tag{B11}$$

which in turn leads to

$$\overline{\omega}_{TS}'^{2} \approx \frac{1 + (r_x' + \chi')m^2}{r_x'\chi'} + \tau m^4 - m^2k_x' \tag{B12}$$

and

$$\overline{\omega}_{B}'^{2} \approx \frac{m^4\left(\tau + \dfrac{1}{1 + r_x'm^2}\right) - m^2k_x'}{1 + \sigma} \tag{B13}$$

---

[12]For identical face sheets and $f/c \leq 0.632$,

$$\tau = \frac{1}{3}\left(\frac{\frac{f}{c}}{1 + \frac{f}{c}}\right)^2 \leq 0.05$$

Positive values of the in-plane load parameter are limited by the buckling value, $k_x' = \tau + [1/(1 + r_x')]$ (for no airflow). For lightweight cores and identical face sheets the ratio χ'/r_x' is approximately equal to

$$\left(\frac{G_{c_x}}{E_f}\right)\left(\frac{c}{f}\right)\left(\frac{1 - \mu^2}{2}\right)\left(1 + \frac{f}{c}\right)^2$$

Numerically, this ratio often has a value considerably less than 1.

[13]One notable exception is when $r_x'\tau m^2 >> \chi'\tau m^2 \geq 1$.

where

$$\sigma = m^2\chi' \left(\frac{1 - r_x' k_x' + r_x' \tau m^2}{1 + r_x' m^2} \right)$$

In many instances σ is also much less than 1. For example, if $k_x' = \tau = 0$ then $\sigma = m^2\chi'/(1 + r_x' m^2) < \chi'/r_x'$ which is normally small compared to 1.

Substitution of the above approximate expressions for the thickness-shear and bending frequencies into the second of equations (B7) yields

$$\left.\begin{aligned} \left.\frac{\gamma_x}{w,x}\right|_{\overline{\omega}_{TS}'^2} &\approx 1 + \frac{1 + r_x' m^2}{m^2\chi'} \\ \left.\frac{\gamma_x}{w,x}\right|_{\overline{\omega}_{B}'^2} &\approx \frac{m^2 r_x'}{1 + m^2 r_x'} \end{aligned}\right\} \qquad \text{(B14)}$$

where σ has been neglected with respect to unity. Since $w_{,x} = \alpha_x + \gamma_x$, and since no term on the right hand side of equations (B14) can be less than zero, the *approximate* bounds on γ_x and α_x are

$$\left.\begin{aligned} 0 \le \frac{\gamma_x}{w,x} < 1 \\ 0 < \frac{\alpha_x}{w,x} \le 1 \end{aligned}\right\} \quad \text{for the bending modes} \qquad \text{(B15)}$$

$$\left.\begin{aligned} \frac{\gamma_x}{w_{,x}} &> 1 \\ \frac{\alpha_x}{w_{,x}} &< 0 \end{aligned}\right\} \text{ for the thickness-shear modes} \qquad \text{(B16)}$$

The mode shapes resulting from these restrictions on γ_x and α_x are illustrated in figures 3(c) and 3(d) for the bending and thickness-shear modes, respectively.

Numerical values for $\overline{\omega}'^2$ and $\gamma_x/w_{,x}$ as predicted by the approximate expressions (eqs. (B12), (B13), and (B14)) and by the exact equations ((B5) and (B7)) are compared in table II for three sets of parameters.

TABLE II.- COMPARISON OF IN-VACUO BENDING AND THICKNESS-SHEAR FREQUENCIES AND MODE SHAPES AS PREDICTED BY EXACT AND APPROXIMATE SOLUTIONS FOR A SIMPLY SUPPORTED BEAM

			1	2	3
	k_x'		0.0	-1.0	0.0
	f/c		0.04	0.04	0.0
	χ'		0.01	0.01	0.002
	r_x'		1.0	0.1	0.2
	m		2	1	2
$\overline{\omega}'^2$	Bending	Exact	3.203	1.894	8.867
		Approximate	3.208	1.910	8.889
	Thickness-shear	Exact	500.8	1109	4511
		Approximate	504.0	1111	4520
$\frac{\gamma_x}{w,x}$	Bending	Exact	0.799	0.0894	0.443
		Approximate	0.800	0.0909	0.444
	Thickness-shear	Exact	125.2	110.8	225.6
		Approximate	126.0	111.0	226.0

C. Two-Mode Galerkin Solution of Reference 9

In reference 9 a two-mode Galerkin solution for flutter was obtained for a simply supported panel having:

1. Two transverse shear stiffnesses (D_{Q_x}, D_{Q_y}).
2. Two bending stiffnesses (D_x, D_y).
3. Two Poisson ratios (μ_x, μ_y).
4. A twisting stiffness D_{xy}.

For isotropic face sheets and an orthotropic core with negligible bending stiffnesses, one can set (ref. 14)

$$\mu_x = \mu_y = \mu$$

$$D_x = D_y = D_s\ (1 - \mu^2)$$

$$D_{xy} = D_s\ (1 - \mu)$$

By use of the above relations, the two-mode solution (in terms of the notation used herein) is given by

$$\lambda = \frac{\pi^4}{4\eta}\ |i^2 - j^2|\sqrt{-p(i)p(j)} \tag{C1}$$

where i and j are integers whose sum is an odd integer and

$$p(m) = \frac{\left[-c2(m) - \left(\frac{m}{\eta}\right)^4 + \left(\frac{m}{\eta}\right)^2 c3(m) + c4(m)\right]}{\left(\frac{m}{\eta}\right)^2 c1(m)}$$

$$c1(m) = 1 + \left(\frac{1-\mu}{2}\right)\left[\left(\frac{m}{\eta}\right)^2 r_y + n^2 r_x\right] + \left(\frac{1-\mu}{2}\right) r_x r_y \left[\left(\frac{m}{\eta}\right)^2 + n^2\right]^2 + \left[\left(\frac{m}{\eta}\right)^2 r_x + n^2 r_y\right]$$

$$c2(m) = \left[\left(\frac{m}{\eta}\right)^2 + n^2\right]^2 \left[\left(\frac{m}{\eta}\right)^2 r_y + n^2 r_x\right] \left(\frac{1 - \mu}{2}\right)$$

$$c3(m) = c1(m)k_x - 2n^2$$

$$c4(m) = c1(m)[\overline{\omega}^2 + n^2 k_y] - n^4$$

The solution for λ_{cr} (at $\partial\lambda/\partial\omega^2 = 0$) is given by

$$\lambda_{cr} = \frac{\pi^4\eta}{8ij}\left|i^2 - j^2\right|[E(i) - E(j) + n^4F(i,j)] \tag{C2}$$

where

$$E(m) = \frac{c2(m) + \left(\frac{m}{\eta}\right)^4 - \left(\frac{m}{\eta}\right)^2 c3(m)}{c1(m)}$$

and

$$F(i,j) = \frac{c1(j) - c1(i)}{c1(i)c1(j)}$$

Equations (C1) and (C2) provide an estimate for the flutter behavior of a simply supported sandwich panel having an orthotropic core and isotropic face sheets. Note that this solution does not account for rotary inertia, nor for the face sheet bending stiffness contribution to lateral equilibrium (i.e., $\chi = \tau = 0$).

For $\lambda = 0$, equation (C1) can be solved for $\bar{\omega}^2$ and, except for the absence of τ, yields the same in-vacuo frequency equation as given by equation (18a). This observation allows equation (C1) to be written as

$$\lambda(\bar{\omega}^2) = \frac{\pi^4\eta}{4ij}\left|i^2 - j^2\right|\sqrt{\left(\frac{\bar{\omega}_j^2 - \bar{\omega}_i^2}{2}\right)^2 - \varepsilon^2} \tag{C3}$$

where $\varepsilon = \bar{\omega}^2 - [(\bar{\omega}_i^2 + \bar{\omega}_j^2)/2]$ is shown in figure 20. The quantity $\bar{\omega}_i^2$ is the in-vacuo frequency of the ith mode (i.e., m = i in eq. (18a)). It is seen that $\lambda(\bar{\omega}^2)$ is symmetric about the line $(\bar{\omega}_i^2 + \bar{\omega}_j^2)/2$.

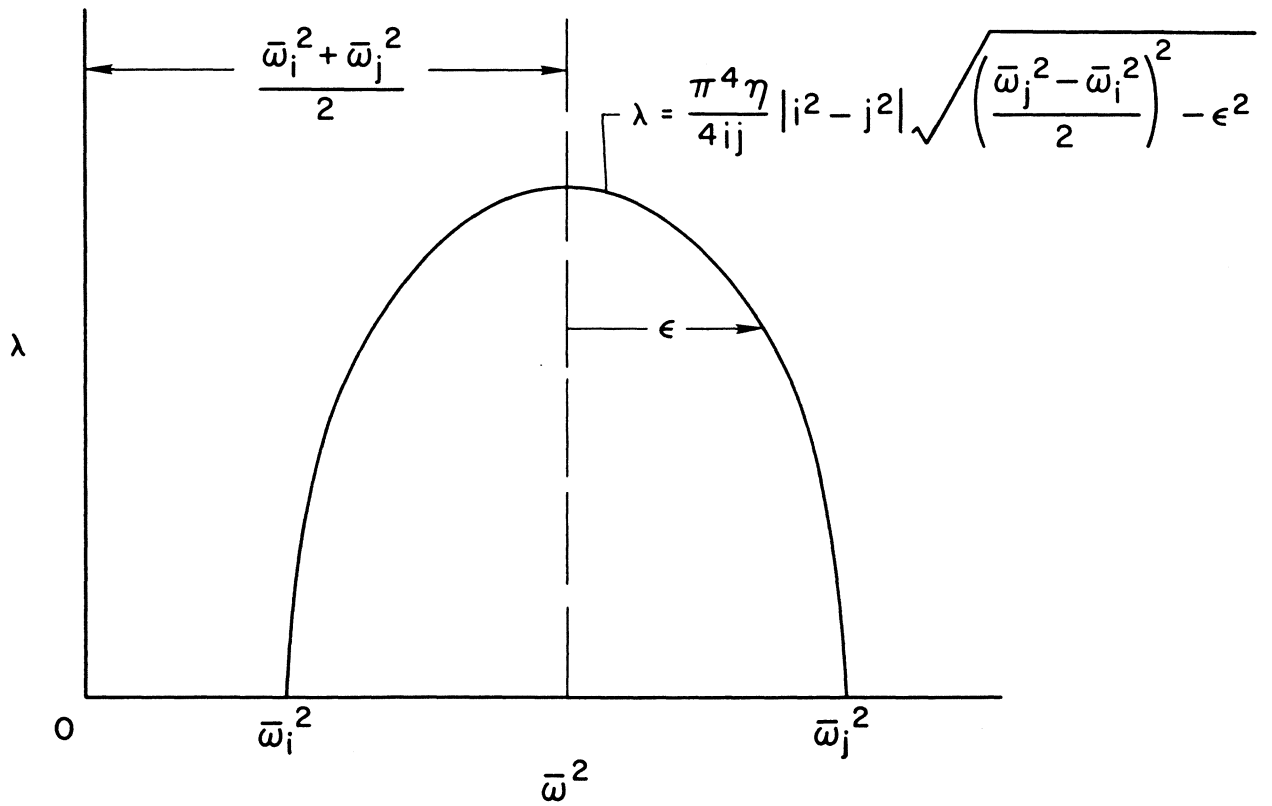

Figure 20.- Symmetric behavior of two-mode Galerkin solution.

D. Comments on Solution of Reference 27[14]

It was noted on page 26 that the thickness-shear and thickness-twist motions are due to the combined influence of core shear deformations and rotary inertia moments. In reference 27 the flutter analysis of reference 5 (isotropic core, face bending stiffness and rotary inertia neglected) was extended to include the effects of rotary inertia. Unfortunately, the analysis of reference 27 is based on differential equations that do not properly account for the rotary inertia moments.

The moments due to rotary inertia are proportional to the acceleration of the *rotation* of the panel cross sections, for example, $\alpha_{x,tt} = [w_{,x} - (Q_x/D_{Q_x})]_{,tt}$ (see appendix A). In reference 27, however, the rotary inertia moments are taken proportional to the acceleration of the *slopes* of the panel cross sections, for example, $(w_{,x})_{,tt}$. The rotation and the slope of a cross section are not equal unless the core shear deformation vanishes ($D_Q = \infty$); hence the analysis in reference 27 leads to erroneous results since it is based on an incorrect description of the rotary inertia moments. For example, the characteristic equation of reference 27 is linear, rather than cubic, in $\bar{\omega}^2$ and does not predict the thickness-shear or the thickness-twist frequencies. Also, the "bending" frequencies are correct only if the rotary inertia or the shear flexibility is neglected. Consequently, the results presented in reference 27 are of questionable value.

---

[14]This appendix is introduced in chapter II (p. 11), prior to the mention of appendix B. Since reference 27 was published shortly before the publication of this thesis, this appendix has been added out of sequence.

The vita has been removed from the scanned document

VIII. REFERENCES

1. Hedgepeth, John M.: Flutter of Rectangular Simply Supported Panels at High Supersonic Speeds. J. Aeron. Sci., vol. 24, no. 8, Aug. 1957, pp. 563-573, 586.

2. Movchan, A. A.: On the Stability of a Panel Moving in a Gas. NASA RE 11-21-58W, 1959.

3. McElman, John A.: Flutter of Curved and Flat Sandwich Panels Subjected to Supersonic Flow. NASA TN D-2192, 1964.

4. Anderson, Melvin S.: Flutter of Sandwich Panels at Supersonic Speeds. Ph. D. Thesis, Dept. of Engineering Mechanics, Virginia Polytechnic Institute, Blacksburg, Virginia, June 1965.

5. Erickson, Larry L.; and Anderson, Melvin S.: Supersonic Flutter of Simply Supported Isotropic Sandwich Panels. NASA TN D-3171, 1966.

6. Mindlin, R. D.; Schacknow, A.; and Deresiewicz, H.: Flexural Vibrations of Rectangular Plates. J. Appl. Mech., vol. 23, no. 3, Sept. 1956, pp. 430-436.

7. Smirnov, A. I.: Dynamic Stability and Vibrations of Sandwich Panels in a Supersonic Gas Flow. Soviet Phys.-Doklady, vol. 13, no. 6, Dec. 1968, pp. 609-612.

8. Smirnov, A. I.: Supersonic Flutter of Sandwich Plates. Soviet Phys.-Doklady, vol. 13, no. 11, May 1969, pp. 1179-1181.

9. Weidman, Deene J.: Effects of Side-Edge Boundary Conditions and Transverse Shear Stiffnesses on the Flutter of Orthotropic Panels in Supersonic Flow. NASA TN D-3302, 1966.

10. Shore, Charles P.: Effects of Structural Damping on Flutter of Stressed Panels. NASA TN D-4990, 1969.

11. Dixon, Sidney C.: Comparison of Panel Flutter Results from Approximate Aerodynamic Theory with Results from Exact Inviscid Theory and Experiment. NASA TN D-3649, 1966.

12. Muhlstein, Lado, Jr.; Gaspers, Peter A., Jr.; and Riddle, Dennis W.: An Experimental Study of the Influence of the Turbulent Boundary Layer on Panel Flutter. NASA TN D-4486, 1968.

13. Gaspers, Peter A., Jr.; Muhlstein, Lado, Jr.; and Petroff, Daniel N.: Further Experimental Results on the Influence of the Turbulent Boundary Layer on Panel Flutter. NASA TN D-5798, 1970.

14. Libove, Charles; and Batdorf, S. B.: A General Small-Deflection Theory for Flat Sandwich Plates. NACA Rep. 899, 1948. (Supersedes NACA TN 1526.)

15. Fulton, Robert E.: Nonlinear Equations for a Shallow Unsymmetrical Sandwich Shell of Double Curvature. Vol. 1 of Developments in Mechanics, J. E. Lay and L. E. Malvern, eds., Plenum Press, 1961, pp. 365-380.

16. Wylie, C. R., Jr.: Advanced Engineering Mathematics. Second ed., McGraw-Hill Book Co., Inc., New York, 1960.

17. Benson, A. S.; and Mayers, J.: General Instability and Face Wrinkling of Sandwich Plates - Unified Theory and Applications. AIAA J., vol. 5, no. 4, April 1967, pp. 729-739.

18. Bolotin, V. V. (T. K. Lusher, trans.; G. Herrmann, ed.): Nonconservative Problems of the Theory of Elastic Stability. The Macmillan Co., New York, 1963.

19. Anon.: Subroutine DPRBM, Roots of a Real Polynomial by Bairstow's Algorithm, IBM System/360 Scientific Subroutine Package (360A-CM-03X), Version III, Programmer's Manual, Fourth ed., 1968, pp. 189-192.

20. Churchill, Ruel V.: Complex Variables and Applications. Second ed., McGraw-Hill Book Co., Inc., New York, 1960, p. 265.

21. Jordan, P. F.; and Shelley, P. E.: Effect of Small Bending Stiffness on Deformation of Inflated Structures. International Astronautical Federation, International Astronautical Congress, 18th, Belgrade, Yugoslavia, Sept. 24-30, 1967, Proceedings, vol. 2, Spacecraft Systems, Education, Oxford, England, Pergamon Press, 1968, pp. 209-217, Michal Lunc, ed.

22. Gol'denveĭser, A. L. (G. Herrmann, ed.): Theory of Elastic Thin Shells. Pergamon Press, New York, 1961, p. 115.

23. Bohon, Herman L.; and Anderson, Melvin S.: Role of Boundary Conditions on Flutter of Orthotropic Panels. AIAA J., vol. 4, no. 7, July 1966, pp. 1241-1248.

24. Zimmerman, N. H.; and Lemley, C. E.: Cavity Effect on Panel Flutter - Just How Significant? The Shock and Vibration Bulletin, Bulletin 40, Part 4 (of 7 parts), Dec. 1969, pp. 139-145.

25. Erickson, Larry L.: Modal Density Estimates for Sandwich Panels: Theory and Experiment. NASA TN D-5771, 1970.

26. Greenwood, Donald T.: Principles of Dynamics. Prentice Hall, Inc., 1965, pp. 145-147.

27. Marafioti, F. A.; and Johnston, E. R., Jr.: Effects of Rotary Inertia on the Supersonic Flutter of Sandwich Panels. AIAA J., vol. 9, no. 2, Feb. 1971, pp. 245-249.

SUPERSONIC FLUTTER OF SANDWICH PANELS: EFFECTS OF FACE SHEET BENDING STIFFNESS, ROTARY INERTIA, AND ORTHOTROPIC CORE SHEAR STIFFNESSES

Larry L. Erickson

Abstract

A theoretical analysis is presented for the supersonic flutter of flat rectangular, biaxially stressed sandwich panels. On the basis of two-dimensional static aerodynamic theory an exact solution is obtained for panels having simply supported edges parallel to the airflow. The leading and trailing edges may be simply supported or clamped. The mathematical model describing the panel motion includes terms that account for rotary inertia, face sheet bending deformations, and transverse shear deformations of an orthotropic core such as honeycomb. Damping forces are neglected.

The linear system of partial differential equations governing the lateral deflection and the two transverse shear angles is eighth order and has constant coefficients. For simply supported edges parallel to the flow these equations have a separable solution. The characteristic equation associated with this solution is an eighth-order polynomial; its roots are determined numerically for given values of dynamic pressure and panel frequency. For each of the two sets of leading and trailing-edge boundary conditions considered, a corresponding frequency determinant is obtained that provides a second relation between the dynamic pressure and frequency. For either set of boundary conditions the corresponding frequency determinant equation and the characteristic equation are simultaneously satisfied by various combinations of

dynamic pressure and frequency. Flutter occurs when the dynamic pressure attains a level that causes two panel frequencies to coalesce and become complex.

For a panel with an isotropic core, a second-order differential operator factors from the eighth-order system of differential equations. The remaining sixth-order system has been used in a previous flutter analysis (but with rotary inertia neglected). Flutter solutions based on the sixth-order system are shown to be correct when the complete solution from the eighth-order system uncouples. (This occurs for the isotropic panel if all edges are simply supported.) The sixth-order system, however, is inherently incomplete and is generally not applicable to the more general case where the solutions from the eighth-order system do not uncouple.

Numerical results from the complete eighth-order system show that the face sheet bending stiffness has a negligible effect on flutter if the faces are thin compared to the core thickness. As the face-to-core thickness ratio increases, the face bending stiffness becomes more important, especially for panels having relatively flexible cores.

The frequency coalescence behavior can be markedly changed by the combined effects of rotary inertia and core shear flexibility. Failure to account for this combined effect can lead to significant overestimates of flutter dynamic pressure values. Rotary inertia also causes the flutter solution to depend slightly on the crossflow in-plane loading.

The directional shear stiffness properties of the core are of comparable importance for square panels. As the panel width increases,

the importance of the shear stiffness in the crossflow direction decreases.